SOLAR ENERGY COLLECTION USING VEE-GROOVED SURFACES

by

JENS PETER KEMPER *

Submitted to the University of Cape Town in fulfilment of the requirements for the degree of Doctor of Philosophy

September 1977

* Dipl.-Wirtschaftsingenieur, TH Karlsruhe, Germany

ABSTRACT

The thesis presented is a study of the absorption characteristics of diffusely and specularly reflecting V-grooved surfaces. Concepts are developed for the so-called "apparent" absorptance of a V-groove cavity, as well as for the "effective" absorptance of a V-grooved surface. These concepts are formulated in closed form mathematical equations, which facilitate both the optimization of V-grooved surfaces and their engineering design.

In order to verify the theoretical analysis, experiments are carried out on 34 V-grooved brass specimens. In addition, the experiments are meant to provide information about the behaviour of such surfaces used for solar energy collection. For that purpose, the specimens are exposed to simulated sunlight, and their effective absorptances, as well as their absorption efficiencies, are determined by a calorimetric method.

The highlights among the results are:

1. V-grooves--carefully optimized and applied to a solar energy absorbing surface--can raise its absorptance almost to unity and improve its absorption efficiency.

2. Best performances at elevated temperatures can be expected from using metal surfaces which are provided with specular V-grooves having a small groove angle ($< 30^{o}$).

3. The optimal groove angle is dependent on (1) the reflection properties of the surface, (2) the absorptance of the surface material, and (3) the ratio of groove depth to width of land which occurs between grooves.

ACKNOWLEDGEMENTS

This thesis was supported by the Council for Scientific and Industrial Research (C.S.I.R.), Pretoria, Republic of South Africa.

The author also wishes to acknowledge his indebtedness to Dr. R. K. Dutkiewicz, Professor of the Department of Mechanical Engineering, University of Cape Town, for suggesting the study and for his helpful guidance and encouragement throughout this project.

Special thanks are due to the staff members of the workshop of the Department of Mechanical Engineering for their help in building the experimental apparatus, particularly with respect to the extremely arduous task of machining the specimens.

Finally, the author wishes to express his deep appreciation to his wife, Gisela, for her understanding and patience during the period of this project.

TABLE OF CONTENTS

TABLE OF CONTENTS (continued)

TABLE OF CONTENTS (continued)

LIST OF FIGURES

LIST OF FIGURES (continued)

LIST OF FIGURES (continued)

NOMENCLATURE

(For quick access to the nomenclature a fold-out version is included after the appendices.
Symbols cited in the literature survey as well as common mathematical symbols are not listed to avoid confusion.)

Symbol		Unit
A	projected surface area of specimen	m^2
A'	grooved surface area of specimen	m^2
a	constant	-
b	constant	-
c_p	specific heat capacity of glycol	Wh/kg^oC
D	diameter of specimens	mm
d	depth of V-groove	mm
E	irradiance per unit area (radiant flux density)	W/m^2
E' (x,y)	local irradiance per unit surface area	W/m^2
e	error as defined in App. H	-
F	configuration factor (angle factor)	-
f	blackbody function	-
G	mass of glycol	kg
H	thickness of specimens	mm
i	number of reflections	-
K	kernel of integral equation	-
k	quantity as defined by Eq. (36)	-
L	width of V-groove side	mm

NOMENCLATURE (continued)

Symbol		Unit
L'	width of V-groove side as shown in Fig. 6	mm
l	width of land between V-grooves as shown in Figs. 9 and 13	mm
$\dot{m}$	flow rate of glycol	kg/h
n	total number of V-grooves on a specimen	-
p	pitch of V-grooves as shown in Fig. 13	mm
q	heat transfer rate	W
T	temperature	^{o}C
t	time interval	sec
U	thermocouple EMF	mV
w	width of V-groove opening	mm
X	dimensionless coordinate (x/L)	-
x	coordinate	mm
Y	dimensionless coordinate (y/L)	-
y	coordinate	mm
z	coordinate	mm
	...	
α	absorptance	-
β	substituted function as defined by Eqs. (14) and (16)	-
γ	substitution as defined by Eq. (15)	-
δ	angle of reflection	deg
ϵ	emittance	-
η	absorption efficiency	%
θ	groove angle	deg

NOMENCLATURE (continued)

Symbol		Unit
λ	wavelength	μm
ξ	dimensionless variable	-
ρ	reflectance	-
σ	Stefan-Boltzmann constant	W/m^2K^4
τ	transmittance	-
Φ	radiant flux	W
φ	image angle as shown in Fig. 6	deg

Subscripts / Superscripts

a	apparent
c	cutoff
d	diffuse
eff	effective
i	number of reflections
l	losses
rel	relative
s	specular, or surface
α	absorbed
0	ambient
1	inlet of calorimeter
2	outlet of calorimeter
3	surface of specimen
*	quantity related to $(T_3 - T_0)^*$
'	auxiliary quantity

CHAPTER 1

INTRODUCTION

1.1 ORIGIN OF THE PROBLEM

In recent years, marked attention has been paid to radiation heat transfer in surfaces as a result of the growing interest in the utilization of solar energy and the development of so-called "selective" surfaces. Although all natural surfaces may be termed selective in the sense that their radiative properties are wavelength dependent, the term is also used to refer to an artificially increased ratio of total absorptance for solar radiation to total emittance for infrared radiation. To achieve such selective properties, a number of techniques have been developed during the last 20 years. These techniques are based upon the following principles:

1. Selective absorption coatings
2. Optical interference
3. Dielectric reflectors
4. Microporous surface textures
5. Grooved or corrugated surfaces

Since the greatest drawback to the use of solar energy over conventional energy (at the present) is the long payback period, the collection of solar energy must be optimized on an economic basis. Of the five methods mentioned above, the grooving or corrugating of absorber

surfaces offers great potential in this respect.

Typically, as will be shown in the literature survey, grooves or corrugations are applied to metallic solar absorber surfaces in wedge or V-shaped profiles. This configuration facilitates both the manufacturing process and a possible heat transfer analysis. Furthermore, a V-shaped metallic surface takes advantage of the effect that the moderate absorptance of metals increases almost to unity by multiple reflection (as will be demonstrated in this thesis), whereas their emissivity remains at a relatively low level.

However, there is recent experimental evidence [1] that the above effect is a function of parameters which have not been adequately investigated. It therefore appears to be useful, particularly with respect to the design of solar collectors, to examine more closely the interdependence of such parameters, and to enable the performance of V-grooved absorber surfaces to be optimized.

1.2 LITERATURE SURVEY

The effect of surface texture on its radiation heat transfer properties did not receive significant attention before the middle of this century. However, as far as grooved surfaces of solid and opaque materials are concerned, some early observations and fundamental experi-

ments are noteworthy to demonstrate the development and limits of a theoretical approach to the problem.

Probably one of the earliest references to the effect of surface texture was by P. Bouguer (1698-1758). Studying the reflection of sunlight from polished and rough surfaces [2], he observed that the intensity of the reflected light decreased with decreasing angle of incidence, as well as with the degree of roughness. He explained the latter by assuming that the roughness of a surface can be represented by little hemisheres as shown in his illustration:

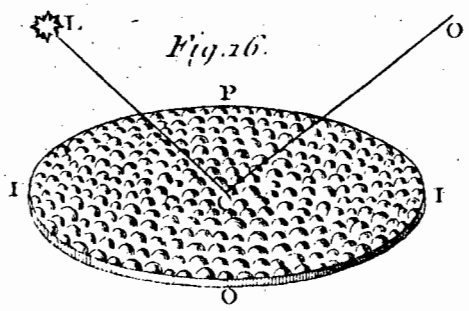

Bouguer's original illustration [2] of a rough surface.

A beam of light falling on above surface suffers more than one reflection within the small hemispheres and is consequently attenuated. What is more, Bouguer concluded that this multiple reflection contributes to the heating of the surface. The present thesis will show that this observation is perfectly true.

Almost a century later, Bouguer's discovery was investigated from a different point of view by J. Leslie (1766-1832). Leslie observed [3] that by grooving the surface of a heated metallic body, its emission of radiant heat increased in proportion to the extent of grooving. As a result of his experiments he stated that the absorptive power of a surface is proportional to its emissive power, and inversely proportional to its reflective power. This can be regarded as the simplified "Kirchhoff's Law", which was laid down 50 years later.

However, Leslie's statements may be expressed by using the proportionality factors C_1 and C_2, and by defining a factor K = f(surface texture) as follows:

$$\epsilon_{total} = C_1 \alpha_{total} = C_1 K \alpha_{surface} = K (C_2/\rho_{surface})$$

The first theoretical explanation for Leslie's experimental results was given by W. Ritchie [4] in 1824. Ritchie assumed that a cross section of a grooved surface could be represented by equilateral triangles joined closely together:

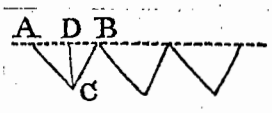

Ritchie's original illustration [4] of a grooved surface.

By purely trigonometrical considerations for a single triangle he came to the following conclusion. The heat Q_{AB} radiated from the opening AB of a triangular cavity is given by

$$Q_{AB} = (Q_{AC} + Q_{BC})\sin\sphericalangle\frac{ACB}{2} + (\frac{Q_{BC}}{2} + \frac{Q_{AC}}{2})_{\text{reflected}}$$

and consequently almost doubled since

$$Q_{AC} = Q_{BC}$$

$$\sin\sphericalangle\frac{ACB}{2} = \sin 30^{o} = 1/2 \ ,$$

and since reflection on a metal surface can approach total reflection. Designating $\sphericalangle$ ACB as θ, Ritchie's conclusions may be expressed as

$$\Phi_{\text{total}} = 2\Phi_{\text{side}}\sin\frac{\theta}{2} + \rho\Phi_{\text{side}} \ .$$

The similarity of this expression with Eq. (12) given in Chapter 2 is remarkable.

Leslie's experiments, in conjunction with similar experiments carried out by M. Melloni during the period 1838-1841 [5,6], H. Knoblauch in 1847 [7,8], and G. Magnus during the period 1865-1869 [9,10], led to a noteworthy controversy about what was causing the augmentation of the emissive and absorptive power of rough surfaces. Melloni and Knoblauch were of the opinion that the process of roughening or grooving had reduced the density of the surface material and thereby given rise to an increased emission and absorption. Their basic idea was that radiation does not only emerge from the

outer surface,but also from layers inside the material. Using a similar concept Magnus, on the other hand, believed that a grooved surface (which he assumed to be saw-tooth shaped) reduces the index of refraction for thermal radiation. This reduced refraction index, especially of metals, he regarded as being responsible for the observed increase in emission.

The controversy continued, but research gradually resumed along the path of Ritchie's work in an effort to find a surface geometry which might be representative of a grooved surface as a whole.

In the search for an ideal and neutral receiver for radiation (black body), C. Féry investigated in 1909 [11] a corrugated surface made of wedge-shaped cavities blackened on the inside. He believed that each beam of rays having entered a cavity was subject to the same interreflection pattern, irrespective of its location of incidence:

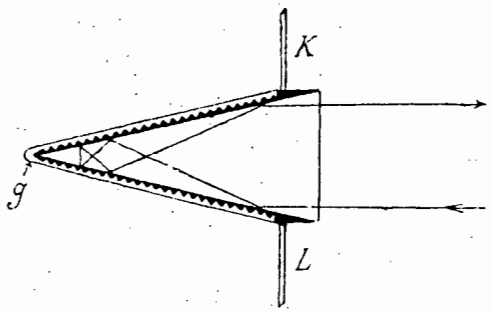

Féry's original illustration [11] of multiple reflection in a wedge-shaped cavity.

In this way the absorptive power of the cavity was substantially increased, an effect which Féry explained as follows: Assuming that the number of reflections suffered by a single ray is $N = 180/\alpha$, where α is the angle at the vertex of the cavity, he stated that the reflective power of the cavity is K^N, and the

$$\text{Absorptive power} = 1 - K^N. \qquad (1)$$

It is interesting to note that Eq. (1) is identical to Eq. (38) which is set up for a cavity with specular sides and does not hold for blackened sides as assumed by Féry.

That Féry was mistaken in treating a black surface as being specular was realized by C. E. Mendenhall in 1910 [12]. Mendenhall carried out similar experiments on V-groove cavities made of platinum strips. Trying to find out how closely the radiation from the inside of his cavity approximated that of a black body at the same temperature, he defined an effective absorbing power, A, for two different cavities. For a cavity with specular sides, he agreed with Féry's equation, which he wrote in the form

$$A = 1 - r^n.$$

For a cavity with a matt surface, Mendenhall could only give an estimate of the average absorbing power by considering the diffuse reflection pattern at the centre of

the cavity side. His estimate may be rewritten in a general form:

$$\bar{\alpha}_{eff} = \alpha_{side}[1-\rho_{side}(1- \arctan(\sin\theta/(\cos\theta-0,5))\,/180)]^{-1} \quad (2)$$

Inspection of Eqs. (2) and (30) reveals a remarkable similarity, the only difference being the last term. This term in Eq. (30), $(1 - \sin\theta/2)$, is a configuration factor, which was not known at that time, but which is well approximated in Eq. (2).

As mentioned at the beginning of this survey, radiation heat transfer properties of grooved surfaces received intensified attention after the 1960's. As far as V-grooved surfaces are concerned, the main interest pertained to questions of their thermal emissivity or heat emission [13-22]. Only a few papers are known dealing with the absorption characteristics of V-grooved surfaces or V-groove cavities, though these are similar to the emission characteristics.

The first, and probably the only mathematically exact analysis of thermal radiation absorption in single V-groove cavities was given by E. M. Sparrow and S. H. Lin in 1962 [23], with reference to a preceding analysis of 1961 [24]. Sparrow and Lin gave consideration to cavities whose sides are either diffuse or specular reflectors (receiving radiant energy in a diffuse form or as a bundle of parallel rays). Since the latter problem is

the object of this investigation, Sparrow and Lin's results will be summarized in some detail:

As far as parallel rays entering a specular cavity are concerned, Sparrow and Lin followed Mendenhall's results by defining an "apparent" absorptivity, α_a, of a cavity, such that

$$\alpha_a = 1 - \rho_s^i = 1 - (1 - \alpha)^i. \tag{3}$$

Realizing that the number of reflections, i, is dependent on groove angle, θ, and angle of incidence, γ, they extended Eq. (3) into

$$\alpha_a = \left[(1-(1-\alpha)^{i'-1}(1-\alpha(\sin((i'-\tfrac{1}{2})\theta+\gamma))/\sin(\tfrac{\theta}{2}+\gamma))\sin(\tfrac{\theta}{2}+\gamma)\right.$$
$$+ \left.(1-(1-\alpha)^{i''-1}(1-\alpha(\sin((i''-\tfrac{1}{2})\theta-\gamma))/\sin(\tfrac{\theta}{2}-\gamma))\sin(\tfrac{\theta}{2}-\gamma)\right]$$
$$\times (2\cos\gamma\sin\tfrac{\theta}{2})^{-1}. \tag{4}$$

As far as diffuse reflecting cavities are concerned, they considered the energy locally incident per unit surface area, the integration of which resulted in the total incident energy per cavity side. This led to a pair of dimensionless integral equations,

$$f(\xi) = \alpha + \rho\int_0^1 g(\eta)\, dF_{\xi-\eta}\ ,\quad g(\eta) = \alpha + \rho\int_0^1 f(\xi)\, dF_{\eta-\xi}, \tag{5}$$

whose solution was obtained numerically for certain α and θ-values. With this solution the apparent absorptivity

could be evaluated by performing the integration

$$\alpha_a = \int_0^1 f(\xi)\, d\xi + \int_0^1 g(\eta)\, d\eta \ . \qquad (6)$$

Some final results are shown in App. A and are replotted in Fig. 2 ; they will be discussed in more detail in Section 2.2.1.4 .

Sparrow's method of analysing the heat transfer behaviour of V-shaped (and similar) cavities became the underlying principle for all further theoretical investigations. Recent work [16-22] has been merely a refinement of Sparrow's approach with respect to various surface properties.

The use of V-grooved or V-corrugated surfaces for solar energy collectors--particularly for solar air heaters--was suggested for the first time by H. Tabor in 1957 [25], and has since been studied by teams in France, Australia, Israel, and U.S.A.

Trombe and Foex in France demonstrated in 1958 [26] that the peculiar radiative characteristic of polished zinc (very low emissivity in the infrared and moderate absorptivity in the visible spectrum) could be favourably utilized for solar air heaters. Folding the zinc absorber plate into, for example, 30° Vees, would result in an effective absorption of more than 90%, and the emission loss would be not more than 10-15% at a working

temperature of 100 ^{o}C.

A different aspect of V-corrugated absorbers for solar collectors was studied by K. G. T. Hollands [27] and D. J. Close [28] in 1963 in Australia. Hollands utilized the directionally selective properties of a V-groove to optimize the absorptive power, taking into account that the solar radiation over a year is directional in character. Realizing that the sun's incidence angle throughout the year is 50% more often in the range 15 to 30 deg than it is within the range 0 to 15 deg, he defined an average yearly solar absorptance α_{sy} as follows:

$$\alpha_{sy} = [2\alpha(7\tfrac{1}{2}^{o}) + 3\alpha(22\tfrac{1}{2}^{o})]/5 \qquad (7)$$

The additional application of a spectrally selective coating would make such a selected V-corrugation both directionally and spectrally selective.

In a theoretical design study of solar air heaters, Close demonstrated that a V-corrugation, designed according to Holland's principles and having a heat transfer surface double that for a flat plate, would be superior to flat black and flat selective surfaces under all test conditions.

The fact that a V-corrugation of an absorber plate, whilst increasing the collector efficiency, also involves higher costs of material, was pointed out by W. W. S. Charters in 1972 [29]. Using a computerized analysis for

two different types of V-corrugated (Height = 5 cm) air heaters, Charters investigated the heat gain per unit actual surface area, thus taking into account the amount of material required to fabricate the absorber plate. On this basis the performance of a 120^{o} V-corrugation turned out to be most economical; but such a wide-angled groove has little advantage over a flat surface as will be shown later.

Up to this point, all the work discussed has involved large V-grooves (in the order of centimetres). These grooves are normally manufactured by the bending of sheet metal, and typical applications include their use in air heaters. For some solar applications, however, smaller grooves (in the order of millimetres) are found to be more suitable. This is particularly true if grooves are to be cut into thin surfaces.

Only two experimental investigations of very small V-grooves are known so far, the first being reported by C. P. Butler et al. in 1962 [30]. Their report is concerned with the selection and testing of surfaces which exhibit spectrally selective properties suitable for conversion of solar radiation to sensible heat. Among others, a micro-V-grooved surface was produced by pressing an assembly of 250 razor blades into a gold specimen. It was shown, by exposing both a flat and a grooved gold specimen to simulated sunlight, that the effective

absorptance and emittance had increased approximately as predicted. These results will be discussed in more detail in Chapter 5.

A different use of small V-grooves (width = 1,5 mm) was reported by O. W. Clausen and J. T. Neu in 1965 [31]. By blackening one side of specular aluminium V-grooves, they obtained a strongly directional absorption characteristic, which could be utilized for the thermal control of space vehicles. The experimental absorptance data (for 45^{o} and 60^{o} groove angle) were calculated from reflectance measurements taken on a modified spectrometer.

Finally, work has recently been re-initiated into the use of V-grooves as solar concentrating devices [32-39]. This form of application, although based upon the above principle of interreflection, is beyond the scope of the present investigation, and therefore no details are presented.

1.3 OBJECTIVE

The preceding literature survey is not intended as a complete review of publications related to this work, rather it should become evident that -

1. Theoretically, V-grooves or V-corrugations applied to solar energy absorbers are suitable

means for increasing the absorptive power, an effect, however, which does not always results in a worthwhile improvement of the overall absorption efficiency;

2. Closed Form Mathematical Formulae describing the above effects, and suitable for engineering use, are not available;

3. Very little attention has been given (theoretically and experimentally) to the impact of small V-grooves on the radiation heat transfer properties of a real surface to which they are applied.

In view of this information gap, the aim of the present investigation is as follows:

In Chapter 2 , closed form theoretical formulae will be developed, describing the absorption characteristics of diffusely and specularly reflecting surfaces. The applicability of these formulae in an engineering sense will be taken into account.

An experimental verification of the formulae derived will be presented in Chapter 3 and Chapter 4 . For that purpose, the absorption characteristics of specially prepared V-grooved brass specimens will be investigated.

It is worth mentioning that J. Leslie stated already in 1804

> "...that the propellent power (of a grooved surface) increases in proportion as the scratches or striae become multiplied on the surface. There is no doubt some limit where the effect reaches its maximum, and which might be discovered, by having plates of metal manufactured with a variety of delicate flutings" [3, p. 82].

It will be shown that such maxima exist and that the prepared V-grooved metal surfaces, acting as an absober for sunlight, behave largely as theoretically predicted. In addition, the advantage of V-grooved surfaces for solar energy collection will be demonstrated.

CHAPTER 2

THEORETICAL ANALYSIS

2.1 INTRODUCTION

It has been shown in Chapter 1 that the radiation heat transfer properties of a V-grooved surface are governed by the overall absorption and emission of single V-groove cavities of which the surface is composed. Moreover, the absorption of radiation within such a cavity is governed by an apparent absorptance, α_a, which exceeds the absorptance, α, of the surface material.

It will be shown in Section 2.2 that, ideally, α_a is a function of surface absorptance, surface reflectance and groove opening angle:

$$\alpha_a = f(\alpha, \rho, \theta)$$

In the following Section 2.3 this functional dependence will be extended to make allowance for a real V-grooved surface.

At this point, it is appropriate to give consideration to some assumptions under which the forthcoming analysis of radiation interchange is carried out. These are:

(I) The surfaces are "semi-gray"

(II) The reflection from any surface is either diffuse and hemispherically uniform, or specular and unidirectional

(III) The V-groove cavities are perfect axially symmetric

(IV) The irradiance is uniform and normal to the opening of a cavity

To item (I):

Engineering heat transfer calculations, for example, are usually carried out under the assumption that the participating surfaces are gray, i.e.,

$$\epsilon(T_s) = \alpha(T_s) = 1 - \rho(T_s) \neq f(\lambda, \text{ solid angles}).$$

This gray-body assumption is reasonable, but it may cause serious errors if the wavelength range in which the absorption occurs is broad and very different from that in which the reradiation (emission) takes place. This is usually the case in solar energy collectors, where the peak emission of solar radiation to be absorbed occurs at 0,48 µm (6000 K) whereas the peak emission of reradiation at, say, 400 K occurs at 7,24 µm. Thus α and ϵ should be treated seperately and monochromatically or at least in a semi-gray approach assuming that α and ϵ are constant within certain spectral bands.

However, as far as the present investigation is concerned, it is assumed that α is constant within the solar spectrum, and ϵ is constant within the temperature range under consideration.

The advantage of the fact that, in general,

$$\alpha(T_s) \neq \epsilon(T_s)$$

is that large practical α/ϵ ratios are attainable. For a surface receiving solar energy this may be achieved by making provisions for both a low operating temperature and a low emittance of the absorbing material. Simultaneously increased absorptance will then be an additional advantage. This will be discussed in more detail in Chapter 5 .

To item (II):

The reflective properties of a plane surface are more complicated to specify than either the emittance or absorptance. This is because the reflected energy depends not only on wavelength and direction being considered for the reflected energy, but additionally depends on the angle at which the incident energy impinges on the surface. Thus the assumption that the reflection from any participating surface is both independent of the wavelength within the solar spectrum and perfectly diffuse or perfectly specular provides two special cases, which facilitate the calculation of radiation interchange.

It can be expected that the above assumptions do not produce serious errors on two conditions: firstly, α is considered as being the total averagé solar absorptance, and, secondly, the purely diffuse or specular properties are considered as being the limiting cases for any real surface property. The latter will be explained in more detail in Section 2.2.1.4 .

To item (IV):

The assumption that the V-groove cavities are irradiated by parallel rays normal to the opening of a cavity, is also a special case. That this is the optimal case with respect to the absorptive power of a cavity may be seen in App. A , which shows a copy of the results obtained by Sparrow et al. [23], as mentioned in the literature survey. Inspection of App. A reveals that, in general, the absorptive power of a V-groove cavity decreases with either increasing angle of incidence or when diffusely irradiated. This holds for both specularly and diffusely reflecting surfaces.

2.2 ABSORPTION IN V-GROOVE CAVITIES

Subject to the assumptions mentioned above, the following analysis refers to cavities having either perfect diffusely or perfect specularly reflecting sides. The diffuse cavity will be analysed first.

2.2.1 Apparent Absorptance of Diffuse Cavities

2.2.1.1 Fundamental Equations. The apparent absorptance of a V-groove cavity may be defined as

$$\alpha_a = \frac{\text{total radiant energy absorbed within the cavity}}{\text{total radiant energy entering the cavity}}$$

$$= \frac{\text{total absorbed radiant flux}}{\text{irradiance} \times \text{cavity aperture area}} , \qquad (8)$$

and with reference to Fig. 1

$$\alpha_a = \frac{\Phi_\alpha}{E\,\omega\,z} . \qquad (9)$$

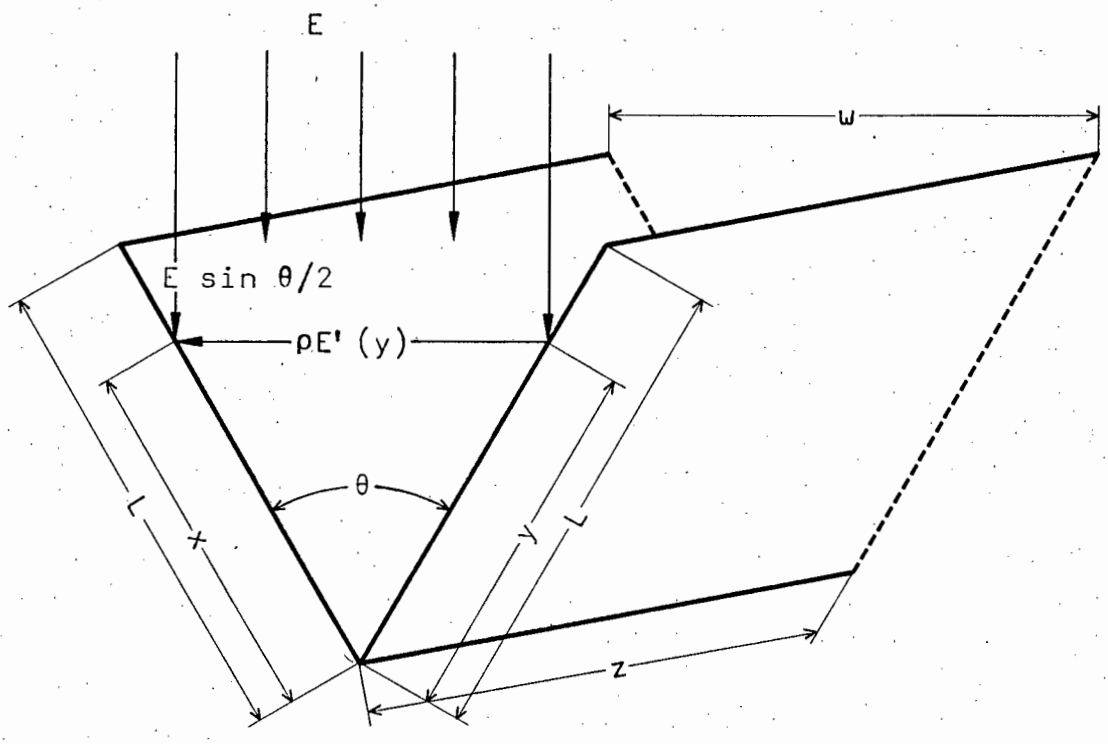

Figure 1. Fundamental configuration of a V-groove cavity.

The total radiant flux, Φ_a, absorbed per unit length of the cavity is obtained by integrating the absorbed local irradiance, $\alpha E'(x)$ and $\alpha E'(y)$, over the surface of the cavity sides (E' is the locally reflected part of E):

$$\frac{\Phi_a}{z} = \alpha \left(\int_0^L E'(x)\, dx + \int_0^L E'(y)\, dy \right) \qquad (10)$$

Because of assumptions (III) and (IV) made in Section 2.1, both cavity sides receive an equal amount of radiant flux making the integrals in Eq. (10) identical. Hence it follows that

$$\frac{\Phi_a}{z} = \alpha\, 2 \int_0^L E'(x)\, dx ,$$

and using Eq. (9)

$$\alpha_a = \alpha \frac{2 \int_0^L E'(x)\, dx}{E w} . \qquad (11)$$

The calculation of α_a from Eq. (11) requires only a solution for the function E'(x) since--in general--all other quantities are known.

Referring to Fig. 1, the local irradiance, E'(x), on one cavity side may be expressed as the sum of direct irradiance, $E \sin\theta/2$, plus that fraction of total irradiance, $\int E'(y)$, which is diffusely reflected from the

opposite side and which strikes location x :

$$E'(x) = E \sin \theta/2 + \rho_d \int_{y=0}^{L} E'(y)\, dF_{dx-dy} \qquad (12)$$

The contribution of emission, $\varepsilon \sigma (T_s^4 - T_0^4)$, is left out of consideration. This is possible because it is the object to determine only the amount of incoming energy which is ultimately absorbed within the cavity. Clearly, it may be assumed that the energy absorbed by the cavity walls is immediately extracted, so that $T_s = T_0$, i.e., no emission occurs.

The term dF_{dx-dy} in Eq. (12) represents the configuration factor (angle factor) for diffuse radiation interchange between two infinitely small strip elements dx and dy within an infinitely long V-groove cavity. This factor is derived in full details in [40] and is defined as

$$dF_{dx-dy} = \frac{\sin^2 \theta}{2} \frac{x\, y}{(x^2 + y^2 - 2\, x\, y \cos \theta)^{3/2}}\, dy . \qquad (13)$$

To simplify the notation, the following dimensionless substitutions may be introduced:

$$\beta(X) = \frac{E'(x)}{E \sin \theta/2} \qquad (14)$$

$$\beta(Y) = \frac{E'(y)}{E \sin \theta/2}$$

where $X = x/L$

$Y = y/L$

$$\gamma = \frac{\rho_d \sin^2 \theta}{2} \tag{15}$$

Using the above substitutions as well as Eq. (13), integral equation (12) can be rewritten in the following form:

$$\beta(X) = 1 + \gamma \int_0^1 \beta(Y) \frac{X\,Y}{(X^2 + Y^2 - 2\,X\,Y \cos\theta)^{3/2}}\, dY \tag{16}$$

Eq. (11) can also be rewritten as

$$\alpha_a = \alpha \frac{E\,2\,L \sin\theta/2 \int_0^1 \beta(X)\, dX}{E\,w} .$$

Since $w = 2\,L \sin\theta/2$, (17)

as may be seen by inspection of Fig. 1, it follows that

$$\alpha_a = \alpha \int_0^1 \beta(X)\, dX . \tag{18}$$

Inspection of Eq. (18) (in contrast to Eq. (11)) reveals that the functional dependence of α_a has been

reduced to

$$\alpha_a = f(\alpha, \beta(X)) = f(\alpha, \rho_d, \theta) .$$

Again, the calculation of α_a from Eq. (18) requires only a solution for the dimensionless function $\beta(X)$, provided that the material properties α and ρ_d are known.

Integral equation (16) in its dimensionless form with the symmetric kernel

$$K(X, Y) = \frac{X\,Y}{(X^2 + Y^2 - 2\,X\,Y\cos\theta)^{3/2}}$$

has received considerable attention in the literature. This is because it represents a standard integral equation of the second Fredholm type, whose solution can be obtained by various approximate methods. A numerical approximation using an iterative process, which is specifically applicable to the present problem, has been performed by Sparrow et al. [23, 24] (cf. p. 9/10). Engineering calculations, however, would be greatly facilitated by a simple--but exact--mathematical solution which, unfortunately, does not appear possible.

To by-pass this problem, a different mathematical approach will be presented in the following sections leading to a straightforward closed form solution. This solution is based on the superposition of two boundary solutions, which are obtained for two singular points of integral equation (16).

2.2.1.2 Boundary Behaviour. Integral equation (16) can be rewritten by means of the substitutions

$$Y = \frac{X}{\xi}$$

$$dY = -\frac{X}{\xi^2}\, d\xi$$

as follows:

$$\beta(X) = 1 - \gamma \int_{\infty}^{X} \beta\left(\frac{X}{\xi}\right) \frac{1}{(\xi^2 + 1 - 2\,\xi \cos\theta)^{3/2}}\, d\xi \qquad (19)$$

A singular point of this integral equation is the irradiance at the vertex of the cavity, which can be obtained by setting $x/L = X = 0$ (cf. Fig. 1):

$$\beta(0) = 1 - \gamma\, \beta(0) \int_{\infty}^{0} \frac{1}{(\xi^2 + 1 - 2\,\xi \cos\theta)^{3/2}}\, d\xi \qquad (20)$$

A direct evaluation of the integral in (20) and solving for $\beta(0)$, as carried out in App. C-2, is now possible and results in

$$\beta(0) = \frac{1}{1 - \rho_d/2\,(1 + \cos\theta)}\,. \qquad (21)$$

A second singular point exists with regard to the irradiance, $\beta(x = L)$, at the upper rim of a cavity side. A solution for $\beta(x = L)$ may be obtained by making use of the additional substitution $X = \xi$ in integral equation

(19) leading to

$$\beta(\xi) = 1 - \gamma\,\beta(1) \int_{\infty}^{\xi} \frac{1}{(\xi^2 + 1 - 2\,\xi \cos\theta)^{3/2}}\, d\xi \,. \qquad (22)$$

Evaluation of the integral in (22) and solving for $\beta(1)$ if $\xi = 1$, as carried out in App. C-3, results in

$$\beta(1) = \frac{1}{1 - \rho_d/2\,(1 - \sin\theta/2)} \,. \qquad (23)$$

With these singular-point-solutions (21) and (23), the local apparent absorptance of a V-groove cavity at its boundaries can be obtained by inserting (21) and (23) respectively into Eq. (18):

$$\alpha_{a,x=0} = \frac{\alpha}{1 - \rho_d/2\,(1 + \cos\theta)} \qquad (24)$$

$$\alpha_{a,x=L} = \frac{\alpha}{1 - \rho_d/2\,(1 - \sin\theta/2)} \qquad (25)$$

An estimate for the validity of Eqs. (24) and (25) can be made by considering an infinitely small cavity ($\theta = 0^o$), which, theoretically, approximates a black body. Solving the above equations for $\theta = 0^o$ and $\alpha = 1$ yields

$$\alpha_{a,x=0} = \alpha_{a,x=L} = 1 \,,$$

as is to be expected. On the other hand, solving Eqs. (24) and (25) for $\theta = 180^o$, i.e., for a flat plate,

yields

$$\alpha_{a,x=0} = \alpha_{a,x=L} = \alpha \ ,$$

also as expected.

It will be shown in the following section that from the foregoing solutions referring to the cavity boundaries, a combined solution for the entire cavity can be deduced by superposition.

2.2.1.3 Superposition of Boundary Solutions.

Equations (24) and (25) can be written alternatively by making use of the fact that $\alpha = 1 - \rho$:

$$\alpha_{a,x=0} = \frac{2\alpha}{2 - (1 - \alpha)(1 + \cos\theta)} \qquad (26)$$

$$\alpha_{a,x=L} = \frac{2\alpha}{2 - (1 - \alpha)(1 - \sin\theta/2)} \qquad (27)$$

A graph for these two equations is plotted in Fig. 2 assuming a surface absorptance of $\alpha = 0{,}5$ (see curves A and B). Fig. 2 shows clearly a general increase of the apparent absorptance with decreasing groove angle, the so-called "cavity effect". Curves A and B demonstrate that this cavity effect is much greater at the vertex (where α_a approaches unity with respect to curve A) than it is at the opening of the cavity.

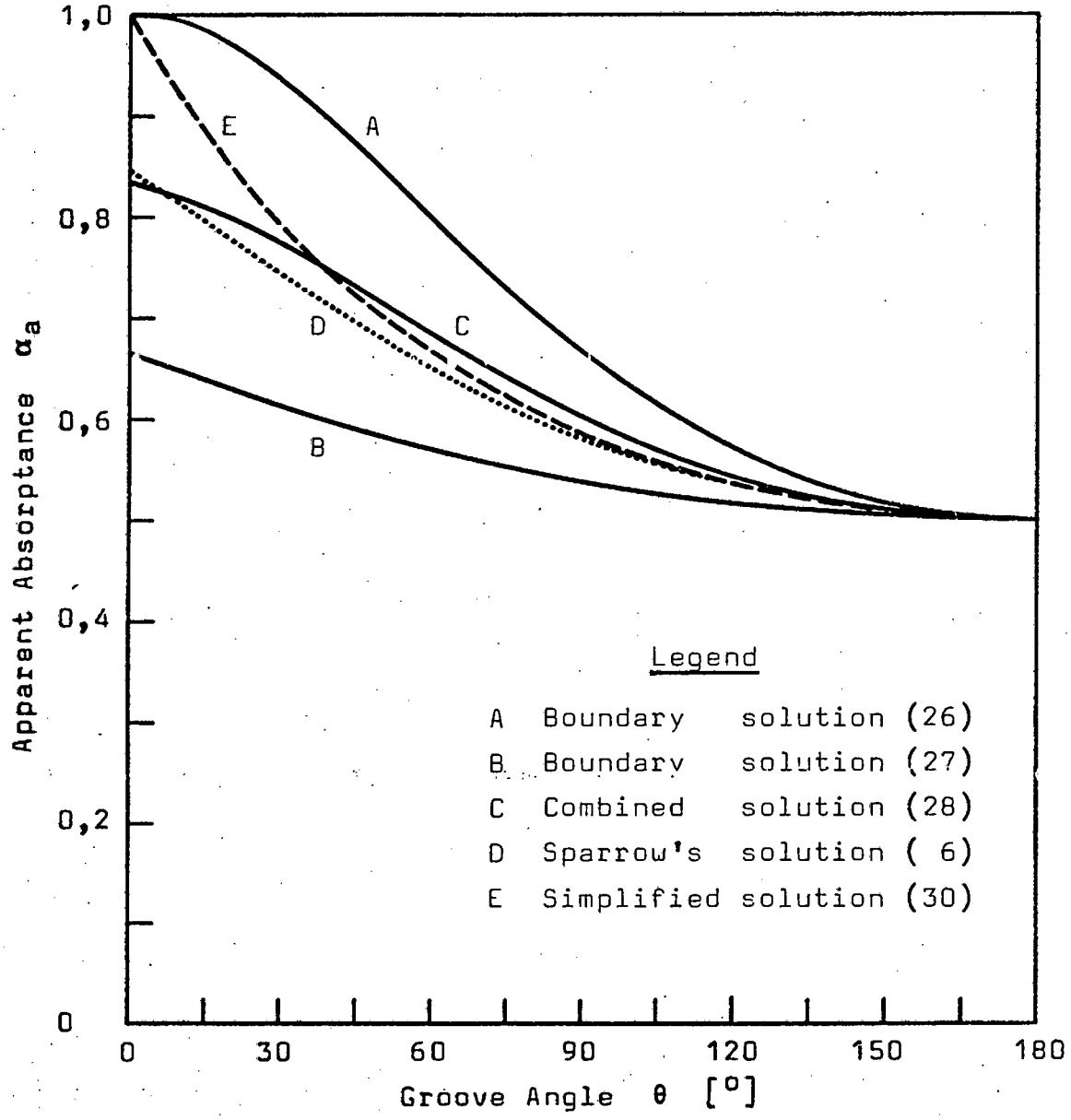

Figure 2. Effect of groove angle on the apparent absorptance of a V-groove cavity having a surface absorptance of $\alpha = 0,5$.

It is noteworthy that even a highly simplified modification of the problem leads to a useful solution, which is represented by curve E in Fig. 2 and plotted in full in Fig. 4. This solution has been obtained as follows:

Assuming that the local irradiance is constant over the sides of the cavity, i.e.,

$$E'(x) = E'(y) = \text{constant},$$

integral equation (12) can be reduced to

$$E'(x) = E \sin\theta/2 + \rho_d E'(x)(1 - \sin\theta/2). \qquad (29)$$

The term $(1 - \sin\theta/2)$ represents the configuration factor for diffuse radiation interchange within an infinitely long V-groove cavity and is given in full details in [40]. Solving Eq. (29) for $E'(x)$ and using (11) and (17) leads to

$$\alpha_a = \frac{\alpha}{1 - (1 - \alpha)(1 - \sin\theta/2)}. \qquad (30)$$

With reference to Fig. 2 (see curve E), it is obvious that Eq. (30) provides a useful formula valid for groove angles in the range of $30^o < \theta < 180^o$. The following Section 2.2.2 and some experimental results will show that Eq. (30) is also a good approximation, as far as groove angles $\theta < 30^o$ and real surfaces with specular components are concerned.

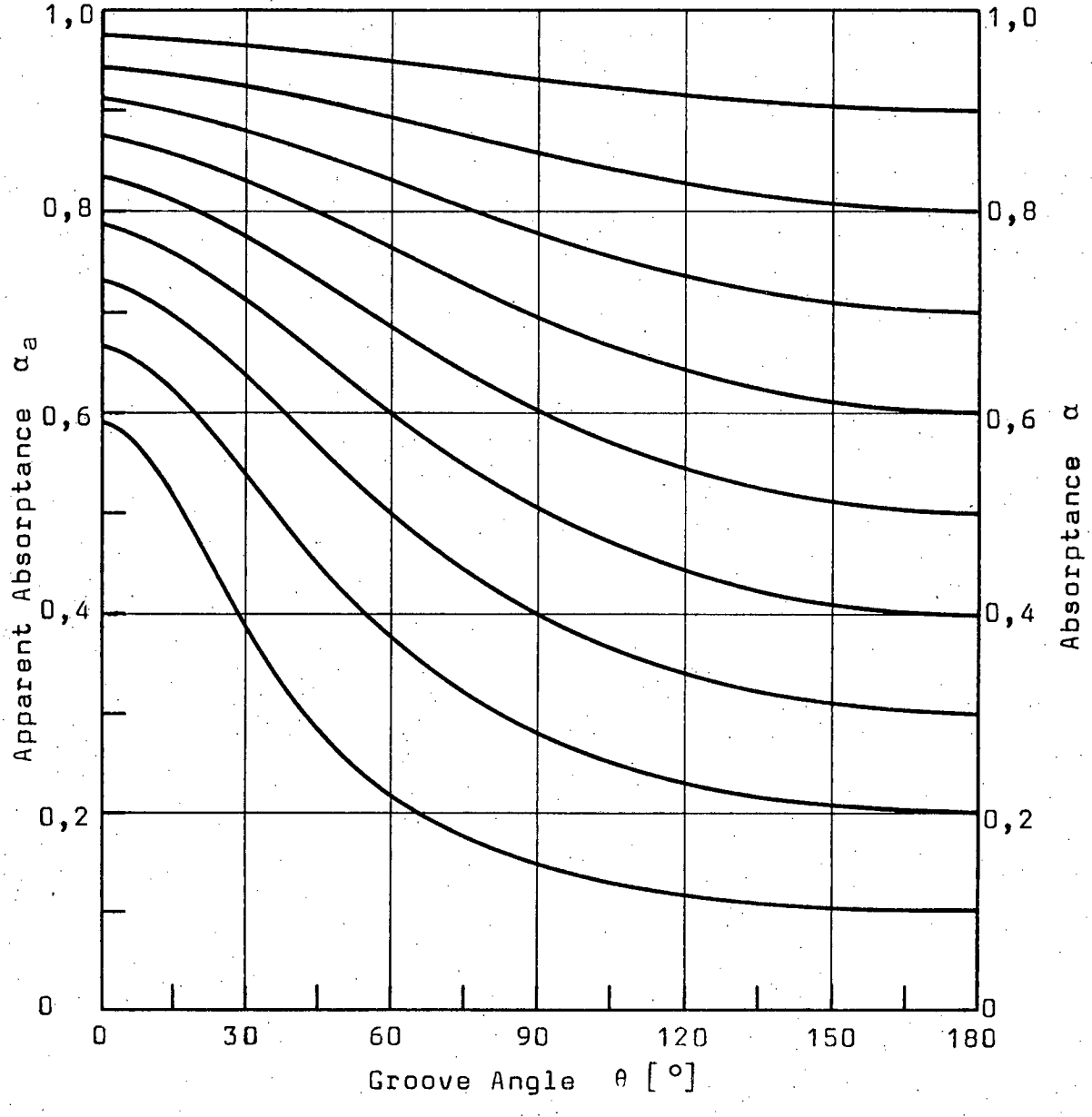

Figure 3. Apparent absorptance of diffuse V-groove cavities as defined by Eq. (28).

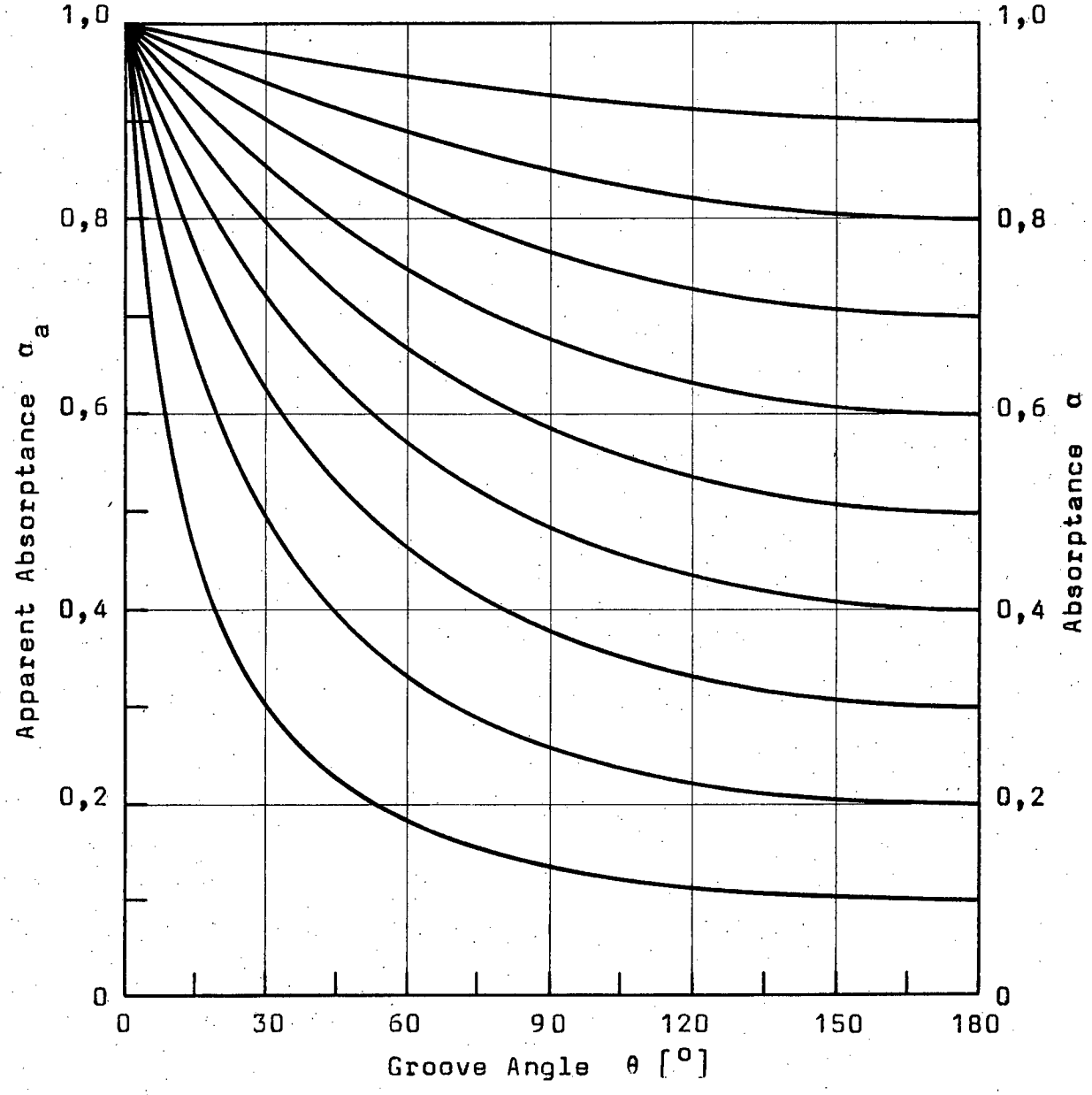

Figure 4. Apparent absorptance of diffuse V-groove cavities as defined by Eq. (30).

2.2.2 Apparent Absorptance of Specular Cavities

2.2.2.1 Basic Reflection Pattern. The surfaces under consideration in this section are mirrorlike or specular, i.e., an unidirectional beam of radiation striking a specular cavity wall is assumed to be partly absorbed and partly reflected according to the well-known laws of reflection. With reference to Fig. 5 , it may be seen that a beam of radiation, E, entering a V-groove cavity with an opening angle of, say, $\theta = 45^{o}$ suffers four reflections. After each reflection, the

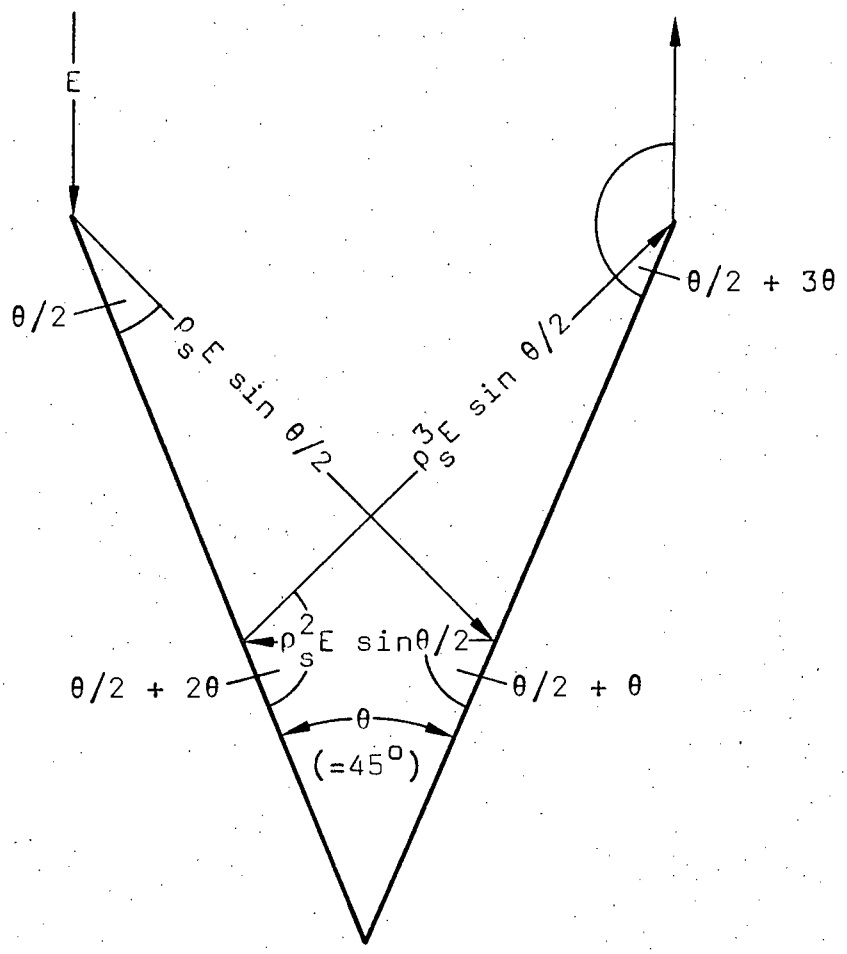

Figure 5. Reflections in a specular V-groove cavity.

original power, $E \sin \theta/2$, is reduced to $\rho_s^i E \sin \theta/2$ if i denotes the number of reflections up to this point. The fraction $\alpha \rho_s^i E \sin \theta/2$ is absorbed at each surface contact. Hence it appears that the apparent absorptance of a specular cavity is governed by a multiple reflection pattern, so that

$$\alpha_a = f(\alpha, \rho_s, i, \theta) .$$

Furthermore, it may be seen from Fig. 5 that the reflection angle, δ, after i reflections is

$$\delta_i = \theta/2 + (i - 1)\,\theta = (i - 1/2)\,\theta .$$

A necessary condition for the last reflection to take place is

$$(i - 1/2)\,\theta < 180^o .$$

Hence, the total number of possible reflections is given by the following expression:

$$i \text{ (integer)} < 180^o/\theta + 1/2 \qquad (31)$$

With this basic information, a fromulation of the apparent absorptance can be carried out as follows:

2.2.2.2 Absorptance as Stepfunction. Adopting the definitions given in Section 2.2.1.1 , the apparent absorptance of a specular cavity can be expressed identically to Eq. (11) :

$$\alpha_a = \alpha \frac{2 \int_0^L E'(x)\, dx}{E\, w}$$

Since the local irradiance, $E'(x)$, can be considered to be composed of two distinct functions E_1' and E_2' which are valid for and constant over the intervals $0 < x_1 < L'$ and $L' < x_2 < L$ respectively, Eq. (11) can be reduced to

$$\alpha_a = \alpha \frac{2\, L\, (E_1' + E_2')}{E\, w} \,. \tag{32}$$

Referring to Fig. 6, E_1' denotes the irradiance on the fraction L'/L of a cavity side for which all incident beams of radiation suffer i reflections, whereas E_2' denotes the irradiance on the fraction $(L - L')/L$ of a cavity side for which all incident rays suffer $i - 1$ reflections. Using these informations, it can be shown (cf. Figs. 5 and 6) that

$$E_1' = (E \sin \theta/2 + \rho_s E \sin \theta/2 + \rho_s^2 E \sin \theta/2 + \ldots + \rho_s^{i-1} E \sin \theta/2) \frac{L'}{L} \tag{33}$$

and

$$E_2' = (E \sin \theta/2 + \rho_s E \sin \theta/2 + \rho_s^2 E \sin \theta/2 + \ldots + \rho_s^{i-2} E \sin \theta/2) \frac{L - L'}{L} \,. \tag{34}$$

Inserting the sum of the above equations, $E_1' + E_2'$, into

Eq. (32) after rearrangements, as carried out in App. C-4, yields

$$\alpha_a = 1 - (1 - \alpha)^{i-1} \left(1 - \alpha \frac{L'}{L}\right) . \qquad (35)$$

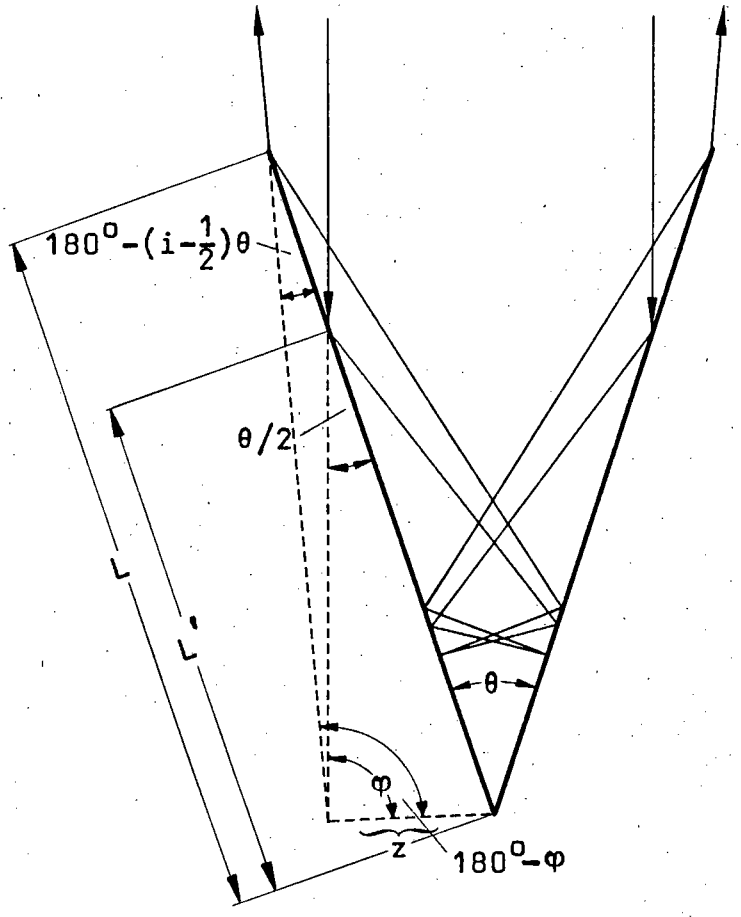

Figure 6. Mirror image of reflection in a specular V-groove cavity.

The term L'/L in Eq. (35) can be evaluated with reference to Fig. 6. By applying the law of sines to the mirror image triangles, which are formed by both an incident and outgoing ray, it can be shown that the following proportions hold true:

$$\frac{z}{\sin\left(180 - (i - 1/2)\,\theta\right)} = \frac{L}{\sin\left(180 - \varphi\right)}$$

$$\frac{z}{\sin \theta/2} = \frac{L'}{\sin\varphi}$$

Solving for z leads to

$$\frac{L'}{L} = \frac{\sin\left(i - 1/2\right)\theta}{\sin \theta/2} = k \ .$$

Since it is obviously necessary that $L'/L \leq 1$, the factor k is to be evaluated as follows:

$$k = \begin{cases} \dfrac{\sin\left(i - 1/2\right)\theta}{\sin \theta/2} & \text{if} < 1 \\ 1 \quad \text{otherwise} \end{cases} \tag{36}$$

Hence it follows:

$$\alpha_a = 1 - (1 - \alpha)^{i-1}\,(1 - k\alpha) \tag{37}$$

This is the final expression for the apparent absorptance of a V-groove cavity with specularly reflecting sides subject to the assumptions made at the beginning of this chapter. With respect to the restrictions given by Eqs. (31) and (36), Eq. (37) is plotted in Fig. 7 for various surface absorptances. The stepfunctional character of α_a will be discussed in the following section. For comparison purposes, Figs. 3, 4 and 7 are replotted on transparencies in App. B .

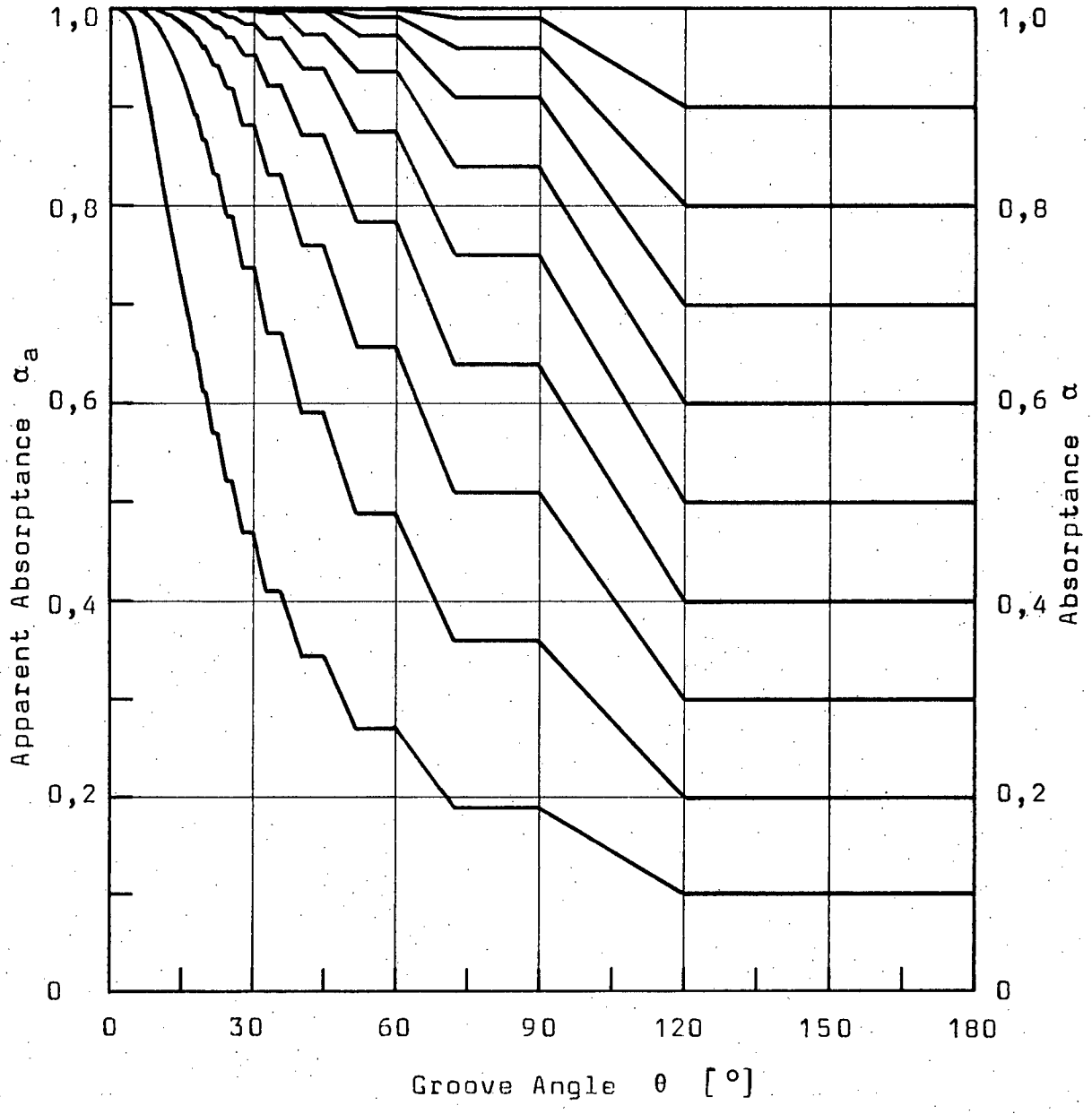

Figure 7. Apparent absorptance of specular V-groove cavities as defined by Eq. (37).

2.2.2.3 Discussion. The characteristic of Eq. (37) is illustrated in Fig. 8 with regard to two intervals for θ ; $[60^{o}<\theta<72^{o}]$ and $[72^{o}\leq\theta\leq90^{o}]$. For some groove angles within these intervals, reflection patterns have been drawn:

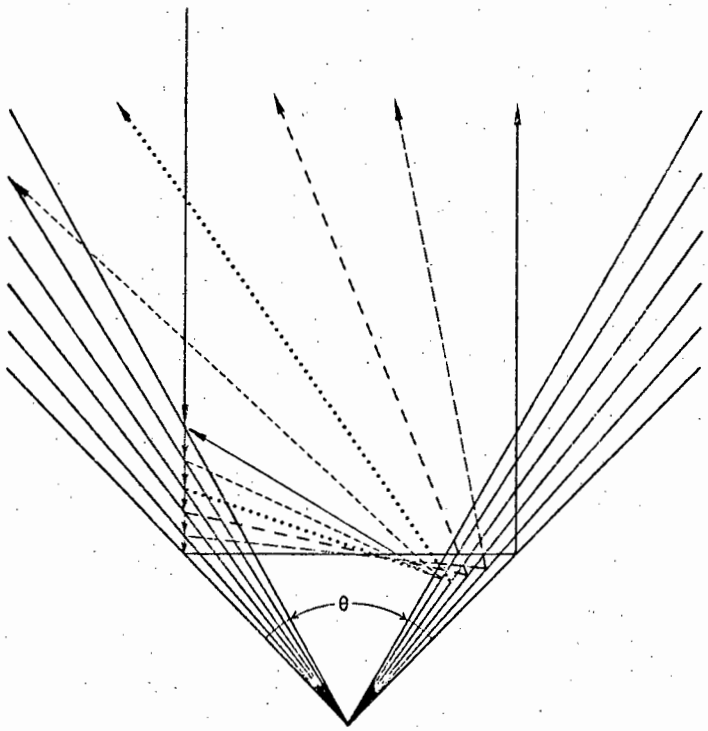

Figure 8. Reflection patterns in specular cavities with groove angles of $\theta = 60^{o}, 66^{o}, 72^{o}, 78^{o}, 84^{o}, 90^{o}$.

Inspection of Fig. 8 shows that parallel rays with normal incidence on a specular V-groove cavity with an opening angle of $60^{o}<\theta<72^{o}$ are reflected two or three times depending on the region of incidence. In short:

$$\alpha_{a,\alpha=\text{const.}} = f(i, \theta)$$

For groove angles of $72^{o}\leq\theta\leq90^{o}$, the same rays are

reflected twice, and only twice, independently of their location of incidence, i.e.,

$$\alpha_{a,\alpha=\text{const.}} = \text{constant} .$$

Hence it appears that for a wide range of selected groove angles, as for instance $\theta = 120^{o}, 90^{o}, 60^{o}, 45^{o}, 30^{o}, 15^{o}$, α_a can be calculated by using the simplified form of Eq. (37) which is

$$\alpha_a = 1 - (1 - \alpha)^i . \qquad (38)$$

Eq. (38) holds only as long as (cf. (36))

$$\sin (i - 1/2)\,\theta \geq \sin \theta/2$$

and is identical to those widely used in literature (cf. Eqs. (1) and (3)).

2.3 ABSORPTION BY V-GROOVED SURFACES

2.3.1 Effective Absorptance

Although it is tacitly assumed in Figs. 3, 4 and 7, it is obvious that the underlying equations can not hold for a groove angle of $\theta = 0^{o}$; such a groove does not exist. Therefore, the absorptance of a surface being composed of V-grooves can not increase to unity with groove angles decreasing to 0^{o}. What is more, a variety of experiments, of which a selection will be presented in

Chapter 4, has shown that the absorptance of a V-grooved surface does not agree with theoretical values calculated from Eqs. (28), (30) or (37). It was found that this was particularly true for small grooves and due to the finite lands which appear between them (cf. App. F). These unavoidable lands, whose percentage of the total projected surface area increases with decreasing groove angle, affect the overall absorption characteristic and must be taken into account.

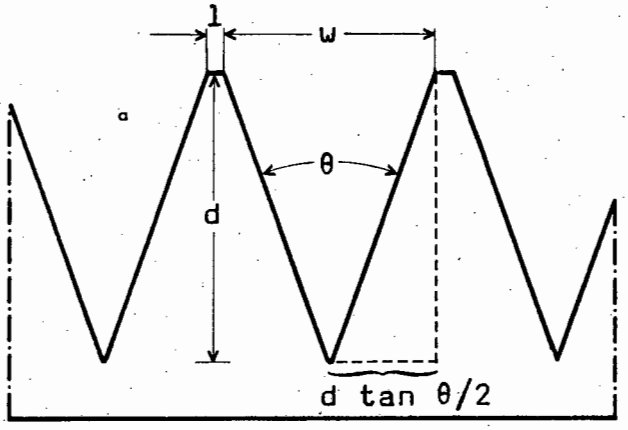

Figure 9. Cross section of a V-grooved surface.

The presence of lands is illustrated in Fig. 9, which shows that the absorptance of a V-grooved surface is composed of both the apparent absorptance, α_a, of groove openings, w, and the absorptance, α, of lands l. Allowance for this may be made by defining an effective absorptance, so that

$$\alpha_{eff} = \alpha_a \frac{w}{l + w} + \alpha \frac{l}{l + w} \quad . \tag{39}$$

It is convenient to express w in terms of groove depth, d, and groove angle θ, parameters which represent manufacturing data. Hence, with $w = 2\,d \tan \theta/2$ (see Fig. 9), Eq. (39) can be rewritten and rearranged, so that finally

$$\alpha_{eff} = \frac{\alpha_a \, 2\frac{d}{l} \tan\frac{\theta}{2} + \alpha}{1 + 2\frac{d}{l}\tan\frac{\theta}{2}} \quad . \tag{40}$$

This is a general expression for the effective absorptance of a V-grooved surface and may be applied to the preceding results as shown in the following sections.

2.3.2 Optimization of Parameters

Equation (40) is plotted in Fig. 10 assuming diffuse surface properties as well as three given values for α and two different values for d/l respectively. Inspection of the six resulting curves reveals that their peaks shift towards smaller groove angles with decreasing α and increasing d/l. It can be shown that this trend is also true for specularly reflecting surfaces. Indeed, in order to achieve a high effective absorptance of a V-grooved surface having a given surface absorptance, α, a small groove angle is required, and very little land should be left between grooves (high d/l ratio). This leads to an optimization problem for α_{eff} since θ, α_a and d/l are interdependent quantities.

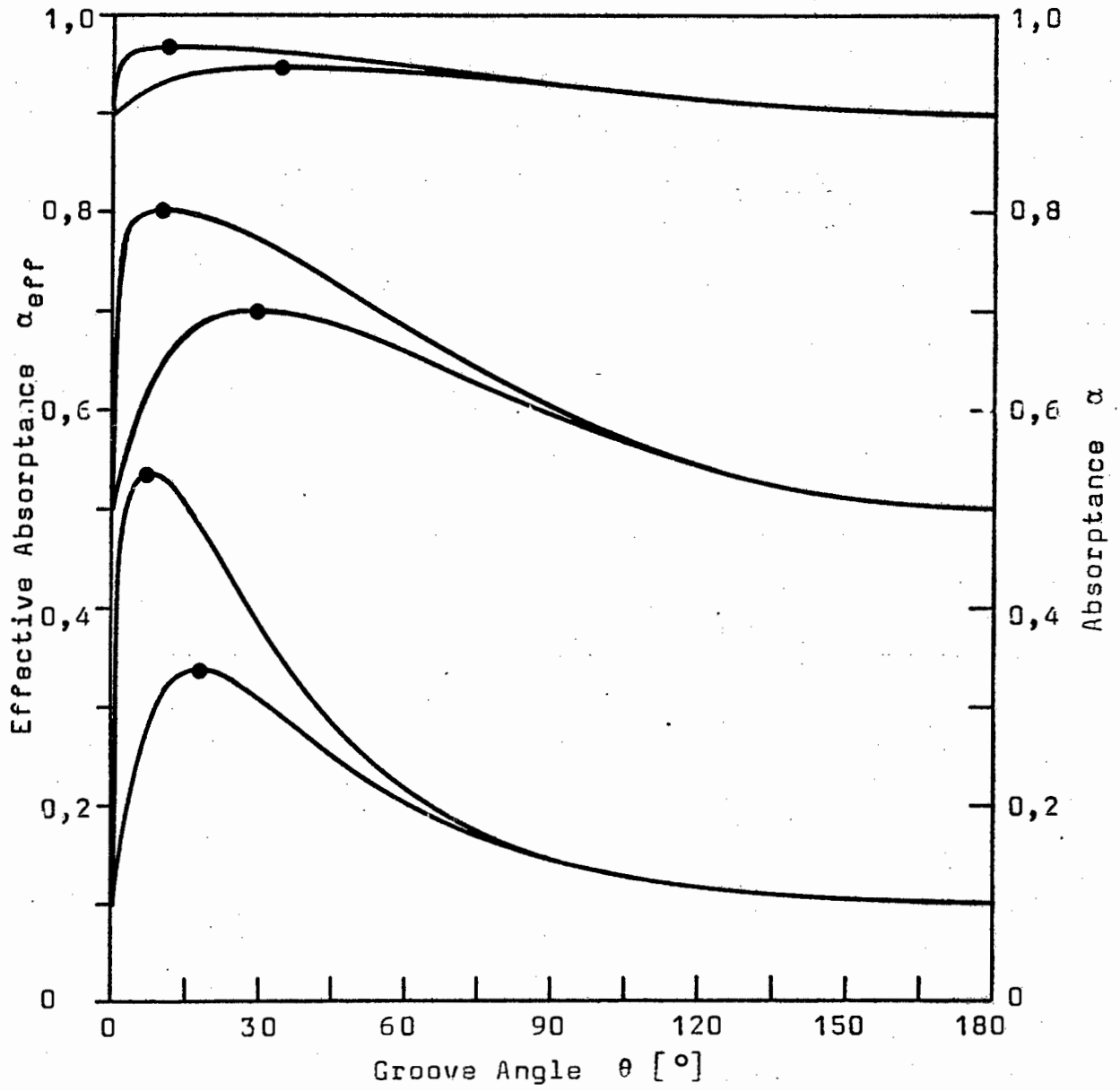

Figure 10. Effective absorptance of diffuse V-grooved surfaces; plotted for 3 values of α and d/l = 100 (upper curves) and d/l = 5 (lower curves).

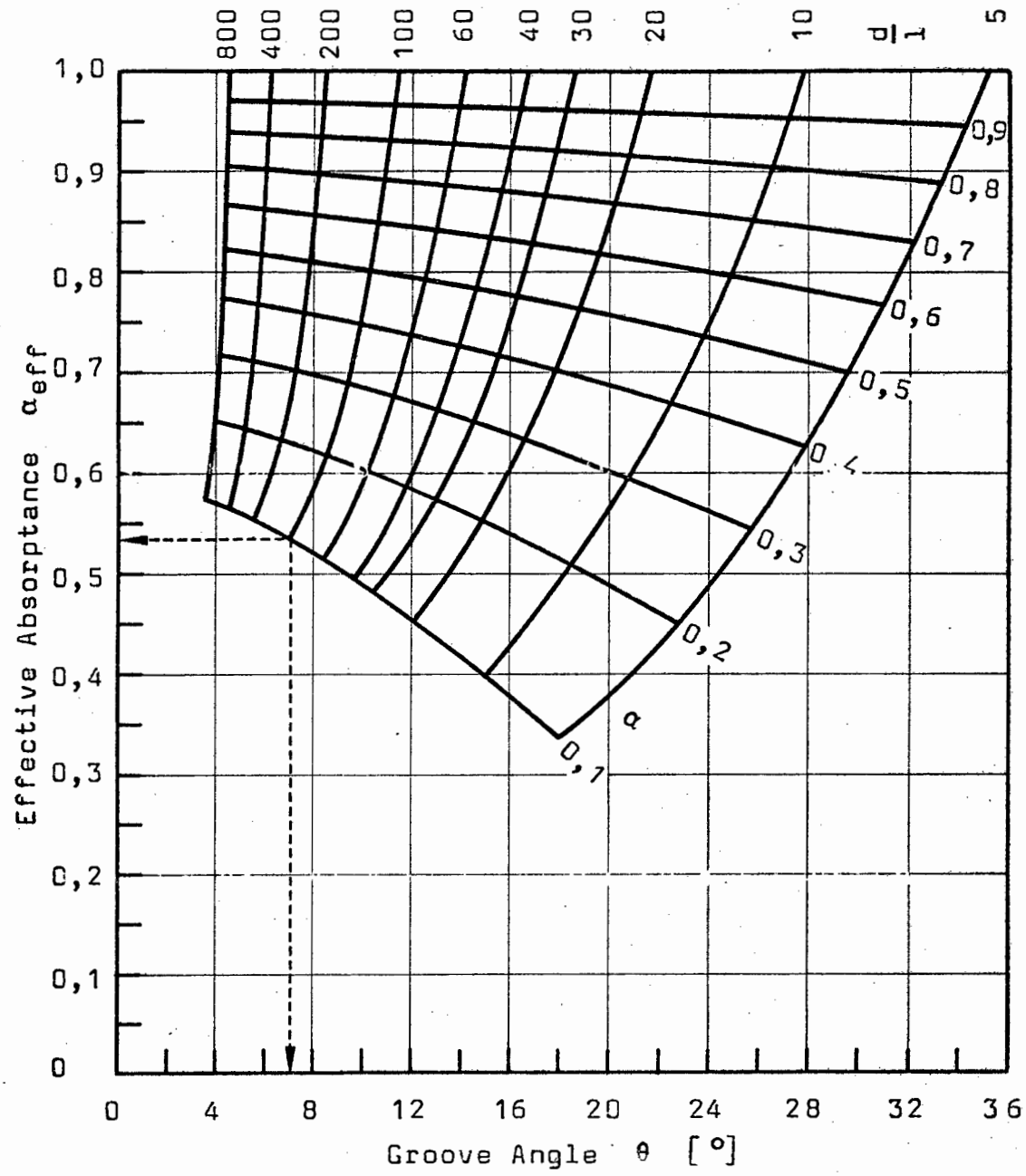

Figure 11. Nomograph for optimization of diffuse V-grooved surfaces. (Example: $\alpha = 0{,}1$ and $d/l = 100$ yield $\theta_{opt.} = 7^{\circ}$ and $\alpha_{eff} = 0{,}53$)

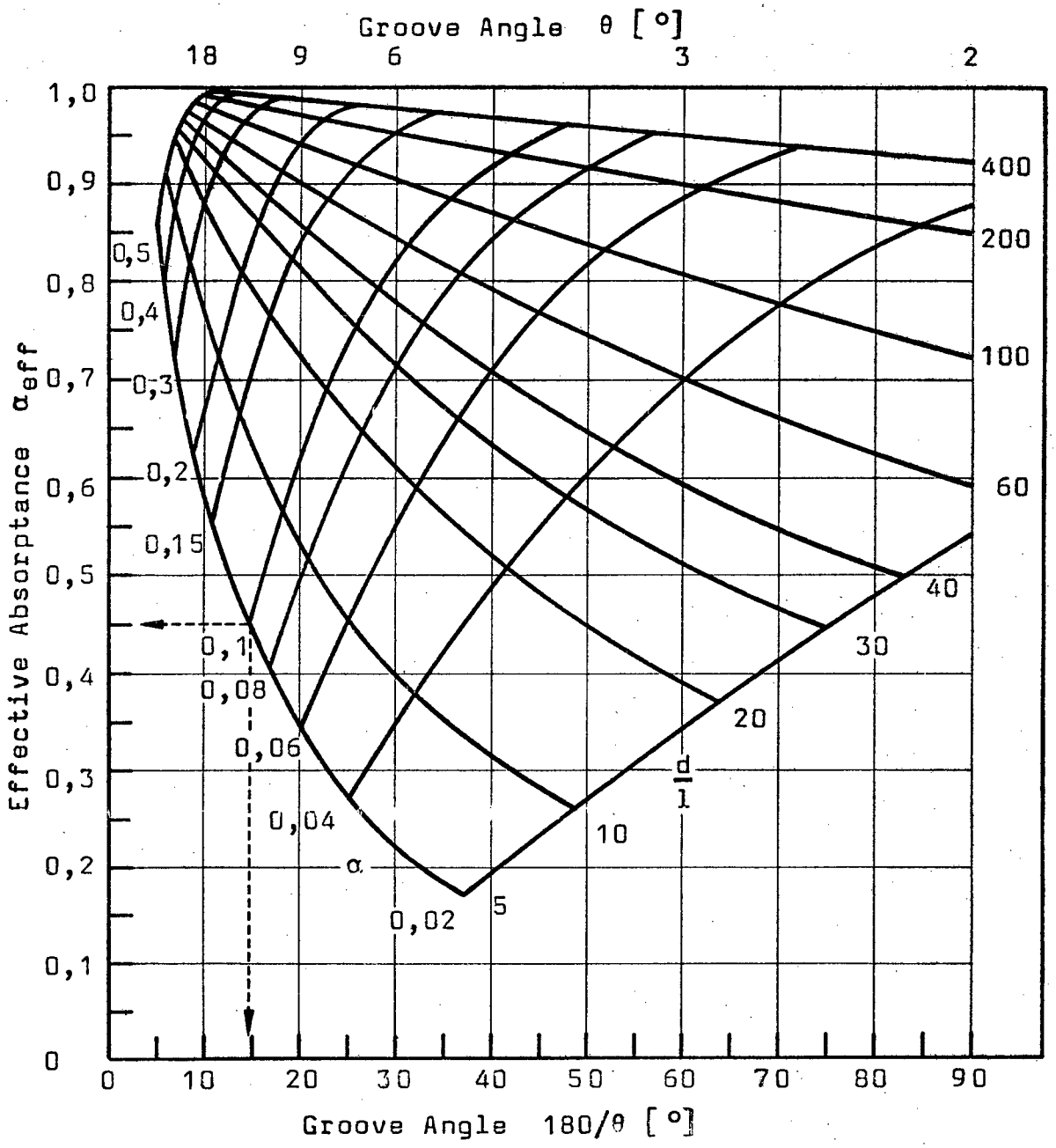

Figure 12. Nomograph for optimization of specular V-grooved surfaces. (Example: $\alpha = 0,1$, $d/l = 5$ yield $\theta_{optimum} = 12^{o}$ and $\alpha_{eff} = 0,45$)

The optimization of α_{eff} may be facilitated by using the nomographs in Figs. 11 and 12. These nomographs are a graphic representation of Eq. (40) being optimized for reasonable intervals of the variables α, d/l and θ. In other words, the grid intersections represent the peaks of the pertinent curves, of which six are plotted in Fig. 10. Consequently, Figs. 11 and 12 provide a means to determine the optimal groove angle for the highest possible effective absorptance of diffuse or specular V-grooved surfaces, subject to a given surface absorptance, α, and d/l - ratio.

2.4 SUMMARY

It has been shown that the effective absorptance of V-grooved surfaces is basically governed by the formula

(40): $$\alpha_{eff} = \frac{\alpha_a \, 2\frac{d}{l} \tan\theta/2 + \alpha}{1 + 2\frac{d}{l}\tan\theta/2} \quad .$$

The main variable α_a depends on α and θ and is also a function of the reflective properties of the surface material. In summary, α_a is given as follows:

1. If all parts of the surface reflect diffusely:

(28): $$\alpha_a = \alpha \left(\frac{1}{2 - (1-\alpha)(1+\cos\theta)} + \frac{1}{2 - (1-\alpha)(1-\sin\theta/2)} \right)$$

2. If all parts of the surface reflect specularly:

(37): $$\alpha_a = 1 - (1 - \alpha)^{i-1} (1 - k\alpha)$$

The parameters i and k are given by Eqs. (31) and (36) respectively.

3. If the reflectance of the surface comprises both diffuse and specular components, α_a may be evaluated by means of a suitable interpolation between the above formulae.

4. For certain groove angles and surface absorptances, α, a useful approximation is given by Eq. (30):

(30): $$\alpha_a = \frac{\alpha}{1 - (1 - \alpha)(1 - \sin \theta/2)}$$

The latter may be seen in App. B, where Eqs. (28), (30) and (37) have been replotted on transparencies for comparison purposes.

CHAPTER 3

EXPERIMENTAL INVESTIGATION

3.1 INTRODUCTION

The purpose of the experimental investigation is two-fold: Firstly, it serves both to verify the formulae derived in the preceding analysis and to determine their practical applicability. Secondly, the experimental results are meant to provide more information about the practical behaviour and properties of real V-grooved surfaces used for solar energy collection. The lack of such information in literature has been shown in Chapter 1 .

Experiments were carried out on five sets of different test specimens, which had been V-grooved according to specifications described in Section 3.2 . The specimens were exposed to simulated solar radiation to determine (1) their effective absorptance and (2) their absorption efficiency.

Since sunlight is subject to large fluctuations (on an hourly and daily basis), the sun is an unsuitable source of radiation for test purposes. It was therefore necessary to build a solar simulator incorporated in a calorimetric test apparatus. Details of this experimental apparatus will be described in Section 3.3 .

Finally, the determination of the absorption properties of a specimen required the use of a calorimetric test method. The mathematical background of this method and the experimental procedure will be explained in the last sections of this chapter.

3.2 DESCRIPTION OF SPECIMENS

The derivation of Eq. (40) has shown that the effective absorptance of a V-grooved surface is influenced by three geometric parameters; the groove angle θ, the groove depth d , and the width of land l between grooves. Accordingly, V-grooves with various angles, depths and lands were milled into circular brass discs. A photograph showing a selection of these discs is given in Fig. 14 , while their basic cross section is illustrated in Fig. 13 :

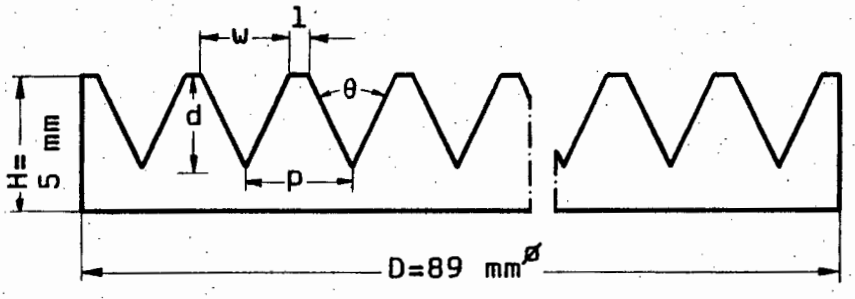

Figure 13. Cross section of specimens.

The specifications for each specimen are tabulated in App. E . Additionally, microscope photographs showing the

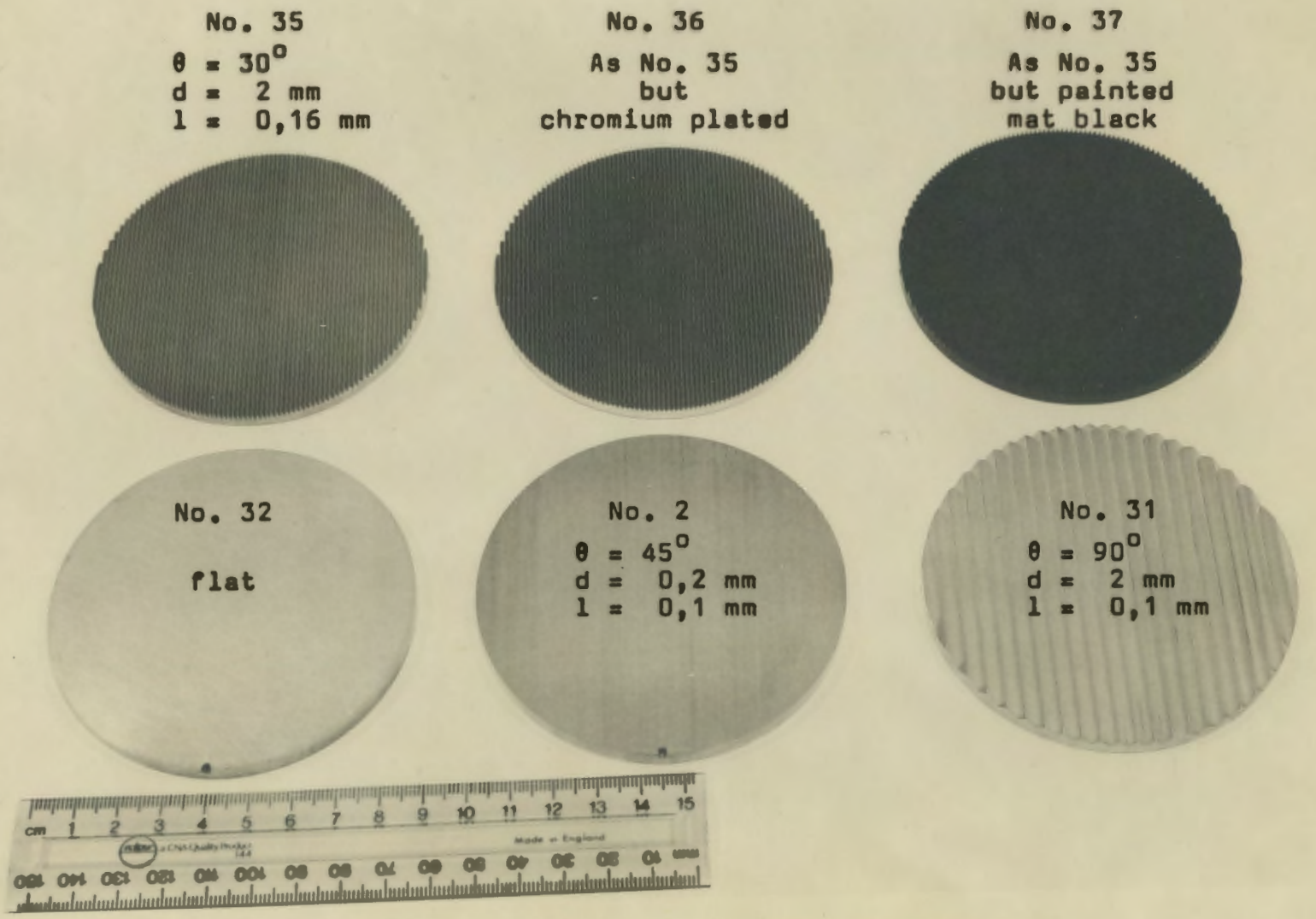

Figure 14. Selection of some specimens.

enlarged cross sections of two sets of specimens are given in App. F .

The circular discs were cut from a 3 1/2 " brass bar. Though brass is not the best material for solar energy collection, it was chosen because of its availability and its desirable properties, such as easy machinability, non-corrodibility, and high thermal conductivity. Furthermore, the milled brass surface guaranteed a fairly constant and moderate absorptance as well as a low emittance.

It can be seen from App. E that five different sets of specimens were manufactured. Without entering into the particulars of the design (which will be explained in Chapter 4), some specific features should be noted.

The first two sets of specimens (No. 1 - 8 and No. 9 - 16) were grooved with a constant angle and with increasing groove depth, whereas specimens No. 17 - 23 and No. 24 - 31 were manufactured with grooves having a constant depth but increasing groove angles. These specimens were designed as to verify the formulae derived in Chapter 2 .

The groove parameters of the fifth set of specimens (No. 32 - 37) were chosen to investigate the effect of different surface absorptances. For this purpose, a black spray paint and a chromium plating were applied.

3.3 DESCRIPTION OF APPARATUS

3.3.1 Solar Simulator

In order to obtain acceptable radiation characteristics, the simulated sunlight had to comply with the following requirements based on ASTM-classifications for solar simulators [41]:

1. Spectral energy distribution as shown in App. D
2. Flux density of approximately 1353 W/m^2 (solar constant)
3. Uniformity of irradiance < 5 %
4. Stability of irradiance < 3 %
5. Beam divergence angle < 4 %

These requirements were met by using a metal halide short arc lamp (OSRAM HMI 575 W) in connection with a system of aluminium-front-coated reflectors. A photograph of the arc lamp and reflector assembly is shown in Fig. 15.

The specially designed mirror system consists of both a spherical and a slightly diffuse parabolic reflector, which produce a parallel and uniform beam of simulated sunlight. In addition, a set of aperture plates and a plane mirror were used to direct the light beam onto a test specimen mounted in a calorimetric specimen holder. All mirrors were front-coated in order to avoid spectral attenuation of the light by transmission through

glass. A photograph showing a general view of this experimental arrangement is given in Fig. 16 . Enlarged partial views are shown in Figs. 17 and 18 .

The spectral energy distribution of the lamp is plotted in App. D showing the desired similarity to solar radiation. In particular, the main three spectral bands correspond very well, as far as radiation quantities are concerned [42, 43] :

	Percentage of Lamp Radiant Energy	Solar Constant
UV-radiation ($\lambda < 0{,}38\,\mu m$)	11,3 %	7 %
Visible light ($0{,}38 < \lambda < 0{,}76\,\mu m$)	45,4 %	45,6 %
IR-radiation ($\lambda > 0{,}76$)	43,3 %	47,4 %

3.3.2 Calorimetric Test Section

The schematic diagram of the experimental apparatus given in Fig. 19 illustrates the functional details of the calorimetric test section. The latter is composed of the following equipment:

1. Storage tank containing the heat transfer medium (ethylene glycol)
2. Float operated constant head device
3. Needle-valve and rotameter for flow control

Figure 15. Arc lamp and reflector assembly.

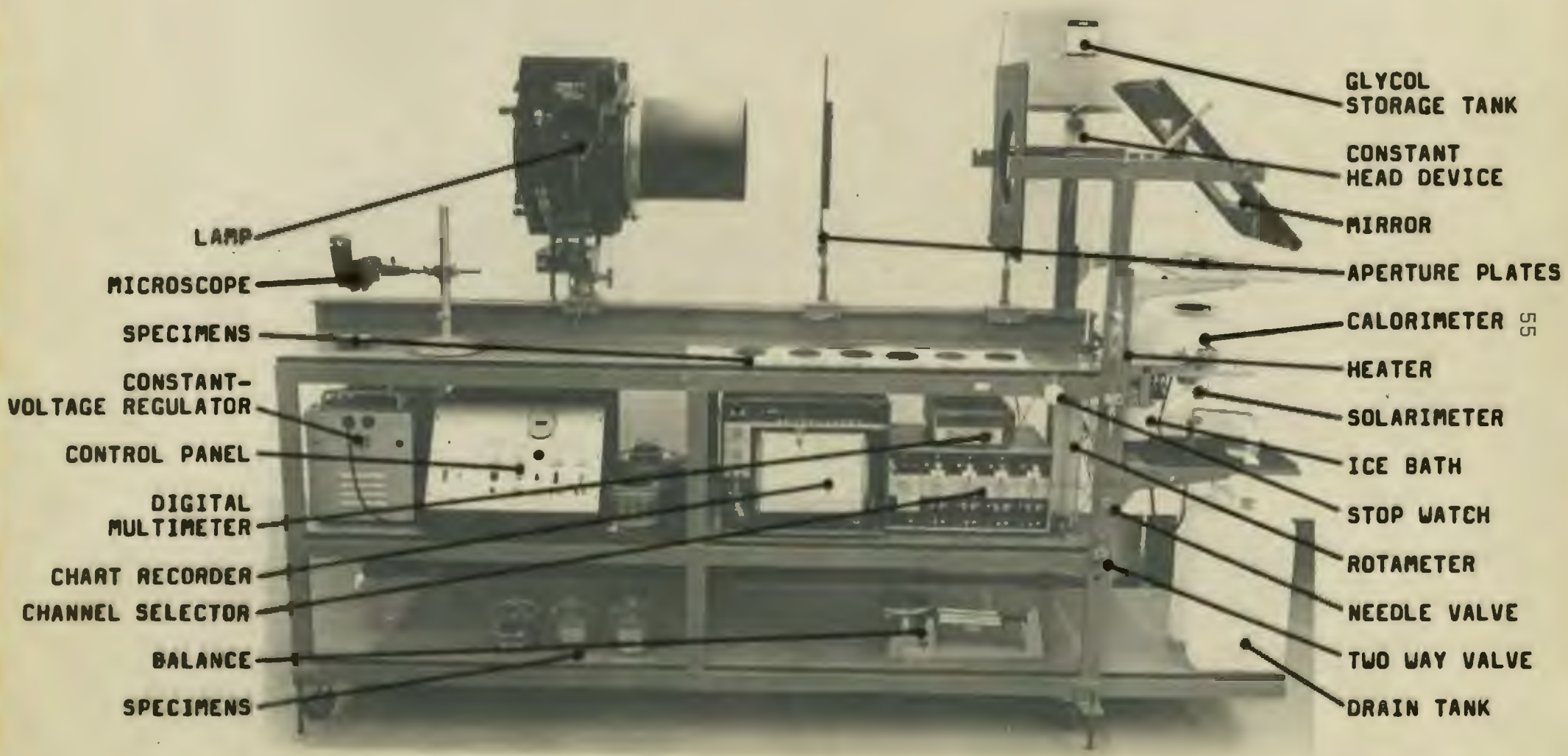

Figure 16. Experimental apparatus.

Figure 17. Partial view of apparatus, calorimetric test section.

Figure 18. View along optical axis on a specimen.

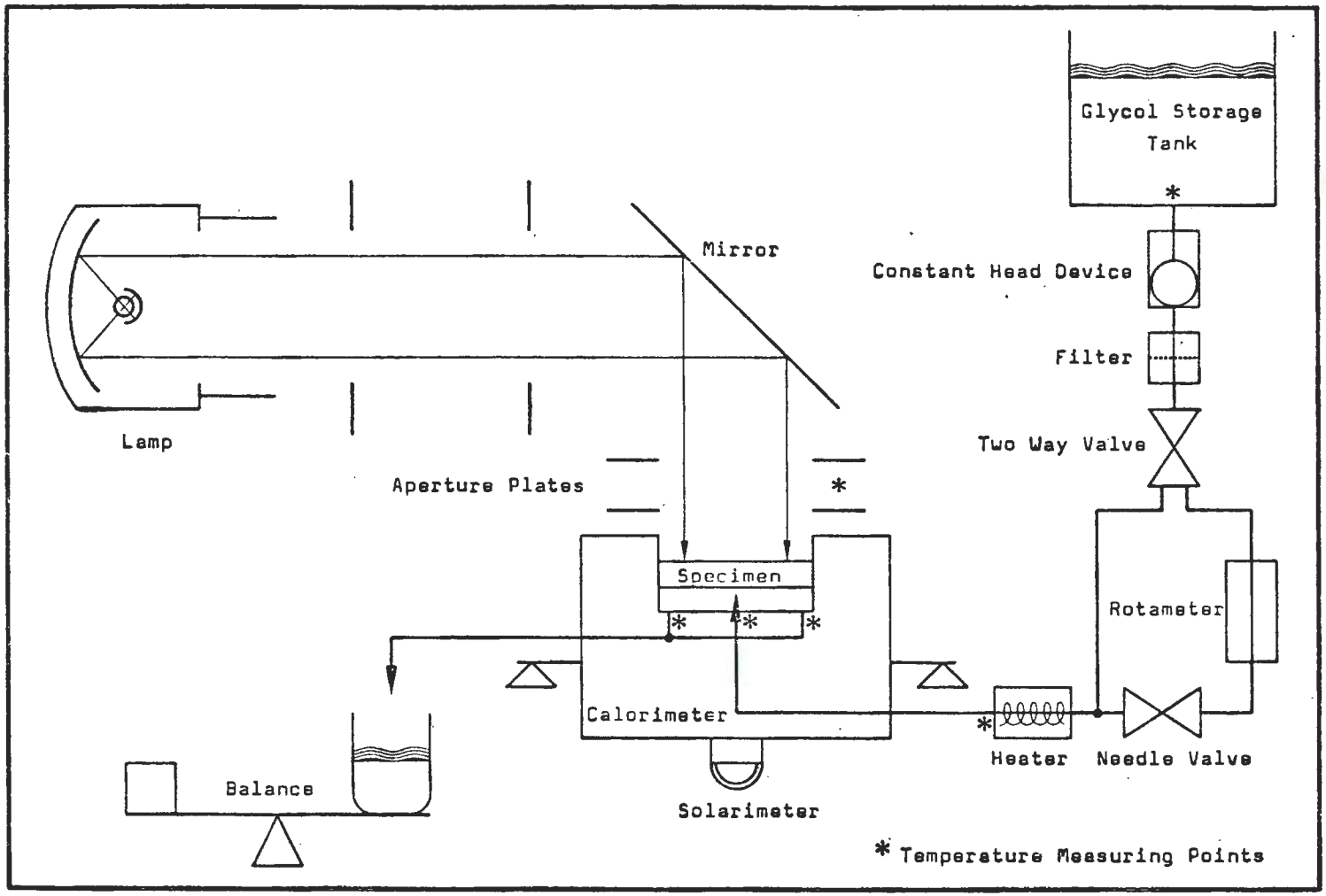

Figure 19. Schematic diagram of apparatus.

4. Flow heater with temperature control equipment

5. Flow-type calorimeter (specimen holder)

6. Drain facilities

7. Balance and stop watch for evaluation of flow rate

Pure ethylene glycol (99 %) was chosen to act as the heat transfer medium. Although all tests were carried out at temperatures below 100 °C, glycol turned out to be superior to water because glycol did not show the tendency of forming disturbing bubbles at temperatures above 80 °C. The disadvantage of glycol was its temperature dependent viscosity and specific heat. While the first rendered the regulation of the flow rate more difficult, the latter, the specific heat, had to be determined by interpolation between key temperatures (see App. G-4).

The functional details of the calorimeter, which is basically a well insulated specimen holder with a built-in flow chamber, are shown in Fig. 20. It is worth mentioning that--because of its short time constant for thermal response--the present polypropylene body of the specimen holder proved to be better than a vacuum insulated mounting.

The calorimeter-box is mounted in bearings allowing

B Polypropylene Body

G Glass Cover (Schott Filter Glass WG 305 , τ = 0,926)

I Polystyrene Insulation

T_1 Inlet Thermocouples (2)

T_2 Outlet Thermocouples (4)

T_3 Surface Thermocouple

Scale 1 : 1

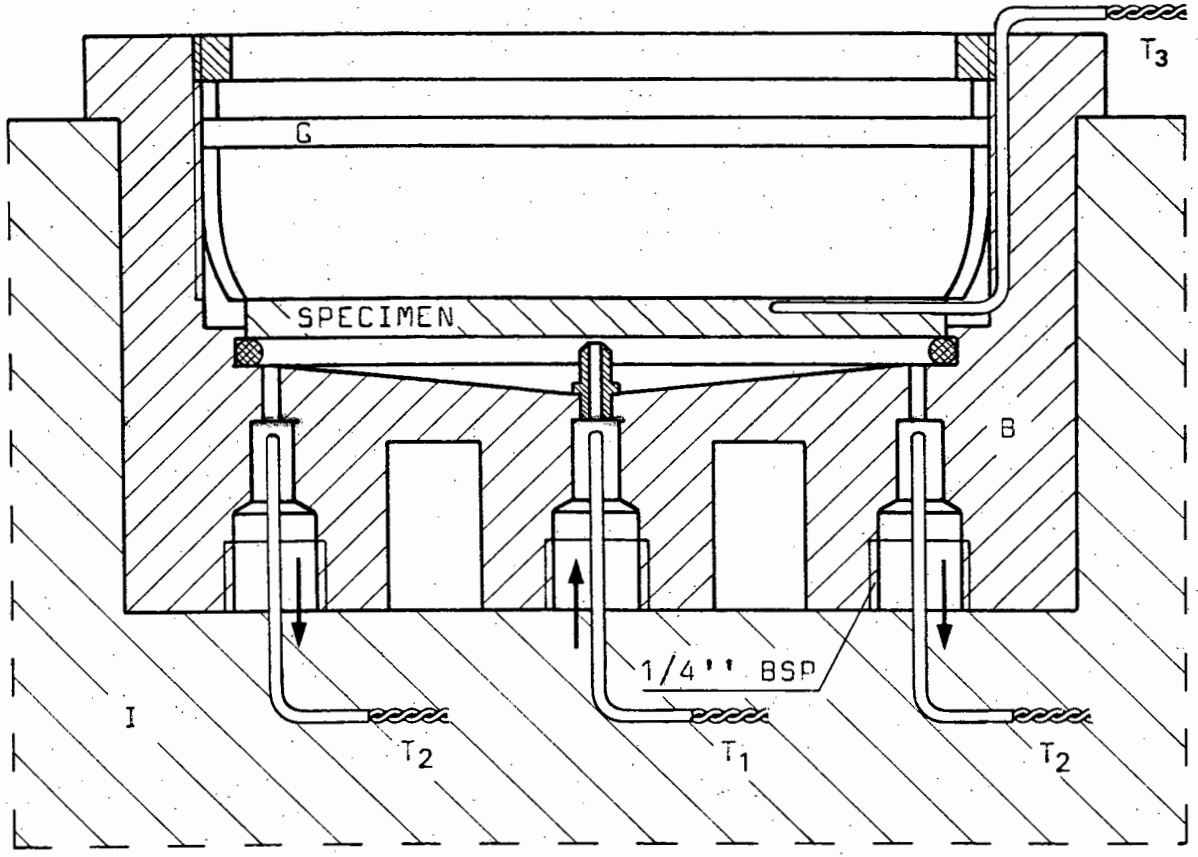

Figure 20. Cross section of calorimeter (specimen holder).

a 180^{o}-rotation. This arrangement facilitated both the operation procedure and the use of a thermopile radiometer, which is fastened to the back of the box and positioned in line with the optical axis of the apparatus (see Figs. 17 and 19).

3.3.3 Instrumentation

Apart from a standard power supply and control unit for the arc lamp and for the flow heater, the instrumentation of the apparatus can be divided into two units: one for measuring the incident radiation, and one unit for recording the temperatures.

The radiation incident upon a test specimen (irradiance E) was measured by means of a precalibrated Kipp & Zonen solarimeter (CM 6) in combination with a Hewlett-Packard digital multimeter (3465 A). These instruments provide a lower threshold for practical radiation detection of 0,8 W/m^2 with an accuracy of $\pm$ 1 % (see Error Analysis, App. H).

For recording the required temperatures, specially designed thermocouple probes and reference junctions in a standard ice bath were used. The copper-constantan probes were calibrated in situ against four key temperatures by means of a third-degree Lagrange interpolation (see App. G-3).

The surface temperature of a specimen was measured by inserting a tubular probe into a small pilot hole beneath the surface. The hole, which is visible in Fig. 14, was drilled 20 mm into the side of each specimen. The positioning of this hole was not very critical, i.e., temperature deviations caused by different probe positions were much smaller than the overall measuring error. This was confirmed by testing a specimen which had five separate probes at different locations.

The temperature difference of the heat transfer medium flowing through the calorimeter was measured by inserting thermocouples into inlet and outlets of the flow chamber (see Fig. 20). The optimal positioning of these probes was determined by a trial and error procedure and also proved to be not very critical.

All thermocouples were connected via extension wires and a selector switch to a Kipp & Zonen channel selector (BA 1). The output of the channel selector was recorded on a Kipp & Zonen micrograph (BD 2), which was also connected to the multimeter mentioned above acting as a controlling instrument. The latter was necessary to eliminate errors caused by a recording drift. The lower threshold for practical temperature detection of this system was 0,02 ^{o}C with an accuracy of ± 0,05 ^{o}C (see Error Analysis, App. H).

3.4 EXPERIMENTAL PROCEDURE

3.4.1 Theoretical Background

The experimental investigation of the specimens by means of the apparatus described was based on the following heat transfer calculations. These calculations determined the steps of the experimental procedure, which will be described in Section 3.4.2 .

The energy balance for the calorimeter can be written down simply in terms of heat transfer rates:

$$q_{in} = q_{out} + q_l \tag{41}$$

The term q_l denotes the sum of convective and radiative heat losses from the surface of the specimen, as well as conductive heat losses through the calorimeter insulation. If q_{in} is defined as the radiant energy incident upon the specimen surface area and q_{out} as the heat quantity transfered via the specimen to the glycol, then Eq. (41) may be written as follows:

$$E\,A\,\alpha_{eff} = \dot{m}\,(\bar{c}_{p2}\,T_2 - \bar{c}_{p1}\,T_1) + q_l \tag{42}$$

where

E	=	irradiance on A
A	=	projected surface area of specimen
$\dot{m}$	=	flow rate of glycol
$\bar{c}_{p1/2}$	=	mean specific heat capacities of glycol between $0^{o}C$ and $T_{1/2}$
$T_{1/2}$	=	glycol temperatures at calorimeter inlet/outlet

The purpose of Eq. (42) is to provide a means for the experimental determination of both the effective absorptance, α_{eff}, of the specimens and their absorption efficiency η. As far as the latter is concerned, Eq. (42) is sufficient, if the efficiency at a certain temperature difference between specimen surface and ambient, $(T_3 - T_0)^*$, is defined as follows:

$$\eta = \frac{q_{out}}{q_{in}} = f(T_3 - T_0)^* \qquad (43)$$

i.e.
$$\eta = \frac{\dot{m}\,(\bar{c}_{p2}\,T_2 - \bar{c}_{p1}\,T_1)}{E\,A}\ 100\,\% \qquad (44)$$

Since η turned out to be negative in some cases, it was more convenient to use a relative efficiency, η_{rel}, which related η of a grooved specimen to η of the flat reference specimen No. 32. Hence the relative efficiency is defined as

$$\eta_{rel} = \frac{\eta}{\eta_{32}} \,. \qquad (45)$$

For computing α_{eff} from Eq. (42), the heat losses q_l at $(T_3 - T_0)^*$ have to be known. These may be found by inversion of Eq. (41), so that

$$q_l = q^*_{in} - q^*_{out} \,. \qquad (46)$$

If the term $(q^*_{in} - q^*_{out})$ is defined as the decrease in

heat content of the heat transfer medium between calorimeter inlet and outlet, then Eq. (46) may be written in the form *(no irradiation)*

$$q_1 = \dot{m}^*(\bar{c}^*_{p1}\, T^*_1 - \bar{c}^*_{p2}\, T^*_2) \quad . \tag{47}$$

Adding Eqs. (42) and (47) yields

$$\alpha_{eff} = \frac{\dot{m}\,(\bar{c}_{p2}\, T_2 - \bar{c}_{p1}\, T_1) + \dot{m}^*(\bar{c}^*_{p1}\, T^*_1 - \bar{c}^*_{p2}\, T^*_2)}{E\,A} \quad . \tag{48}$$

Eqs. (48) and (44) form the basis for the experimental procedure, which is described in the following section.

3.4.2 Basic Procedure

Inspection of Eqs. (44) and (48) reveals that the quantity

$$\frac{\dot{m}\,(\bar{c}_{p2}\, T_2 - \bar{c}_{p1}\, T_1)}{E\,A} \tag{49}$$

is common to both equations, and in addition a similar quantity also occurs in the latter. A basic experimental procedure was therefore followed to evaluate (49), and a modified version (as described in Section 3.4.3) was then used to evaluate the second quantity

$$\frac{\dot{m}^*(\bar{c}^*_{p1}\, T^*_1 - \bar{c}^*_{p2}\, T^*_2)}{E\,A} \quad .$$

The basic procedure was divided into two parts; the first part dealt with the necessary preparations and the second with the actual readings.

Firstly, a specimen was mounted into the specimen holder as shown in Figs. 18 and 20 . The glycol flow was started and checked for possible leakage and formation of air bubbles. Since the glycol, at this stage, was at ambient temperature at the calorimeter inlet and outlet, the temperature recording instruments could be zeroed. The lamp was switched on and after a stabilization period of 30 minutes, the irradiance on the solarimeter was adjusted to approximately 1353 W/m^2. The irradiance produced by the optical system proved to be stable within $\pm$ 3 % and uniform within $\pm$ 5 % . By means of the needle-valve and rotameter, the glycol flow was adjusted to approximately 2 kg/h . This turned out to be a flow rate which ensured both a sufficient turbulence for heat transfer within the flow chamber and a suitable temperature difference between calorimeter inlet and outlet of 2 - 5 ^{o}C. The specimen was now turned into the light beam, and the instruments were switched over to temperature recording (cf. typical recording chart, App. G-2).

The second part of the procedure was to measure the temperature difference between calorimeter inlet and outlet (numerator in (49)), as well as the pertinent flow rate. Since this measurement required a state of equi-

librium, it was necessary to wait until all temperatures had stabilized (30 - 120 min). Thereafter, three control readings were taken of inlet (T_1), outlet (T_2), surface (T_3), and ambient temperature (T_0) over a period of exactly 6 minutes. Simultaneously and for the same period, the glycol was allowed to run into a beaker in place of the drain tank. The collected glycol was weighted in order to accurately determine the flow rate ($\dot{m}$). After this period, the irradiance and the zero point of the instruments were checked again for possible drift.

The data obtained during the above procedure--most of them in the form of mV-readings--were entered in a calculator program (Texas Instruments SR-52) for conversion and immediate computation of expression (49), i.e., of η. The specially developed program took into account the calibration curves for thermocouple outputs, as well as the temperature dependence of the specific heat of glycol (see Sample Calculations, App. G).

3.4.3 Modifications

Due to the small temperature difference of the glycol between calorimeter inlet and outlet (2 - 5 ^{o}C), the efficiency, η, could not be evaluated at elevated temperatures, without additional heating of the system. The basic procedure was therefore modified by preheating the glycol to a desired temperature level, before entering the

calorimeter.

It has been stated that the determination of α_{eff} (see Eq. (48)) required also an experimental evaluation of the expression

$$\dot{m}^*(\bar{c}^*_{p1}\, T^*_1 - \bar{c}^*_{p2}\, T^*_2) \qquad (50)$$

leading to a second modification. Expression (50) was defined as the total heat losses, q_1, of the system at $(T_3 - T_0)^*$. Since the determination of the heat losses did not require an irradiation of the specimens, the glycol was preheated only. Consequently, the cooling of the preheated glycol flowing through the calorimeter was a measure for q_1 at $(T_3 - T_0)^*$. For carrying out this modification, readings were taken for $\dot{m}^*$, T^*_1, T^*_2, and $(T_3 - T_0)^*$ in the same way as described before.

The use of a glass cover over a specimen was the third modification. The glass cover was mounted 20 mm above a specimen, as illustrated in Fig. 20, with the purpose of simulating a glass-covered solar collector. Most of the experiments were then repeated.

The numerical results will be presented in the following chapter and discussed in more detail in the subsequent Chapter 5 .

CHAPTER 4

RESULTS

4.1 INTRODUCTION

The following sections and figures present the main results. These were obtained experimentally as described in the preceding chapter as well as theoretically by applying the relevant formulae derived in Chapter 2 to each specimen. A detailed example of the necessary computation and conversion procedures, which had to be carried out before plotting any data points, is given in App. G.

Figures 21-31 show graphically the effective absorptances and the relative or absolute absorption efficiencies obtained for the investigated specimens. Wherever possible, at least two experimental points are plotted for each specimen representing a repetition of the relevant experiments. The experimental points in Figs. 21, 22, 24, 26, 27, and 29 are accompanied by two limiting curves, which represent the relevant theoretical values, assuming both nominal groove specifications (see App. E) and ideal diffuse or specular surface properties. These curves are plotted as calculated from Eq. (40) in conjunction with Eqs. (28) and (37) respectively.

Furthermore, some experiments were repeated at both low and elevated temperature levels as well as with and without the use of a glass cover. These modifications were necessary to ensure that a variation in both temperature and convective heat losses had no influence on the tests results.

Since experiments were carried out on five different groups of specimens (cf. Section 3.2), the emphasis of the following presentation of results will lie on grouped results rather than on individual results. Particulars of the latter will be given in the course of the discussion in Chapter 5 .

4.2 EFFECT OF GROOVE DEPTH ON ABSORPTION CHARACTERISTICS

Figures 21-23 show the results obtained for specimens No. 1-8 . Originally, these specimens were designed to test the influence of the depth of V-grooves on their apparent absorptance. Previous investigations of similar specimens [1] revealed that such an influence might exist, although there is no theoretical evidence. Accordingly, specimens No. 1-8 were manufactured with grooves having increasing depths and a constant groove angle.

The experimental results show that the effective absorptance, as well as the relative efficiency, increase with increasing groove depth and have the tendency to

reach a maximal value. This observation seems to confirm that there might be an influence of the groove depth on the absorptance.

However, inspection of the groove parameters of specimens No. 1-8 (see App. E) reveals that these specimens are characterized not only by different groove depths but also by different w/l - ratios. In other words, the percentage of lands of the total projected specimen surface area decreases from 27 % (specimen No. 1) to as little as 1,9 % (specimen No. 8). It is obvious that this must affect the absorption characteristic, since the apparent absorptance of the groove openings (w) is higher than the absorptance of the lands (l). The latter equals the absorptance of the flat reference specimen No. 32 (see App. J). It was therefore necessary to eliminate the influence of the ratio w/l. This was achieved by machining the second set of specimens as follows.

Specimens No. 9-16 were grooved in such a way that both the groove angle and the ratio w/l were constant for all different groove depths. The experimental results are plotted in Figs. 24-25. It can be seen that the obtained values for α_{eff} and η_{rel} remain constant for all specimens of this second set. Hence it appears that the groove depth has no direct influence on the absorptive power of a V-grooved surface. The increase in absorptive power with increasing groove depth, as

observed in Figs. 21-23, is a function of the term $w/l = 2\frac{d}{l}\tan\frac{\theta}{2}$ rather than a function of d alone.

The above experimental findings led to the development of Eq. (40), which takes into account the term $w/l = 2\frac{d}{l}\tan\frac{\theta}{2}$. Using this equation in conjunction with Eq. (28) permits a theoretical determination of α_{eff} for specimens No. 1-16 (see App. G). The results are plotted in Figs. 21, 22, and 24 as solid curves (assuming nominal groove specifications). These results have to be corrected as far as actual groove specifications are concerned, and they are plotted also as corrected theoretical values. Inspection of Figs. 21, 22, and 24 shows that the experimental points, in general, follow the shape of the curves of the theoretical values.

In summary, referring particularly to Figs. 21 and 24, it appears that the experimental results are in good agreement with the theoretical predictions, as far as the influence of the groove parameter d/l is concerned. Further details will be discussed in Chapter 5.

4.3 EFFECT OF GROOVE ANGLE ON ABSORPTION CHARATERISTICS

In order to study the effect of increasing or decreasing groove angles, the specimens of the third set (No. 17-23) were manufactured with grooves of various angles ranging from 15^{o} to 90^{o}. To isolate the groove

parameter θ , the ratio w/l , as well as the groove depth were kept constant for all these specimens.

The experimental results are plotted in Figs. 26 to 28 showing that the experimental points follow the corrected theoretical values, especially at low temperatures (cf. Fig. 26). Equally, the relative efficiencies plotted in Fig. 28 follow the trend of increasing absorptive power with decreasing groove angle.

Although a groove angle of less than 15^{o} (in this case) was not tested, it can be expected that the trend mentioned above will not continue for groove angles approaching 0^{o}. The simple reason for this is that the ratio w/l can not be kept constant for groove angles much smaller than 15^{o} unless unrealistic small lands are assumed. Since the latter is of no practical interest (the specifications of specimen No. 17 and No. 18 are already unrealistic), a fourth set of specimens was manufactured.

Specimens No. 24-31 were provided with the same grooves as those of specimens No. 17-23 , with the exception that the lands, and accordingly the ratio w/l , were chosen to fit the pertinent groove angles. In other words, the lands were widened for smaller angles to produce strong groove flanks and lips, which do not bend or break. Thus the specimens of the fourth set represent

realistic V-grooved surfaces.

The results obtained for these specimens are shown in Figs. 29 and 30 . Again, it can be seen that the experimental points follow the theoretical predictions. What is more, an expected optimum occurs, which agrees with the statements made in Section 2.3.2 .

4.4 EFFECT OF SURFACE FINISH ON ABSORPTION EFFICIENCY

The last specimens No. 32-37 were machined to study the effect of black and specular V-grooved surfaces. In addition, it was proposed to test the applicability of such surfaces for solar energy collection.

Since a groove depth of 2 mm and a groove angle of 30^{o} turned out to be favourable groove dimensions (see Figs. 21 and 29), specimens No. 35-37 were grooved accordingly. Specimen No. 35 was left blank (brass surface), whereas specimen No. 36 was spray painted mat black, and specimen No. 37 was made specular by a chromium plating. The flat specimens No. 32-34 served as reference samples.

The experimentally determined absorption efficiencies of these specimens are plotted in Fig. 31 . A study of Fig. 31 reveals three major effects:

Firstly and according to expectations, the application of black paint has increased the absorptive power of both the flat and the grooved specimen (cf. relevant curves for specimens No. 32, 33, 35, and 36).

Secondly, the absorption efficiency of the flat black surface (No. 33), which is very high at low temperatures, is nevertheless exceeded by the grooved black surface (No. 36). This is particularly true at higher temperatures and will be discussed in more detail in Chapter 5.

Finally, as far as the efficiency curve for the specular specimen No. 37 is concerned, a surprising effect occurs. Although the absorptance of the grooved specular surface is lower than that of its black counterpart --a conclusion which can be drawn from the results at low temperatures--, its absorption efficiency at high temperatures is superior to all other surfaces. This observation will also be discussed in more detail in the following Chapter 5.

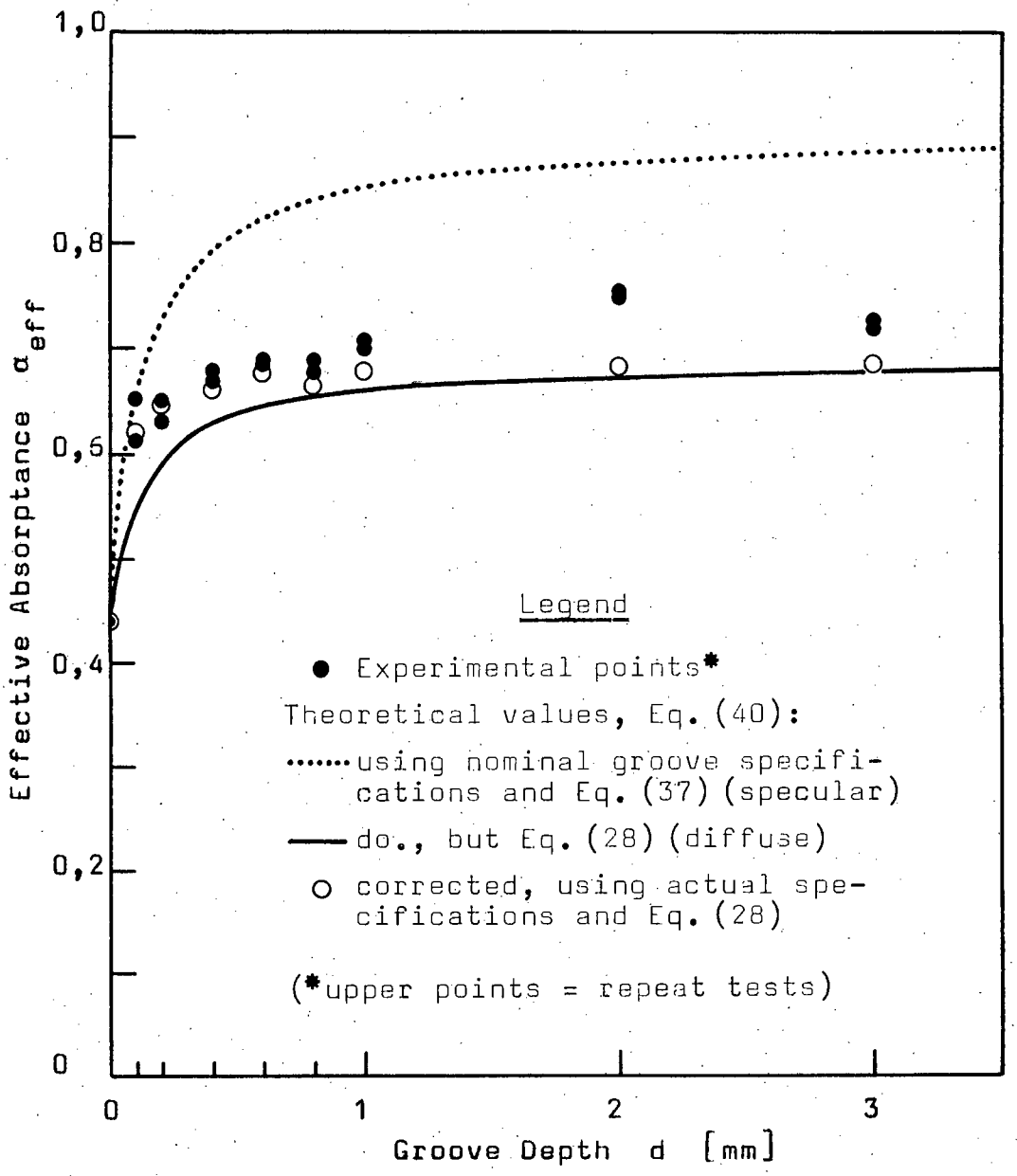

Figure 21. Effective absorptance of specimens No. 1-8 ($\theta = 45^{\circ}$) at $T_3 - T_0 \approx 7\ ^{\circ}C$ compared with theoretical values.

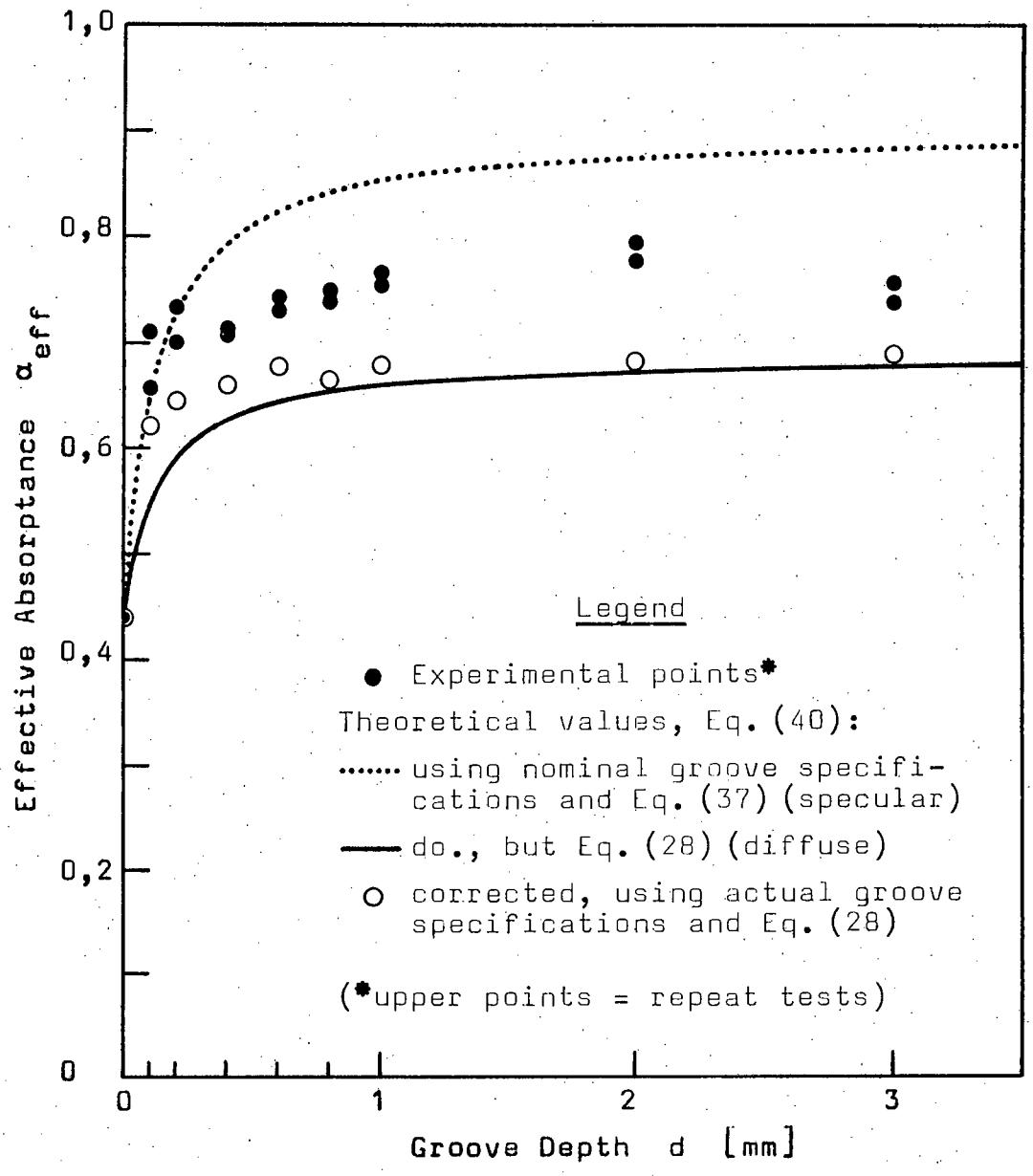

Figure 22. Effective absorptance of specimens No. 1-8 ($\theta = 45^{o}$) at $T_3 - T_0 \approx 53\ ^{o}C$ compared with theoretical values.

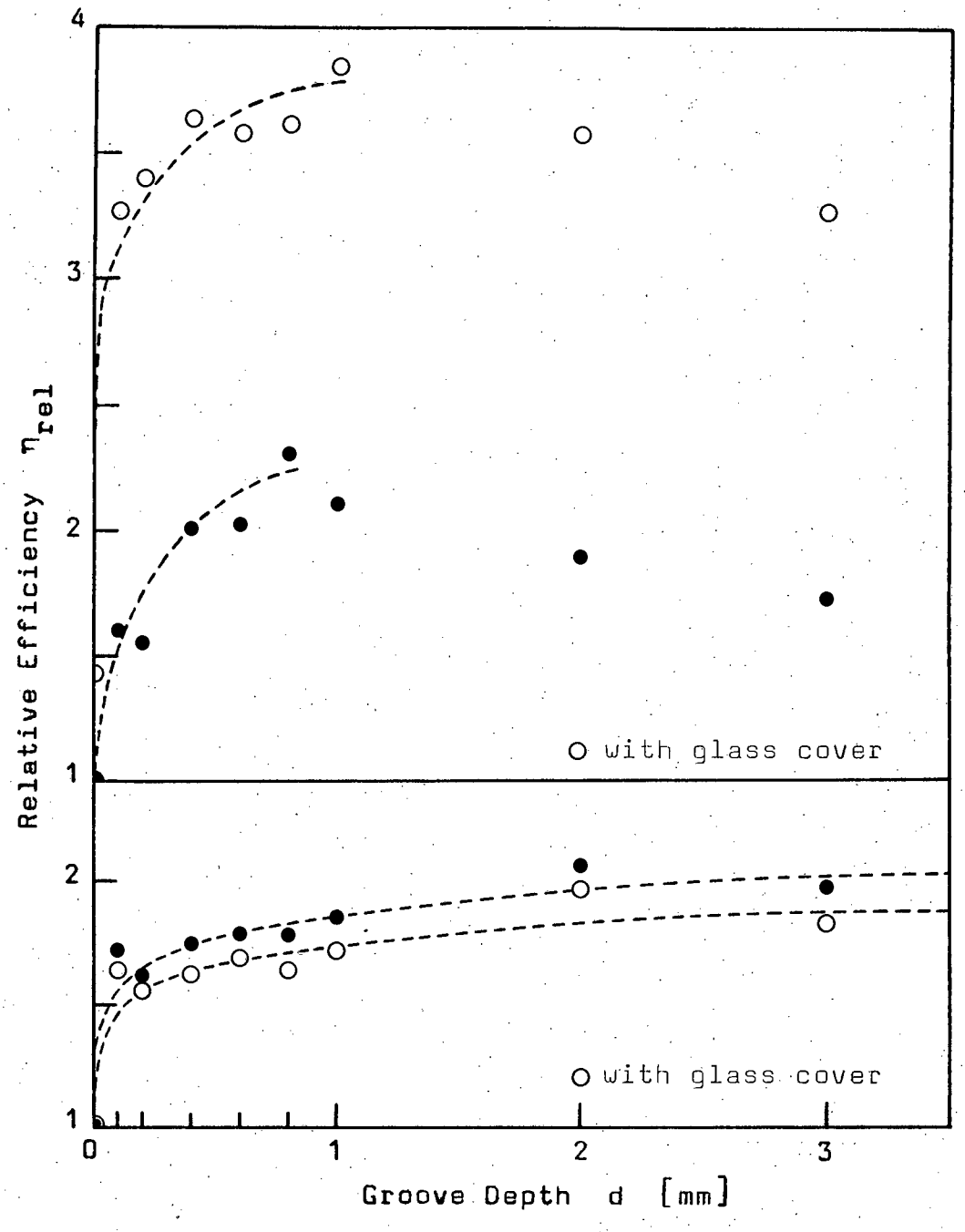

Figure 23. Relative absorption efficiency of specimens No. 1-8 ($\theta = 45^{o}$) at $T_3 - T_0 \approx 7\ ^{o}C$ (lower graph) and at $T_3 - T_0 \approx 53\ ^{o}C$ (upper graph).

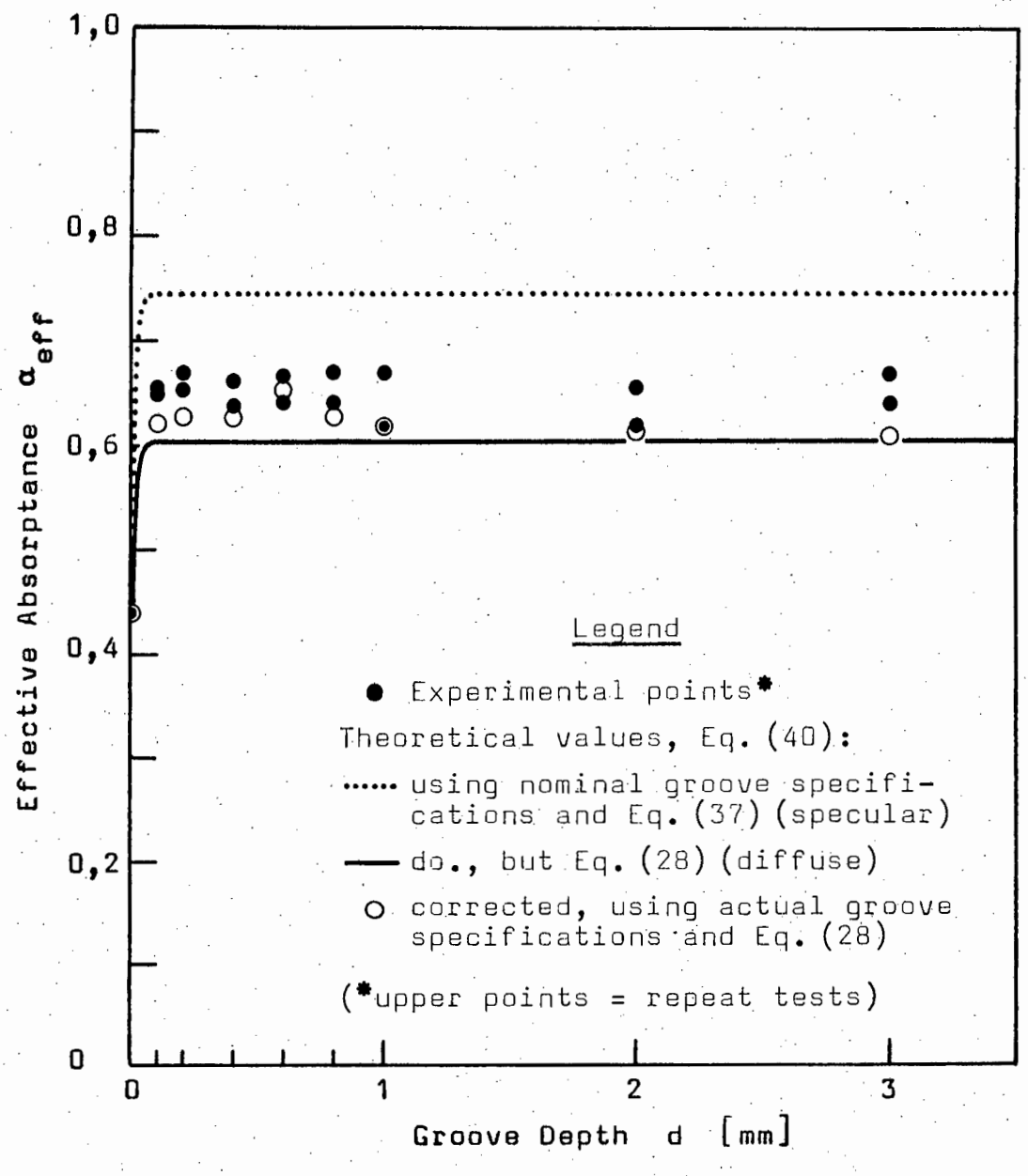

Figure 24. Effective absorptance of specimens No. 9-16 ($\theta = 45^{o}$) at $T_3 - T_0 \approx 7\ ^{o}C$ compared with theoretical values.

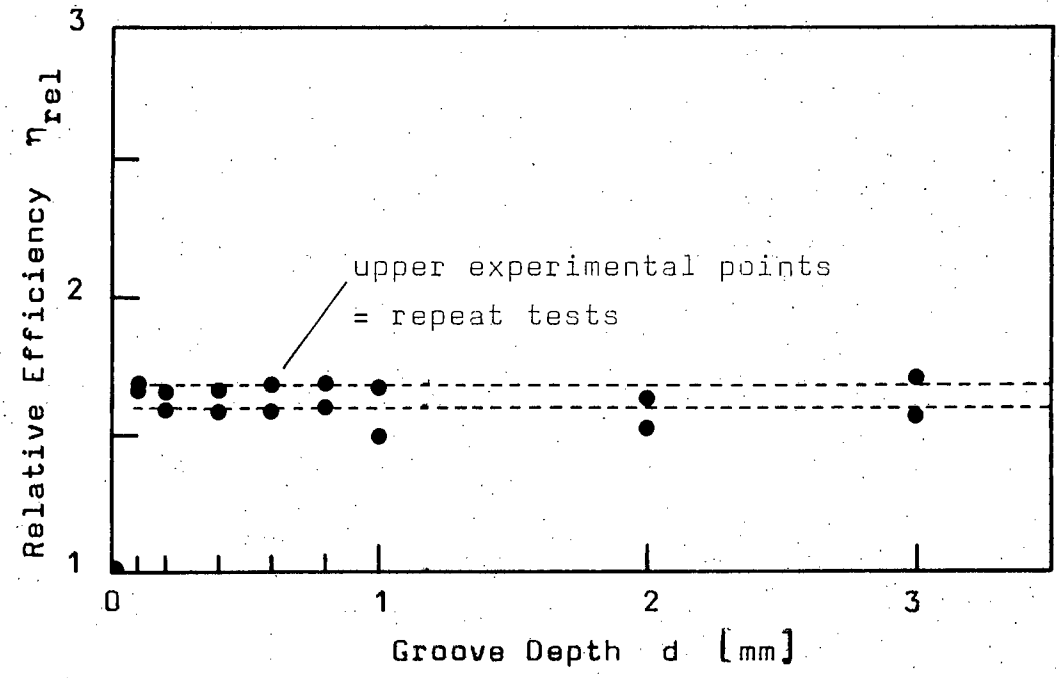

Figure 25. Relative absorption efficiency of specimens No. 9 - 16 at $T_3 - T_0 \approx 7^{\circ}C$.

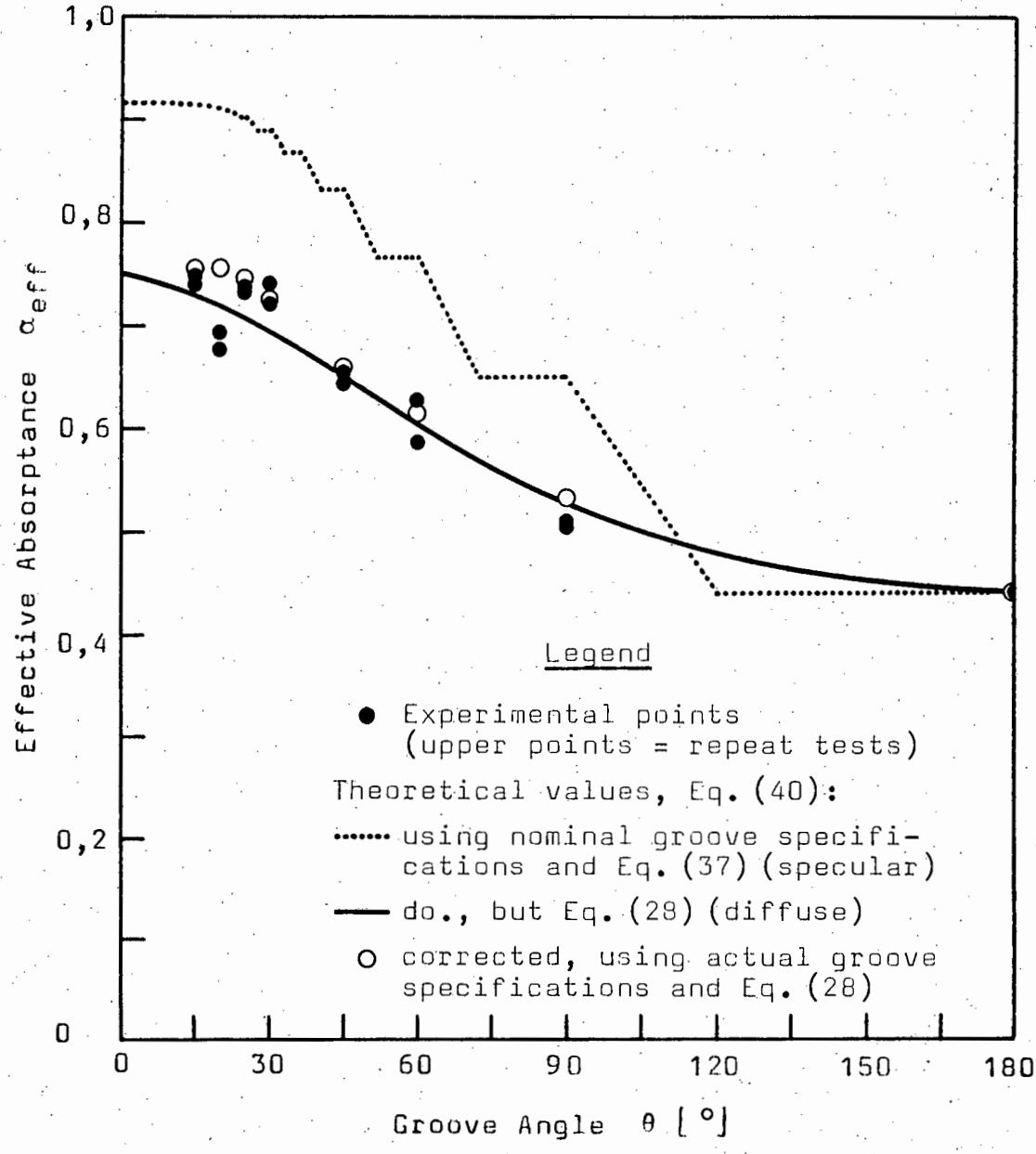

Figure 26. Effective absorptance of specimens No. 17-23 (d = 2 mm) at $T_3 - T_0 \approx 7$ °C compared with theoretical values.

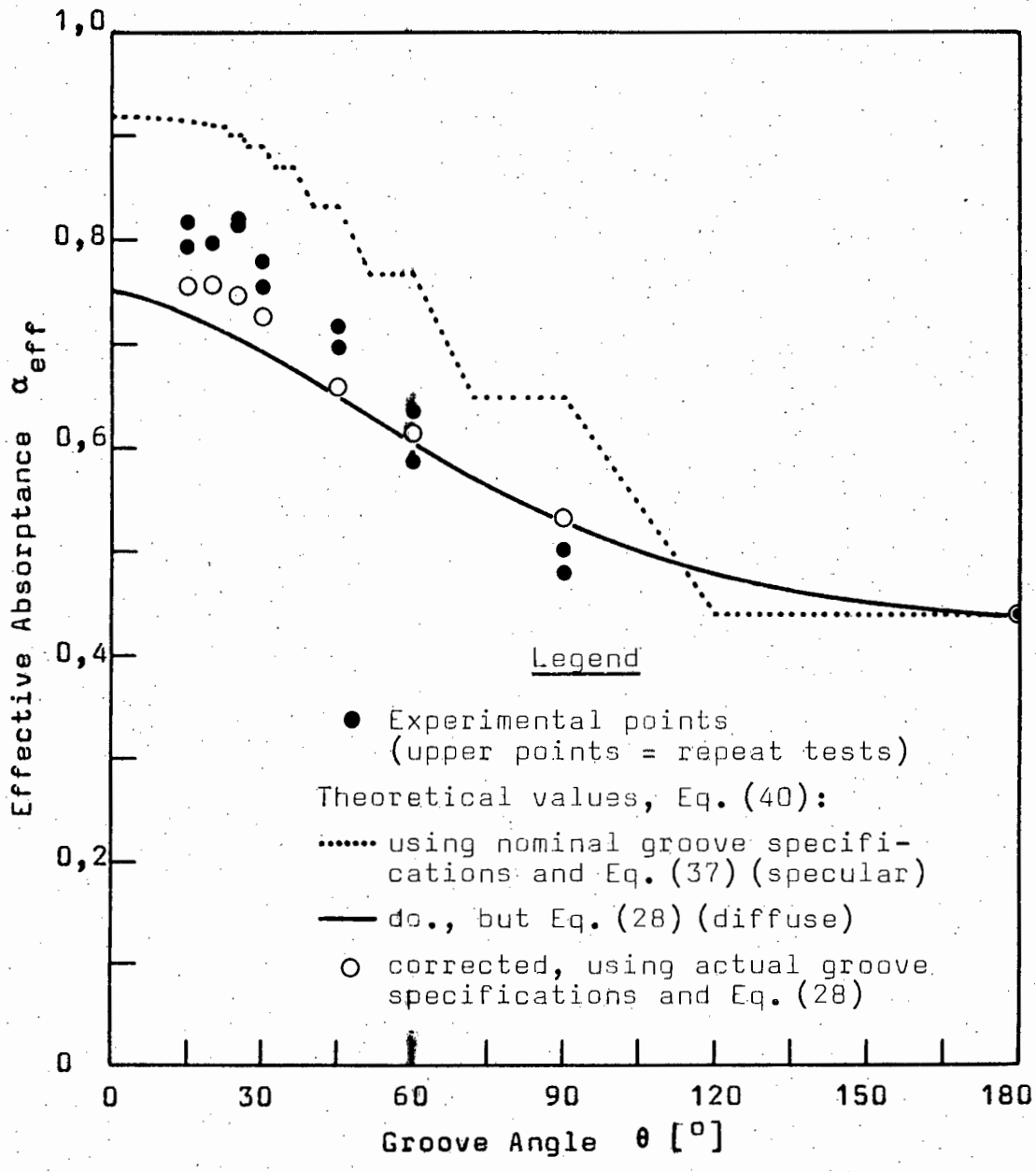

Figure 27. Effective absorptance of specimens No. 17-23 (d = 2 mm) at $T_3 - T_0 \approx 52\ ^{o}C$ compared with theoretical values.

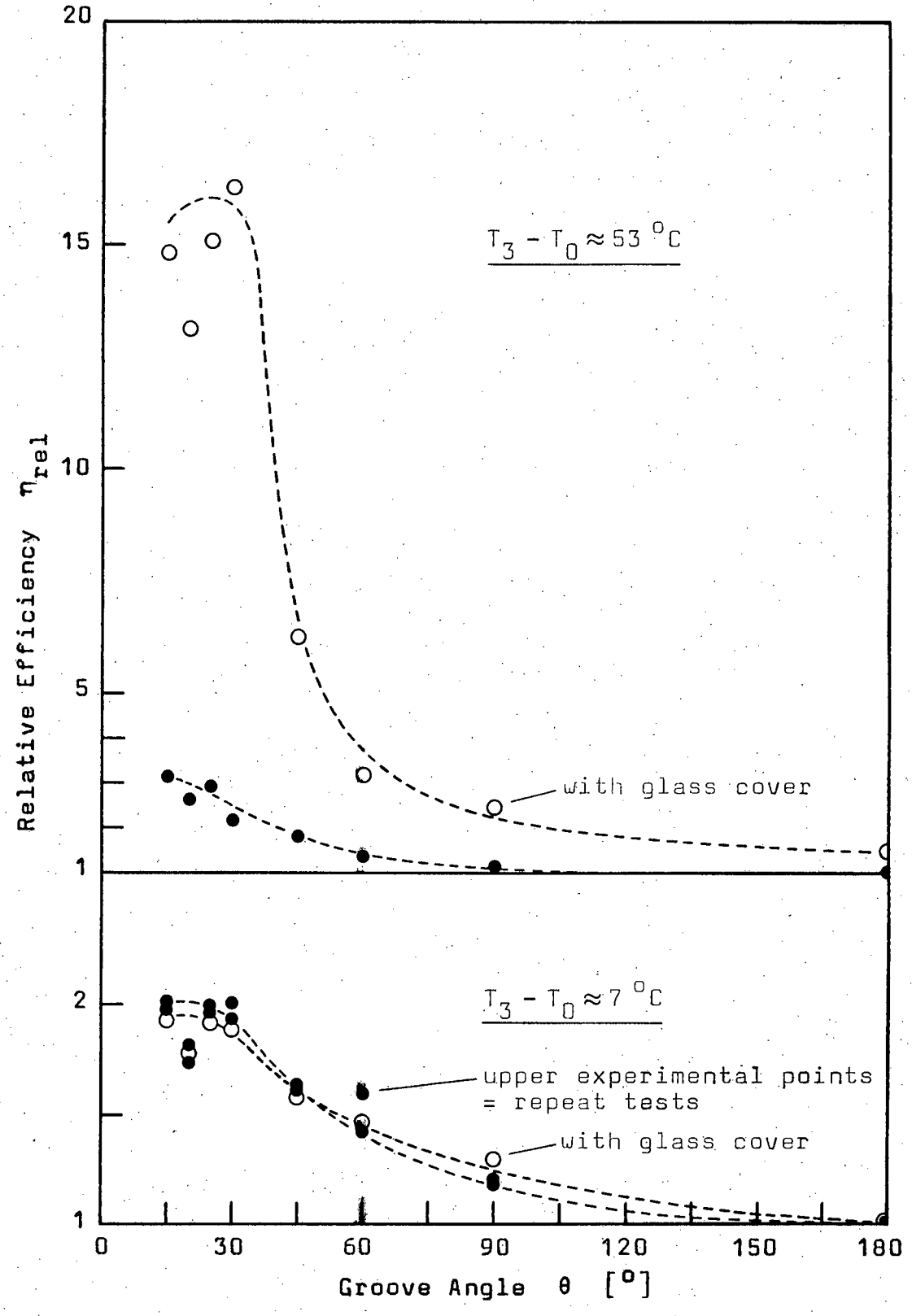

Figure 28. Relative absorption efficiency of specimens No. 17-23 (d = 2 mm) at two different temperatures.

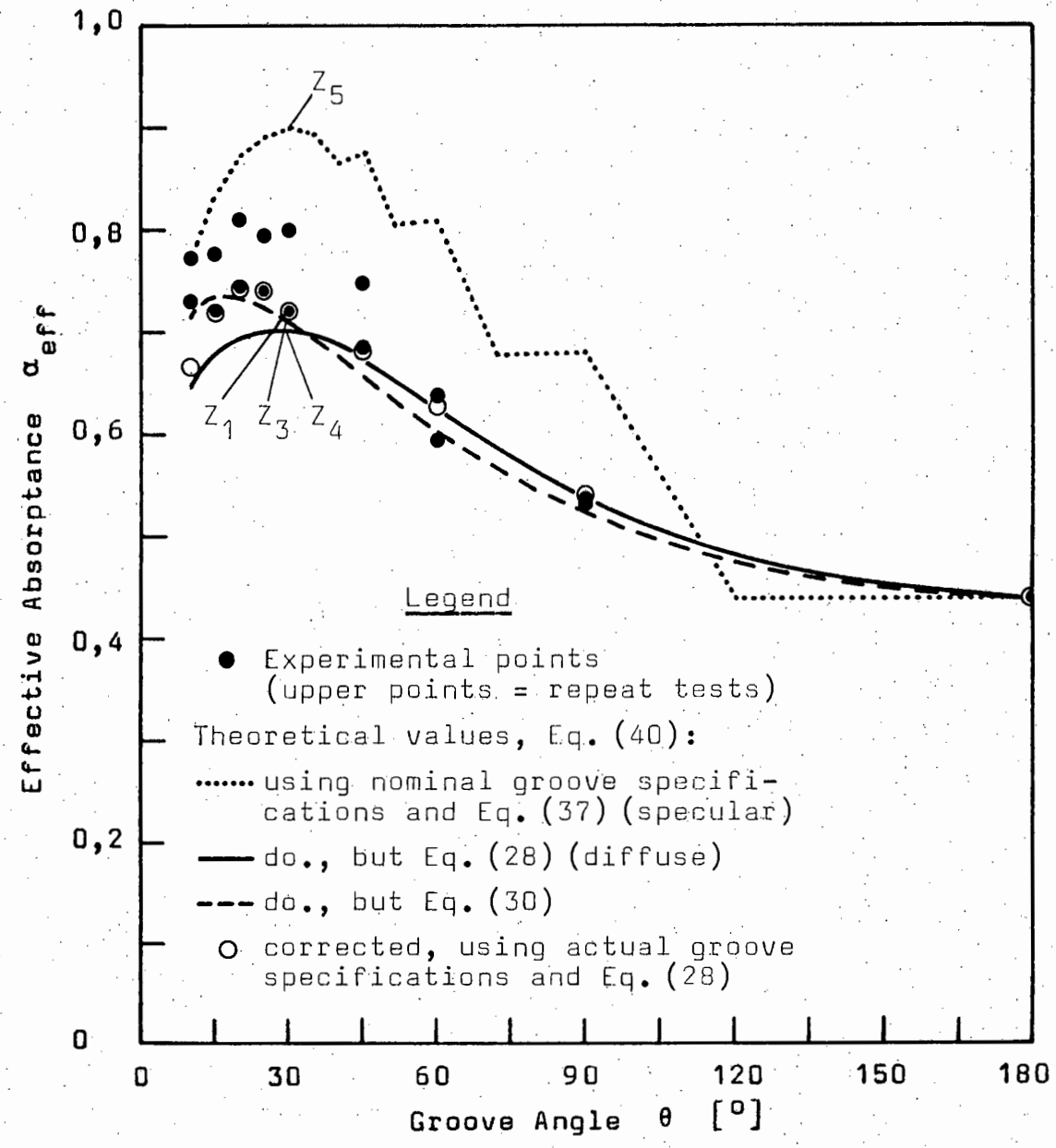

Figure 29. Effective absorptance of specimens No. 24-31 (d = 2 mm) at $T_3 - T_0 \approx 7\ ^{o}C$ compared with theoretical values.

(For Z_{1-5} see App. G-6/7)

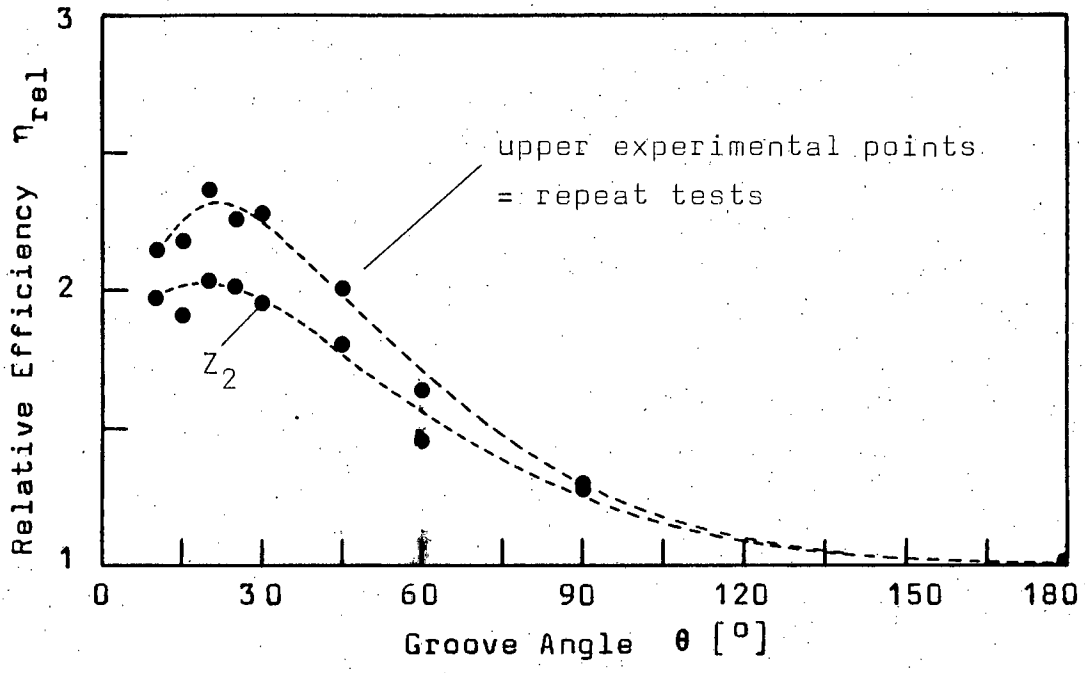

Figure 30. Relative absorption efficiency of specimens No. 24-31 (d = 2 mm) at $T_3 - T_0 \approx 7\ ^{o}C$.

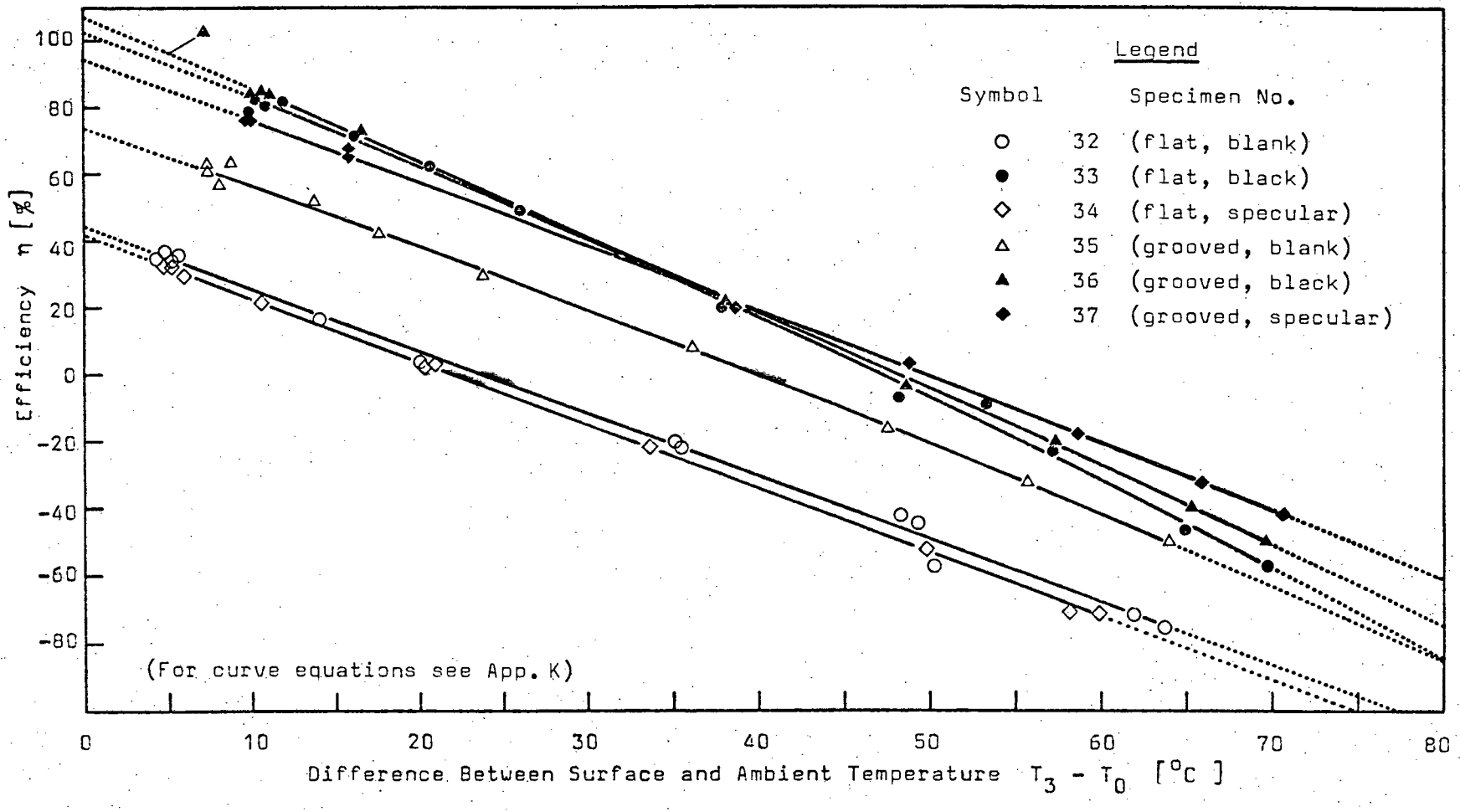

Figure 31. Absorption efficiency of specimens No. 32-37 .
($E = 1353\ W/m^2$)

CHAPTER 5

DISCUSSION

The present research program was carried out to develop closed form solutions to the V-gooved radiation-absorber problem and to verify these experimentally. The results presented in Chapter 4 show that there is a good agreement between the trend of experimental points and the shape of theoretical curves. This is the most important criterion on which the results of the theoretical analysis should be judged. The fact that the experimental and theoretical points in certain graphs are somewhat displaced is of secondary importance, but nevertheless also of interest.

In general, all experimental results are somewhat higher than the predicted values; and in particular, for those cases, where two sets of data under the same conditions were obtained, the first values are always lower than the repeated values. This trend is clearly shown in the preceding graphs, especially in those which are plotted for elevated temperatures (see Figs. 22, 27, and 29). There are two factors which might have contributed to these effects:

1. Although the brass specimens were cleaned carefully

before testing, when irradiated, a slight unavoidable tarnish could be observed getting worse in the course of a test, particularly at elevated temperatures. This tarnish might have increased the absorptance of the surface, which, apart from the groove parameters, has a strong influence on the effective absorptance of a specimen.

2. It has been assumed in Section 2.1 that the reflection on any participating surface is perfectly diffuse. It is well known that this assumption does not hold for real surfaces. Without entering into the underlying theory, it may be stated that the directional components of reflectance increase with increasing angle of incidence; in short, the irradiated sides of small-angled V-grooves become somewhat specular. This explains the generally observed higher values for α_{eff} than those predicted by Eqs. (40) and (28), particularly with respect to smaller groove angles. It therefore seems to be appropriate to replace Eq. (28) by Eq. (30), as far as V-grooves are concerned which have diffuse-specular (real) surfaces and small groove angles. A plot of Eq. (30) (applied in conjunction with Eq. (40) to the relevant specimens) is included in Fig. 29 (dashed curve). It can be seen that this curve is in better agreement with the experimental points, with regard to small groove angles.

An interesting deviation from the above observations

occurs in the case of specimen No. 18 . The experimental values obtained for this specimen are considerably lower than theoretically predicted (see Figs. 26-28 , $\theta = 20^{o}$). The expla nation for this can be found by studying the relevant microscope photograph of the groove profile (see App. F-6). The grooves of specimen No. 18 are badly cut, the vertices being rounded instead of sharp. Since this affects the interreflection pattern at the vertex (where most interreflections occur), the effective absorptance must be expected to decrease.

As previously mentioned, the presence of lands (l) in any grooved surface has a marked effect on all results presented. This is especially noticeable in Figs. 21-23, where the characteristic shape of the curves is due entirely to machining limitations. If perfectly sharp-edged grooves could be machined ($l = 0$), a horizontal α-d trace would result. As the groove depth is decreased, the d/l ratio becomes increasingly significant causing the characteristic droop in the curves towards the origin. For large values of α , the d/l ratio becomes less significant, and the α-d trace tends to the limit given by the value α_a for a single V-groove cavity. It is therefore evident (cf. Figs. 21-23) that, as far as the absorptive power is concerned, there is no advantage to be gained by making 45^{o}-grooves smaller than 1 mm or larger than 3 mm in depth. These figures, of course, hold true only for the present specimens.

It has been stated in Chapter 4 that the grooved black surface (No. 36) is more efficient than the flat black surface (No. 33), particularly at elevated temperatures. This result can be corroborated by extrapolation of the relevant curves in Fig. 31 towards higher temperatures. Carrying out such extrapolations may even show that the absorption efficiency of the grooved brass surface (No. 35) exceeds that of the flat black surface. There are two factors which contribute to this:

1. The small air cells within the grooves suppress the convective heat loss from the surface.

2. The radiative heat loss of the black surface (being a function of the fourth power of its temperature) increases more rapidly than that of the brass surface since $\epsilon_{black} \gg \epsilon_{brass}$.

On this basis it is understandable that the absorption efficiency of the grooved specular surface (No. 37) exceeds that of all other surfaces at higher temperatures. In short, the grooved specular surface takes advantage of the fact that the convective heat loss is partly suppressed and, what is more important, that its absorptance has been increased considerably, whereas its emittance remains at a relatively low level.

The effective absorptance of the grooved specular

surface (No. 37) can be found by extrapolating the relevant efficiency curve in Fig. 31 towards $T_3 - T_0 = 0\,^{o}C$. Since there is no temperature difference between surface and ambient temperature at this point, no heat losses from the surface occur. Consequently, η equals α_{eff} (cf. Eqs. (44) and (48)) and the latter is found to be $\alpha_{eff} = \underline{0,94}$ (see App. K). This experimental value for α_{eff} agrees very well with the theoretical value being obtained as follows: Extrapolating the efficiency curve for the flat specular specimen No. 34 towards $T_3 - T_0 = 0^{o}C$ yields $\alpha = 0,42$ (cf. App. K), which is the absorptance of the chromium plating. Using $\alpha = 0,42$ together with the relevant groove specifications of specimen No. 37 for evaluation of Eqs. (40) and (37) yields $\alpha_{eff} = \underline{0,93}$.

Apart from the above specimens, specular V-grooved surfaces have not been investigated in detail. Too many specimens would have been required to verify the step-functional character of Eq. (37) (cf. Fig. 7). However, it is worth mentioning that the only experimental data, so far available in literature, is in very good agreement with the corresponding values calculated from Eqs. (40) and (37): As mentioned in the literature survey, C. P. Butler et al. [30] pressed an assembly of 250 razor blades into a polished gold specimen. They found out that the original absorptance of the gold specimen increased from 0,24 to 0,31. The area included in their grooves was approximately 8 % of the total (i.e.,

$w/l = 0,08$) and the groove angle approximately 10^{o}. Using these values for evaluation of Eqs. (40) and (37) results in $\alpha_{eff} = 0,3$, a theoretical value which is in very good agreement with Butler's experimental value of $0,31$..

Finally, the following example serves to illustrate the effect the preceding results would have on practical solar energy collection:

Assume that the flat black surface of specimen No. 33 is being used for solar energy collection in space. The surface absorptance for solar radiation is, say, $\alpha = 0,95$ and the infrared-emittance is $\epsilon = 0,94$. The surface is maintained at a temperature of $116\ ^{o}C$ by extracting energy to be used in a power generating cycle. With this, the net energy which can be extracted is

$$q_{net} = q_{absorbed} - q_{emitted}$$

$$= 1285 \quad - 1220 \quad W/m^2$$

$$= 65 \ W/m^2 .$$

The necessary calculations are carried out in App. L.

Using the flat specular surface of specimen No. 34 ($\alpha = 0,42$, $\epsilon = 0,1$) instead of the above black surface, would result in

$$q_{net} = 544 \quad - 130 \quad W/m^2$$

$$= 414 \ W/m^2 .$$

Using the V-grooved specular surface of specimen No. 37 ($\alpha_{eff} = 0,94$, $\epsilon_{eff} = 0,29$) would increase the useful extractable energy to as much as

$$q_{net} = 1223 - 376 \ W/m^2$$

$$= 847 \ W/m^2 \ .$$

CHAPTER 6

CONCLUSIONS

The preceding theoretical and experimental study was carried out to investigate the absorption characteristics of diffusely and specularly reflecting V-grooved surfaces. In the theoretical analysis, formulae are developed for both the apparent absorptance of V-groove cavities and the effective absorptance of V-grooved surfaces. These formulae enable the performance of V-grooved radiation absorbers to be optimized with respect to the various groove parameters and normal incidence.

The experimental part of the study verifies both the theoretical formulae and the predictions inferred from them. In addition, the experiments give some insight into the behaviour of V-grooved surfaces used for solar energy collection.

There are four basic conclusions that can be drawn from the theoretical and experimental results. They are:

1. V-grooves, carefully optimized and applied to a solar energy absorbing surface, can raise its absorptance almost to unity and improve its absorption efficiency.

2. Best performances at high temperatures can be expected from metal surfaces provided with specular V-grooves having a small groove angle ($< 30^{o}$).

3. The optimal groove angle is dependent on three factors: (1) the reflection properties of the groove, (2) the absorptance of the groove surface, and (3) the ratio of groove depth to land width which occurs between the grooves.

4. As far as the effective absorptance of a V-grooved surface is concerned, there is no advantage in choosing a groove depth beyond or above certain limits, which can be found by using the nomographs in Figs. (11) and (12).

During the course of this work it has become evident that there are some areas where further research could be undertaken. These include the effect of selective coatings applied to V-gooved surfaces, the effect of V-grooves or V-corrugations on the transmittance of transparent surfaces, and finally the possible interference effects in very fine V-grooves.

When considering the latter, it is interesting to

note that nature has utilized this principle of interference to increase the transmittance of the cornea of the night moth's eye by developing a nipple array shown in Fig. 32 . The V-shaped profile of this nipple array, as well as its similarity to Bouguer's surface model shown on page 3 , are remarkable.

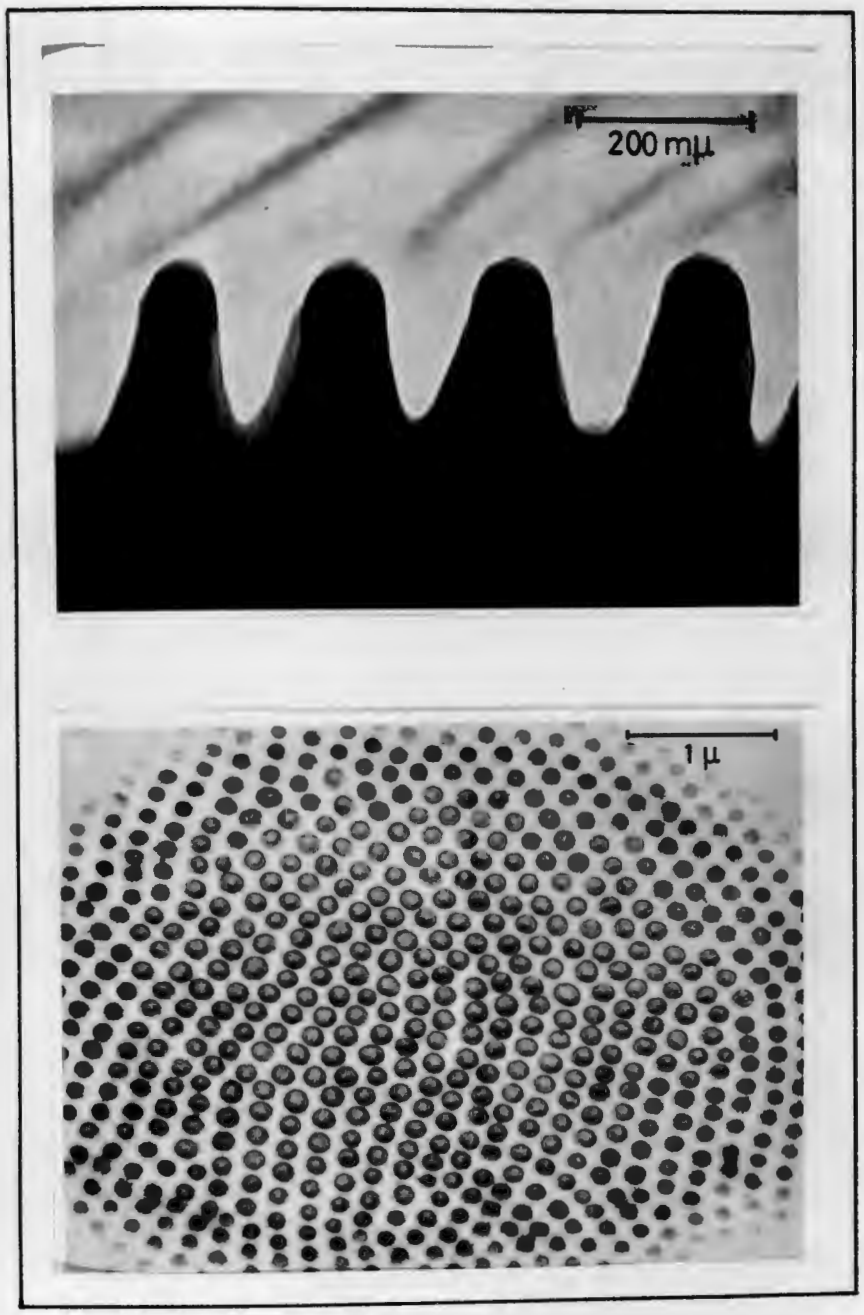

Figure 32. Nipple array of the cornea of a night moth's eye [45].

REFERENCES

1. Haggi, A. S., "Solar collector efficiency", B.Sc. thesis, Department of Mechanical Engineering, University of Cape Town (1974).

2. Bouguer, P., "Traité d'optique sur la gradation de la lumière", ed. De La Caille, Guerin & Delatour, Paris (1760), pp. 161-228 .

3. Leslie, J., "Experimental inquiry into the nature and properties of heat", Mawman, London (1804), pp. 81-85 .

4. Ritchie, W., "Observations on radiant heat", Edinb. Phil. J. 12 (23), 15-18 (1825).

5. Melloni, M., "De la prétendue influence que les aspérités et le poli des surfaces exercent sur le pouvoir émissif des corps", C. r. hebd. Séanc. Acad. Sci., Paris 7, 298-303 (1838).

6. Melloni, M., "Sur la cause des différences que l'on observe entre les pouvoirs absorbants des lames métalliques polies ou rayées, et sur ses applications au perfectionnement des réflecteurs calorifiques", C. r. hebd. Séanc. Acad. Sci., Paris 12, 375-380 (1841).

7. Knoblauch, H., "Ueber die Erwärmung der Körper durch strahlende Wärme", Annln Phys. 70 (2), 230 (1847).

8. Knoblauch, H., "Ueber das Wärmeausstrahlungsvermögen der Körper", Annln Phys. 70 (3), 337-351 (1847).

9. Magnus, G., "Ueber die Verschiedenheit der Wärme welche rauhe und glatte Oberflächen ausstrahlen", Annln Phys. 124, 476-497 (1865).

10. Magnus, G., "Ueber die Veränderung der Wärmestrahlung durch Rauheit der Oberfläche", Annln Phys. 140, 337-348 (1870).

11. Féry, C., "Propriétés sélectives des corps noirs employés comme récepteurs dans la mesure de l'énergie rayonnante et conséquences qui en découlent", J. Phys. 8 (4), 758-770 (1909).

12. Mendenhall, C. E., "On the emissive power of wedge-shaped cavities and their use in temperature measurements", Astrophys. J. 33 (2), 91-97 (1911).

13. Eckert, E. R. G. and Sparrow, E. M., "Radiative heat exchange between surfaces with specular reflection", Int. J. Heat Mass Transf. 3 (1), 42-54 (1961).

14. Psarouthakis, J., "Apparent thermal emissivity from surfaces with multiple V-shaped grooves", AIAA J. 1 (8), 1879-1882 (1963).

15. Brandenberg, W. M. and Clausen, O. W., "The directional spectral emittance of surfaces between 200^{o} and 600 ^{o}C", in Symp. on Thermal Radiation of Solids, San Francisco, 1964, ed. S. Katzoff, NASA SP-55, Washington, D.C. (1965), pp. 313-319.

16. Plamondon, J. A. and Landram, C. S., "Radiant heat transfer from nongray surfaces with external radiation", Prog. in Astronaut. & Aeronaut. 18, 173-197 (1966).

17. Hering, R. G., "Radiative heat exchange between conducting plates with specular reflection", J. Heat Transfer 88 (1), 29-36 (1966).

REFERENCES (continued)

18. Hering, R. G., "Radiative heat exchange between specularly reflecting surfaces with direction-dependent properties", Proc. of the 3rd Int. Heat Transf. Conf., Chicago, 5 (18), 200-206 (1966).

19. McCue, G. A., "A note concerning the effective emittance of certain grooved surfaces", AIAA J. 4 (4), 721-723 (1966).

20. Kimio Kanayana, "Apparent directional emittance of V-groove and circular-groove rough surfaces", Heat Transfer, Japanese Research 1 (1), 11-22 (1972).

21. Gorchakov, V. S. and Panevin, I. G., "The efficiency of radiating fins covered with V-shaped grooves", High Temperature 13 (4), 811-817 (1975).

22. Shimoji, S., "Local Temperatures in semigray non-diffuse cones and V-grooves", AIAA J. 15 (3), 289-290 (1977).

23. Sparrow, E. M. and Lin, S. H., "Absorption of thermal radiation in a V-groove cavity", Int. J. Heat Mass Transf. 5 (Nov.), 1111-1115 (1962).

24. Sparrow, E. M., Gregg, J. L., Szel, J. V. and Manos, P., "Analysis, results, and interpretation for radiation between some simply-arranged gray surfaces", J. Heat Transfer 83 (2), 207-214 (1961).

25. Tabor, H., "Selective surfaces for solar collectors", in Jordan, R. C., "Low temperature engineering applications of solar energy", ASHRAE, New York (1967), pp. 41-52.

26. Trombé, F. and Foex, M., "Études diverses sur les collecteurs plats sans concentration d'énergie", in

REFERENCES (continued)

"Applications thermiques de l'énergie solaire dans le domaine de la recherche et de l'industrie", Colloque International No. 85 , Montlouis (1958), pp. 621-638 .

27. Hollands, K. G. T., "Directional selectivity, emittance, and absorptance properties of Vee corrugated specular surfaces", J. sol. Energy Sci. Engng. 7 (3), 108-116 (1963).

28. Close, D. J., "Solar air heaters for low and moderate temperature applications", J. sol. Energy Sci. Engng. 7 (3), 117-124 (1963).

29. Charters, W. W. S., "Some theoretical heat transfer characteristics of Vee corrugated surfaces for use in solar flat plate absorbers", Annual Conf. of A.I.R.A.H. & I.S.B.S., Adelaide (1972).

30. Butler, C. P., Jenkins, R. J. and Parker, W. J., "Solar absorptance and total hemispherical emittance of surfaces for solar energy collection", U.S. Naval Radiological Defense Laboratory, Technical documentary report No. ASD-TR-61-558, San Francisco (1962).

31. Clausen, O. W. and Neu, J. T., "The use of directionally dependent radiation properties for spacecraft thermal control", Astronautica Acta 2 (5), 328-339 (1965).

32. Perlmutter, M. and Howell, J. R., "A strongly directional emitting and absorbing surface", J. Heat Transfer 85 (3), 282-283 (1963).

33. Black, W. Z. and Schoenhals, R. J., "A study of directional radiation properties of specially prepared V-groove cavities", J. Heat Transfer 90 (4), 420-428 (1968).

REFERENCES (continued)

34. Black, W. Z. and Schoenhals, R. J., "An experimental study of radiation heat transfer from parallel plates with direction-dependent properties", J. Heat Transfer 92 (4), 610-615 (1970).

35. Hollands, K. G. T., "A concentrator for thin-film solar cells", Solar Energy 13 (2), 149-163 (1971).

36. Black, W. Z., "Optimization of the directional emission from V-groove and rectangular cavities", J. Heat Transfer 95 (1), 31-36 (1973).

37. Winston, R., "Principles of solar concentrators of a novel design", Solar Energy 16 (2), 89-95 (1974).

38. Bannerot, R. B. and Howell, J. R., "Moderately concentrating flat-plate solar energy collectors", ASME publication 75-HT-54, New York (1975).

39. Wiebelt, J. A. and Thatree, N., "Design and experimental evaluation of a V-groove solar collector", ASME publication 76-HT-53, New York (1976).

40. Siegel, R. and Howell, J. R., "Thermal radiation heat transfer", McGraw-Hill, New York (1972).

41. ASTM Standard E 491 : 1973, "Standard recommended practice for solar simulation for thermal balance testing of spacecraft", Annual Book of ASTM Standards, Part 41, New York (1974).

42. Thekaekara, M. P., "Data on incident solar energy", Suppl. to the Proc. of the 20th Annual Meet. of the Inst. for Environmental Sci., Vol. 21, 21-49 (1974).

43. Dobrusskin, A., "Metal halide lamps with rare earth additives", Ltg. Res. Technol. 3 (2), 125-132 (1971).

REFERENCES (continued)

44. OSRAM G.m.b.H., "HMI 575W - Spectral radiant intensity", MKFO-Nr. 2032, 2033, 4269, München (1974).

45. Bernhard, C. G., Miller, W. H. and Moller, A. R., "The insect corneal nipple array - a biological, broad-band impedance transformer that acts as an antireflection coating", Acta physiol. scand. 63, Suppl. 243, (1965), p. 19 .

46. Gallant, R. W., "Physical Properties of Hydrocarbons", Gulf Publishing Company, Houston, Texas (1968), Vol. 1, pp. 109-123 .

LIST OF APPENDICES

APPENDIX A

Apparent Absorptance of V-Groove Cavities as Derived by Sparrow and Lin [23]

Comment:

The following graphs show the apparent absorptance of 4 V-groove cavities ($\theta = 30^{o}, 60^{o}, 90^{o}, 120^{o}$) as a function of the -

1. Character of incident radiation
2. Reflective properties of the surface
3. Angle of incidence γ
4. Groove angle θ
5. Surface absorptance α.

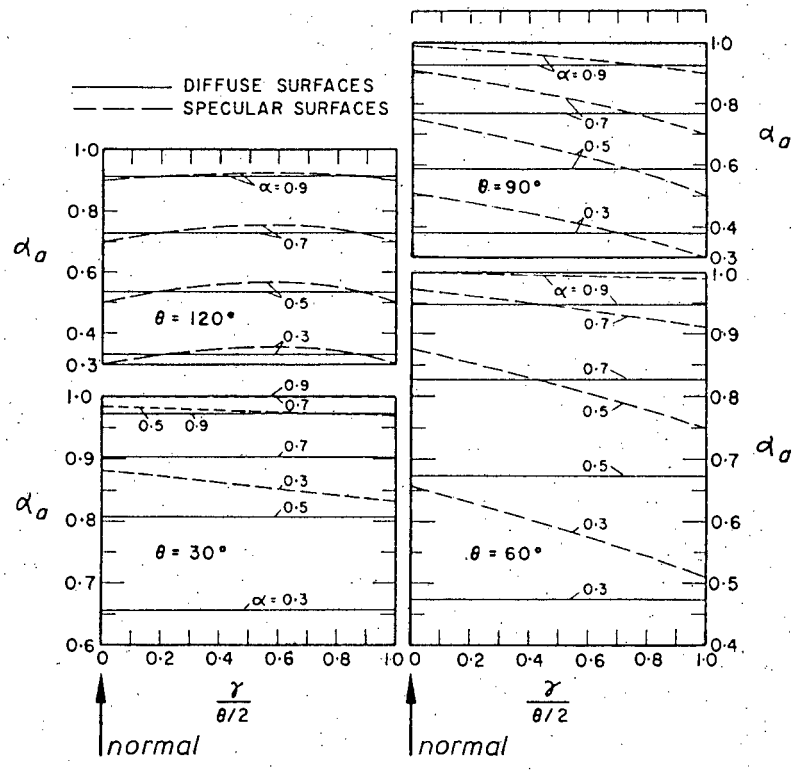

Apparent absorptance for parallel rays incident on a V-groove cavity, (γ = angle of incidence).

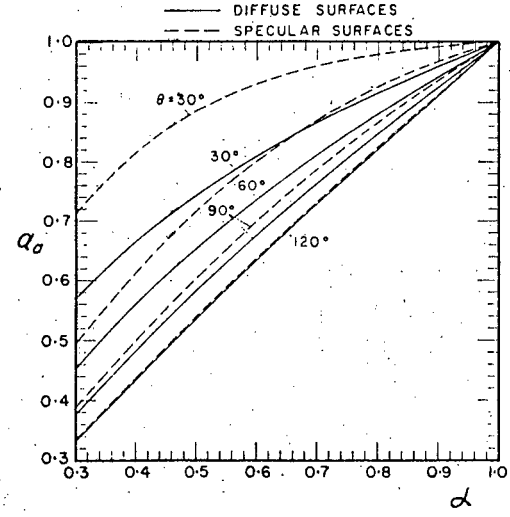

Apparent absorptance for diffuse radiation incident on a V-groove cavity.

APPENDIX B

Apparent Absorptance of V-Groove Cavities as Defined by Equations (28), (30), and (37)

Comment:

The following graphs are reproduced from Figs. 3 - 4 and Fig. 7 on transparencies for comparison purposes.

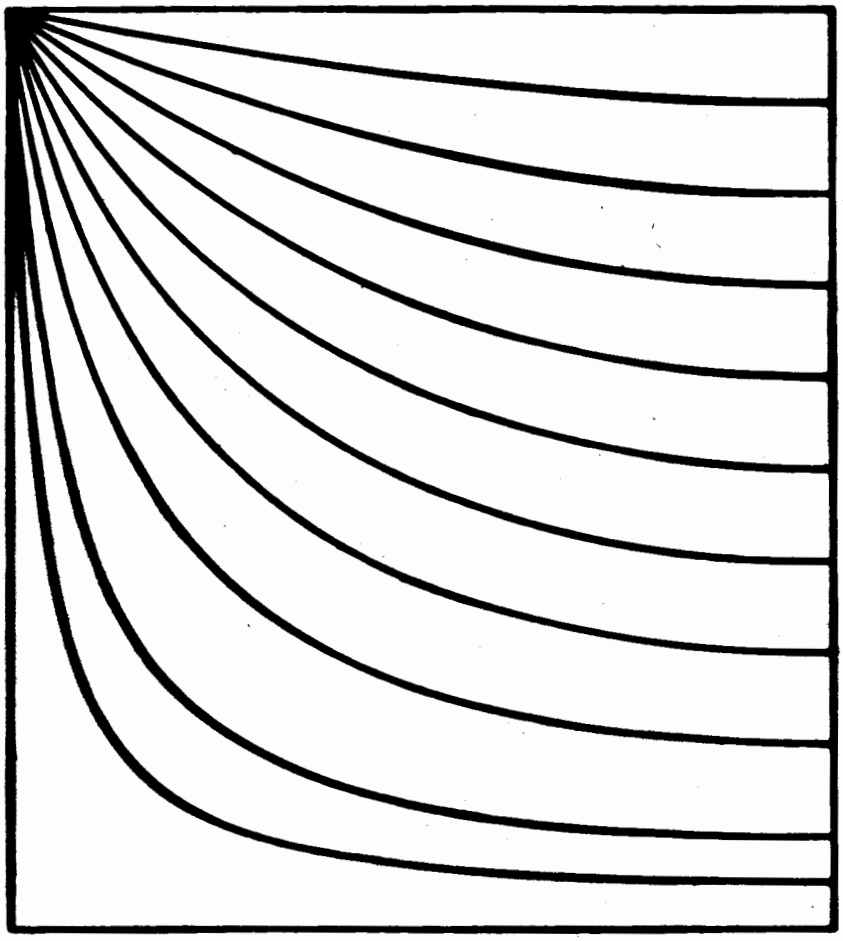

Apparent absorptance of diffuse V-groove cavities as defined by Eq. (30). (Fig. 4)

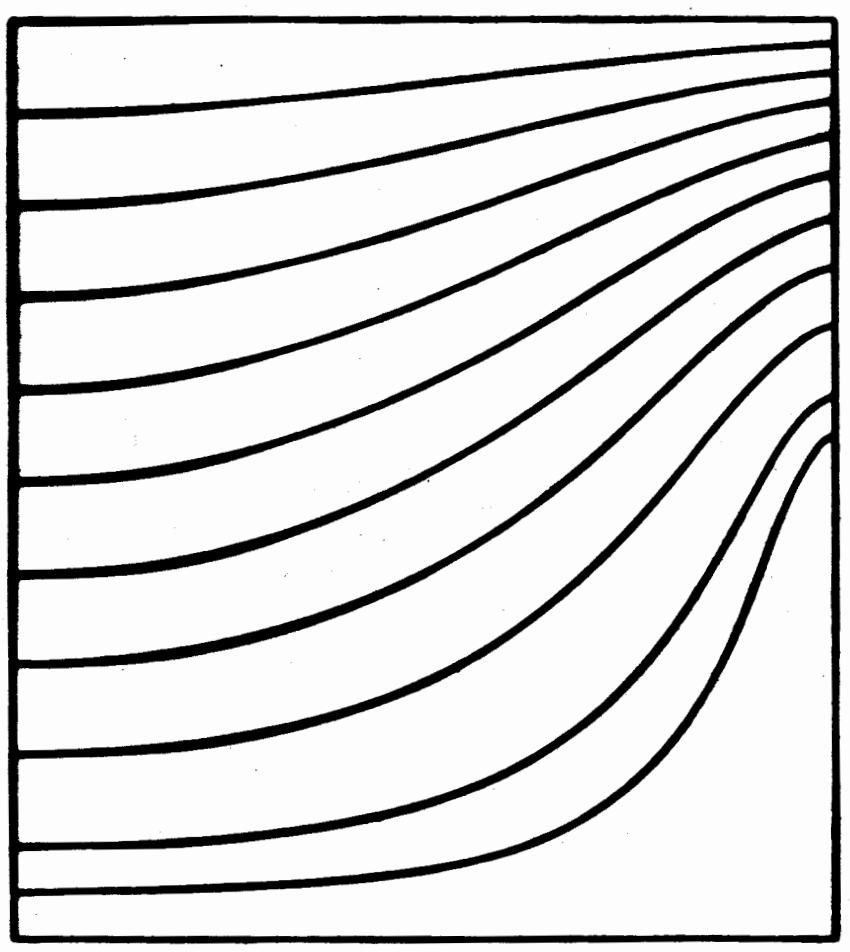

Apparent absorptance of diffuse W-gaseous
cavities as defined by Eq. (28). (Fig. 3)

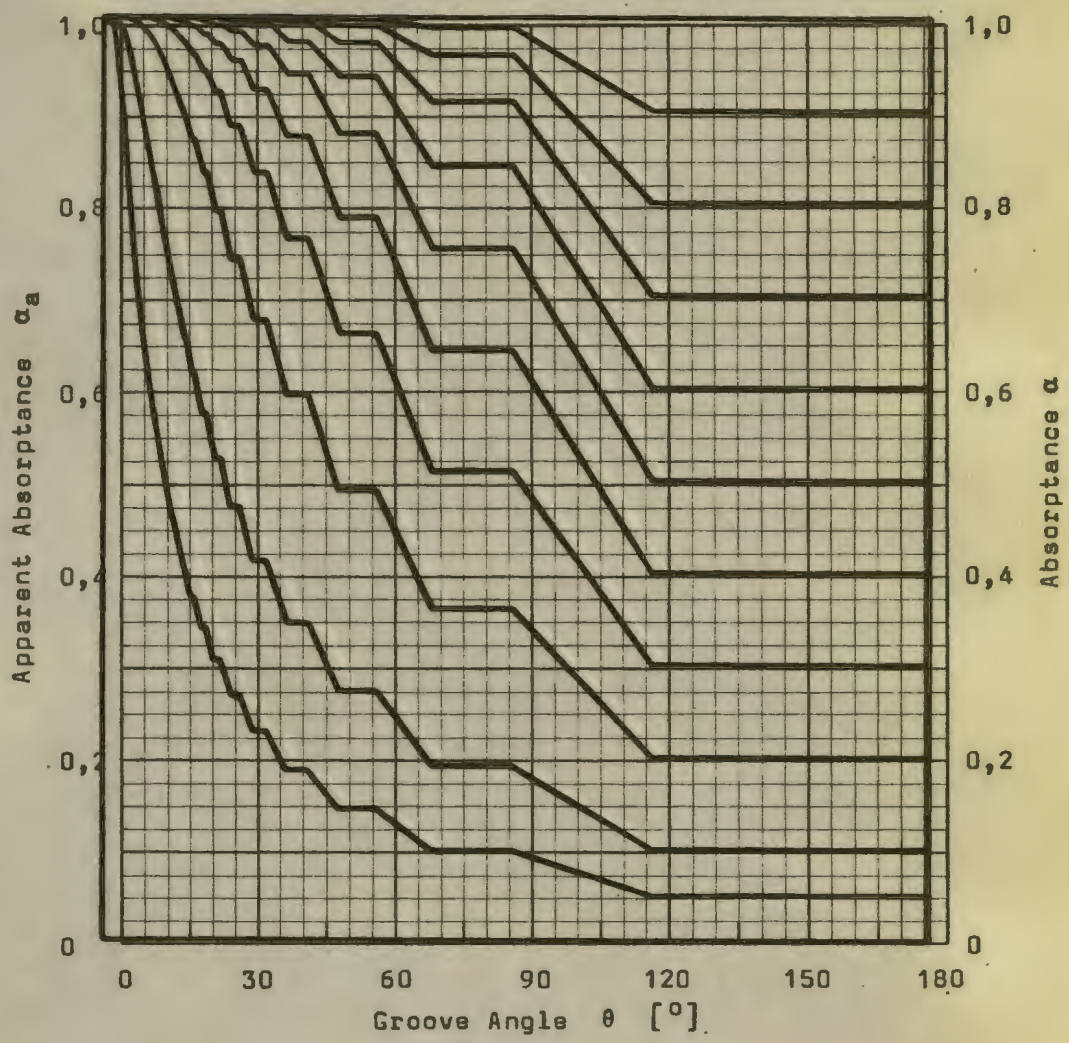

Apparent absorptance of specular V-groove cavities as defined by Eq. (37). (Fig. 7)

APPENDIX C

Solutions for Equations (20),(22),(23) and (34)

Solution for Equation (20)

The integral part $\int_{\infty}^{0} f(\xi,\theta)\, d\xi$ of Equation (20),

$$\beta(0) = 1 - \gamma\beta(0) \int_{\infty}^{0} 1/(\xi^2 + 1 - 2\xi\cos\theta)^{3/2} d\xi ,$$

can be solved by means of standard integral tables. The result is

$$\int_{\infty}^{0} f(\xi,\theta)\, d\xi = \frac{\xi - \cos\theta}{(1 - \cos^2\theta)\sqrt{1 - 2\xi\cos\theta + \xi^2}} \Bigg|_{\infty}^{0}$$

$$= \frac{-\cos\theta}{\sin^2\theta} - \lim_{\xi\to\infty} \frac{1 - (\cos\theta)/\xi}{\sin^2\sqrt{1 - (2\cos\theta)/\xi + 1/\xi^2}}$$

$$= -\frac{\cos\theta}{\sin^2\theta} - \frac{1}{\sin^2\theta}$$

$$= -\frac{1 + \cos\theta}{\sin^2\theta} .$$

With this result, and using the substitution (15), Eq. (20) can be solved for $\beta(0)$:

$$\beta(0) = 1 + \beta(0)\, \frac{\rho\sin^2\theta}{2}\, \frac{1 + \cos\theta}{\sin^2\theta}$$

$$= \frac{1}{1 - \rho/2\ (1 + \cos\theta)}$$

Solution for Equation (22)

The integral part $\int_{\infty}^{\xi} f(\xi,\theta)\, d\xi$ of Eq. (22),

$$\beta(\xi) = 1 - \gamma\,\beta(1) \int_{\infty}^{\xi} 1/(\xi^2 + 1 - 2\,\xi\cos\theta)^{3/2}\, d\xi ,$$

can be solved by means of standard integral tables. The result is (using the integration in App. C-2)

$$f(\xi,\theta) = \frac{\xi - \cos\theta}{(1 - \cos^2\theta)\sqrt{1 - 2\,\xi\cos\theta + \xi^2}} - \frac{1}{\sin^2\theta} \quad .$$

By setting $\xi = 1$ and using substitution (15), Eq. (22) can be solved for $\beta(1)$ as follows:

$$\beta(1) = 1 - \beta(1)\,\frac{\rho\sin^2\theta}{2}\left(\frac{1 - \cos\theta}{\sin^2\theta\; 2\sin\theta/2} - \frac{1}{\sin^2\theta}\right)$$

$$= 1 - \beta(1)\,\frac{\rho\sin^2\theta}{2}\,\frac{\sin\theta/2 - 1}{\sin^2\theta}$$

$$= \frac{1}{1 - \rho/2\,(1 - \sin\theta/2)}$$

Reduction of Equations (33) and (34)

Summing up and rearranging Eqs. (33) and (34) yield

$$\frac{E'_1 + E'_2}{E \sin \theta/2} = (1 + \rho + \rho^2 + \ldots + \rho^{i-2}) \frac{L - L'}{L}$$

$$+ (1 + \rho + \rho^2 + \ldots + \rho^{i-1}) \frac{L'}{L}$$

$$= (1 + \rho + \rho^2 + \ldots + \rho^{i-2})(1 - \frac{L'}{L})$$

$$+ (1 + \rho + \rho^2 + \ldots + \rho^{i-2}) \frac{L'}{L} + \rho^{i-1} \frac{L'}{L}$$

$$= (1 - \rho^{i-1})/(1 - \rho) + \rho^{i-1} \frac{L'}{L}$$

$$= (1 - (1 - \alpha)^{i-1})/\alpha + (1 - \alpha)^{i-1} \frac{L'}{L},$$

since $\rho = 1 - \alpha$.

Inserting this into Eq. (32) yields

$$\alpha_a = \frac{2 L \sin \theta/2}{w} (1 - (1 - \alpha)^{i-1} + \alpha (1 - \alpha)^{i-1} \frac{L'}{L}),$$

and with (17)

$$\alpha_a = 1 - (1 - \alpha)^{i-1} (1 - \alpha \frac{L'}{L}).$$

APPENDIX D

Spectral Energy Distribution of the Metal Halide Lamp Compared with the Solar Spectrum

Comment:

The data for the metal halide short arc lamp OSRAM HMI 575 W is taken from [43, 44]. The data on incident solar radiation is replotted from [42].

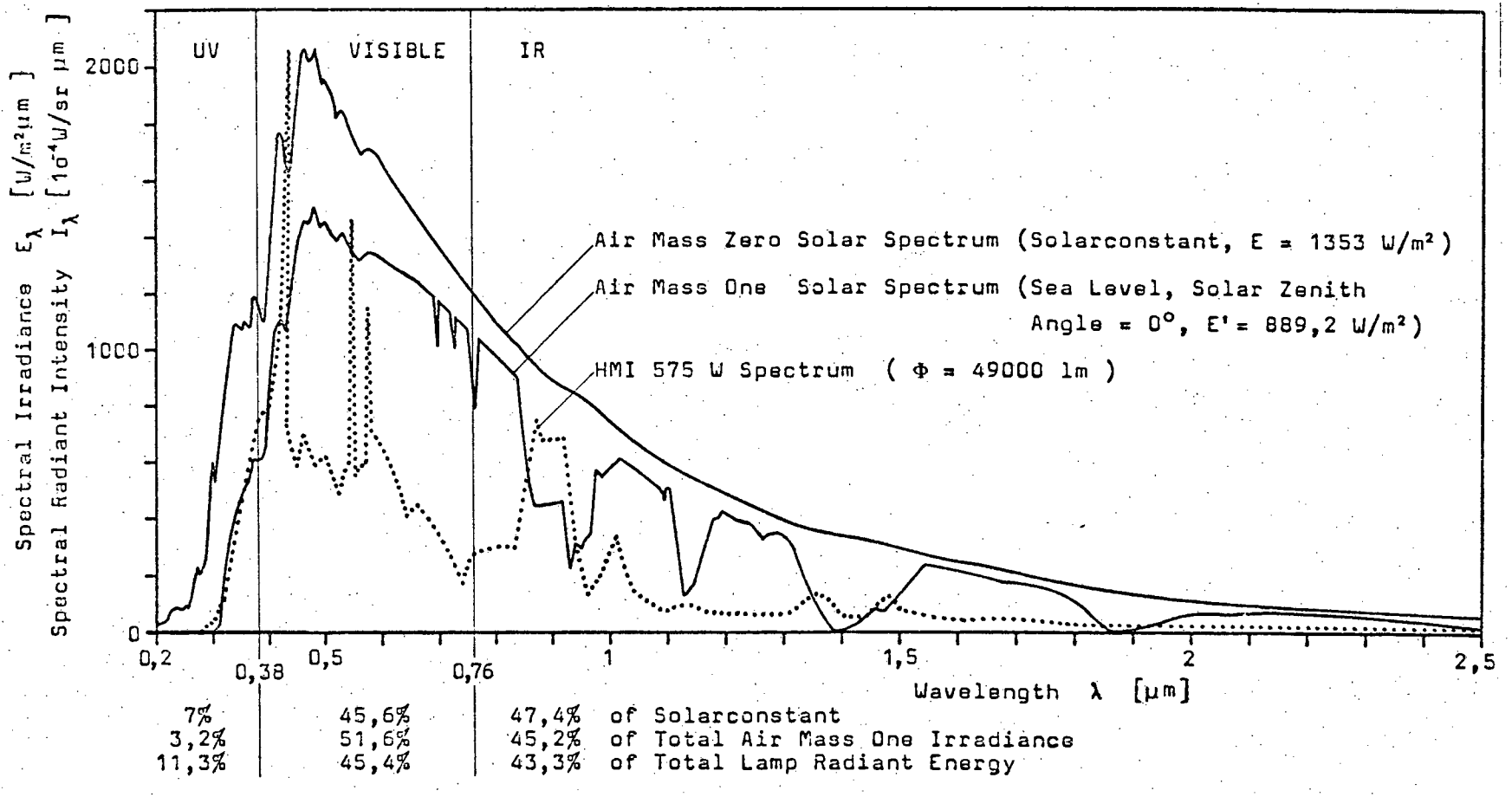

Spectral Energy Distribution of the Metal Halide Lamp Compared with the Solar Spectrum.

APPENDIX E

Tabulated Specifications of Test Specimens

Comment:

The "Actual Specifications" represent the arithmetic means of microscopic measurements. For used symbols see Fig. 13 and nomenclature.

Material of specimens: Brass (DENVA A01)
58% Cu, 39% Zn, 3% Pb

Black spray paint: KRYLON High Heat

	Nominal Specifications								Actual Specifications						
No	θ	d	l	w	w/l	w+l=p	n	A'	l	w	w/l	d/l	n	Fig.	Remarks
	deg	mm	mm	mm		mm		%	mm	mm					
1	45	0,1	0,1	0,083	0,83	0,183	485	173	0,05	0,135	2,7	2	480	21 - 23	off-size
2	"	0,2	"	0,166	1,66	0,266	334	200	0,045	0,223	4,96	4	331		
3	"	0,4	"	0,331	3,31	0,431	205	224	0,048	0,387	8,06	8	204		
4	"	0,6	"	0,497	4,97	0,597	148	234	0,022	0,575	26,14	27	148		
5	"	0,8	"	0,663	6,63	0,763	116	240	0,069	0,694	10,06	12	116		
6	"	1,0	"	0,828	8,28	0,928	95	244	0,035	0,893	25,51	29	95		
7	"	2,0	"	1,657	16,57	1,757	50	252	0,046	1,711	37,2	43	50		
8	"	3,0	"	2,485	24,85	2,585	34	262	0,048	2,537	52,85	63	34		
9	"	0,1	0,042	0,083	1,97	0,125	712	207	0,033	0,092	2,79	3	712	24 - 25	off-size
10	"	0,2	0,084	0,166	"	0,25	356	207	0,06	0,19	3,17	3	356		
11	"	0,4	0,169	0,331	"	0,5	178	207	0,122	0,378	3,1	3	178		
12	"	0,6	0,253	0,497	"	0,75	119	207	0,104	0,646	6,21	6	119		
13	"	0,8	0,337	0,663	"	1,0	89	207	0,24	0,76	3,17	3	89		
14	"	1,0	0,422	0,828	"	1,25	71	207	0,341	0,909	2,67	3	71		
15	"	2,0	0,843	1,657	"	2,5	35	205	0,753	1,747	2,32	3	35		
16	"	3,0	1,265	2,485	"	3,75	24	208	1,186	2,564	2,16	3	24		

H = 5 mm, D = 89 mmØ, A = 0,006221 m^2

Specifications of specimens.

	Nominal Specifications								Actual Specifications						
No	θ	d	l	w	w/l	w+l=p	n	A'	l	w	w/l	d/l	n	Fig.	Remarks
	deg	mm	mm	mm		mm		ft^2	mm	mm					
17	15	2	0,093	0,527	5,67	0,62	143	664	0,044	0,576	13,09	45	143	26 - 28	
18	20	"	0,124	0,705	"	0,83	107	504	0,027	0,803	29,74	74	107		off-size
19	25	"	0,156	0,887	"	1,043	85	407	0,021	1,029	49,0	95	84		off-size
20	30	"	0,189	1,072	"	1,261	70	341	0,054	1,207	22,35	37	70		off-size
21	45	"	0,292	1,657	"	1,949	45	235	0,215	1,734	8,07	9	45		
22	60	"	0,408	2,309	"	2,717	32	183	0,294	2,423	8,24	7	32		
23	90	"	0,706	4,0	"	4,706	19	135	0,538	4,168	7.75	4	19		
24	10	2	0,24	0,35	1,46	0,59	150	736	0,209	0,381	1,82	10	150	29 - 30	
25	15	"	0,22	0,527	2,39	0,747	118	584	0,137	0,61	4,45	15	118		
26	20	"	0,2	0,705	3,53	0,905	98	484	0,074	0,831	11,23	27	98		
27	25	"	0,18	0,887	4,93	1,067	83	413	0,047	1,02	21,7	43	83		off-size
28	30	"	0,16	1,072	6,7	1,232	72	359	0,068	1,164	17,12	30	72		
29	45	"	0,1	1,657	16,57	1,757	50	252	0,046	1,711	37,2	43	50		off-size
30	60	"	0,1	2,309	23,09	2,409	36	203	0,091	2,318	25,47	22	36		
31	90	"	0,1	4,0	40,0	4,1	21	147	0,091	4,009	44,05	22	21		
32	-	-	-	-	-	-	-	100	-	-	-	-	-	31	flat
33	-	-	-	-	-	-	-	"	-	-	-	-	-		flat, black
34	-	-	-	-	-	-	-	"	-	-	-	-	-		flat,specular
35	30	2	0,16	1,072	6,7	1,232	72	359	0,068	1,164	17,12	30	72		
36	"	"	"	"	"	"	"	"	0,082	1,15	14,02	24	"		black
37	"	"	"	"	"	"	"	"	0,07	1,162	16,6	29	"		specular

Specifications of specimens - continued.

APPENDIX F

Microscope Photographs Showing the Cross Sections of Specimens No. 1 - 8 and No. 17 - 23

Note:

Photographs are taken at 4 different magnifications.

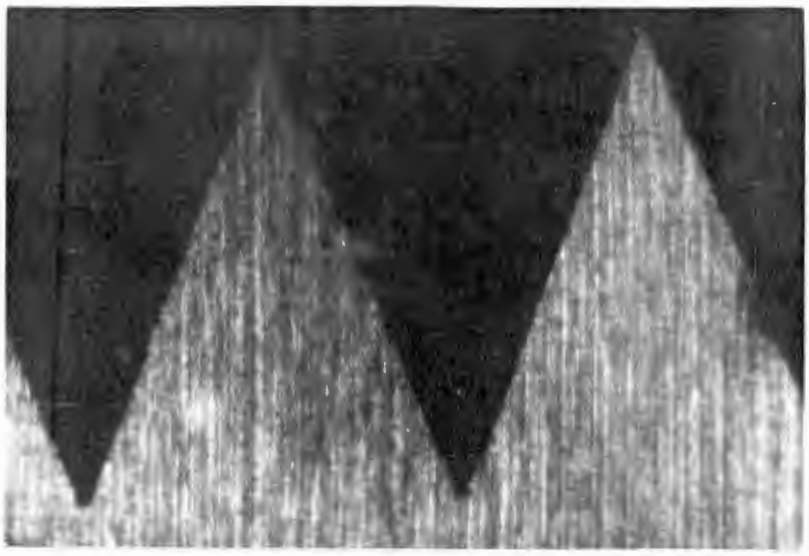

No. 8

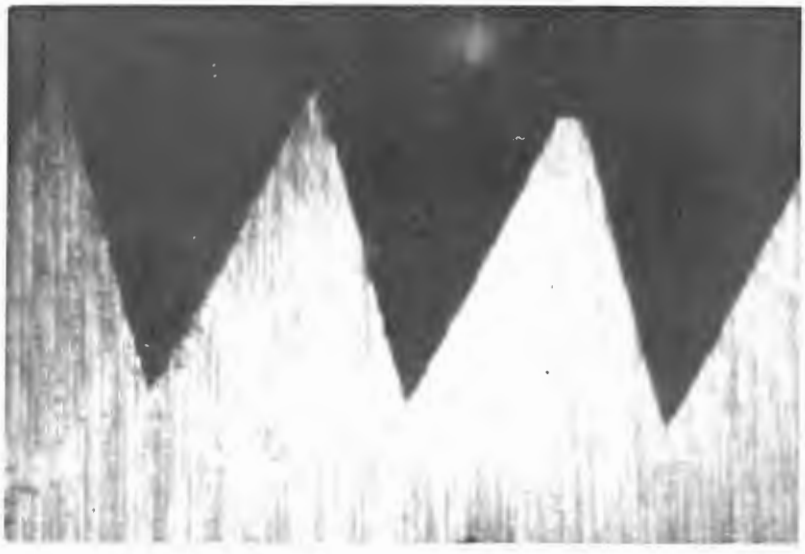

No. 7

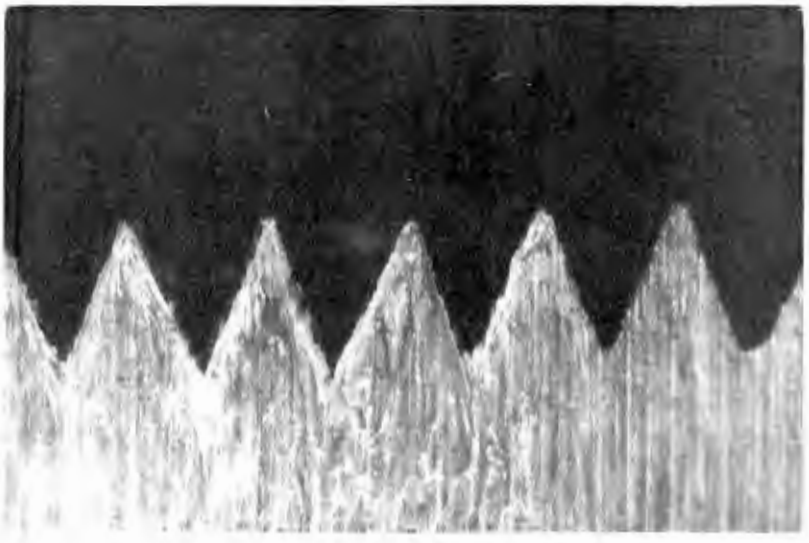

No. 6

Magnification 19x

1 mm

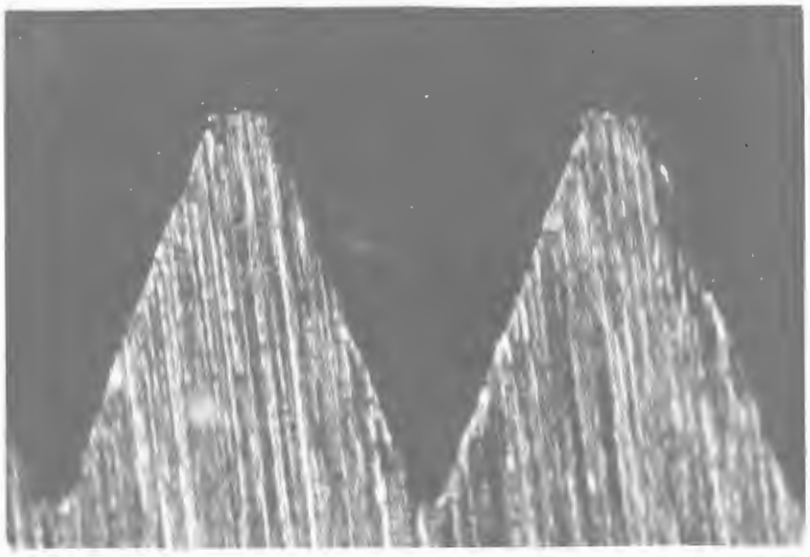

No. 5

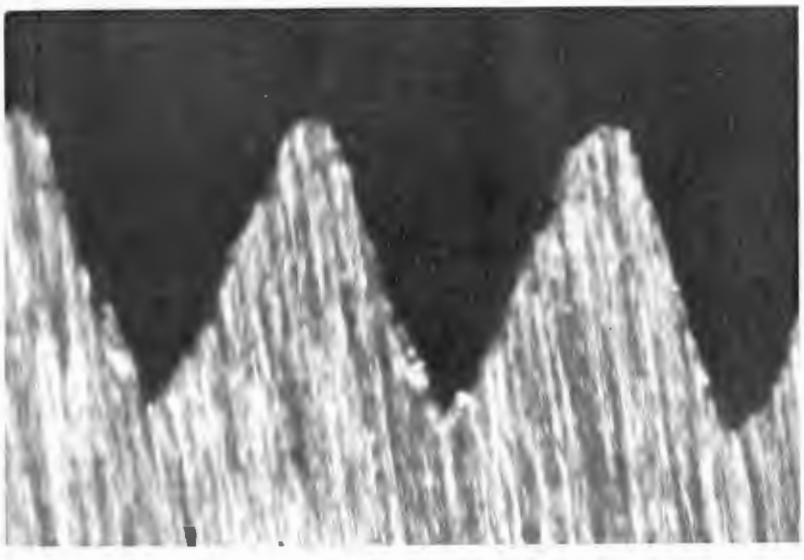

No. 4

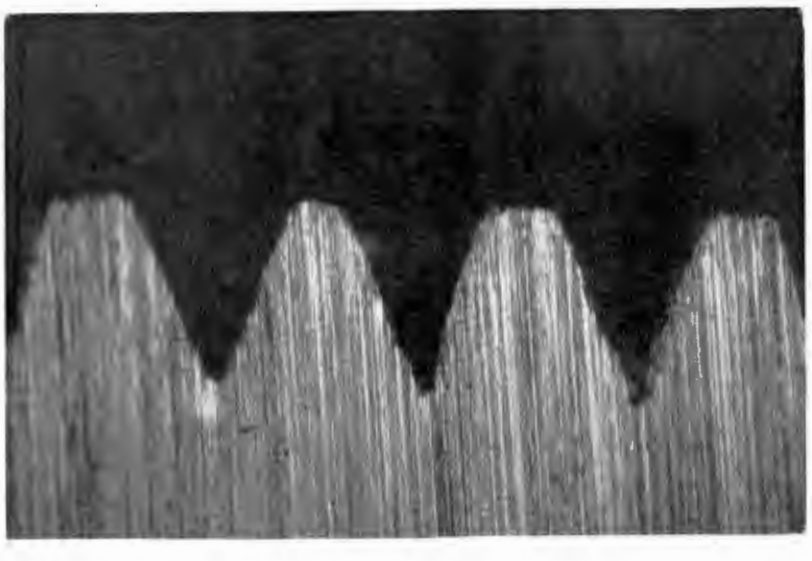

No. 3

Magnification 65x

1 mm

No. 2

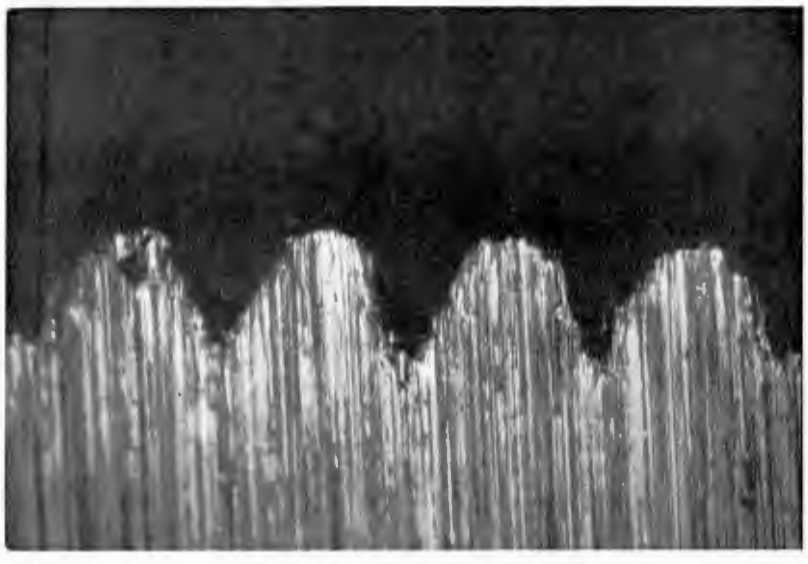

No. 1

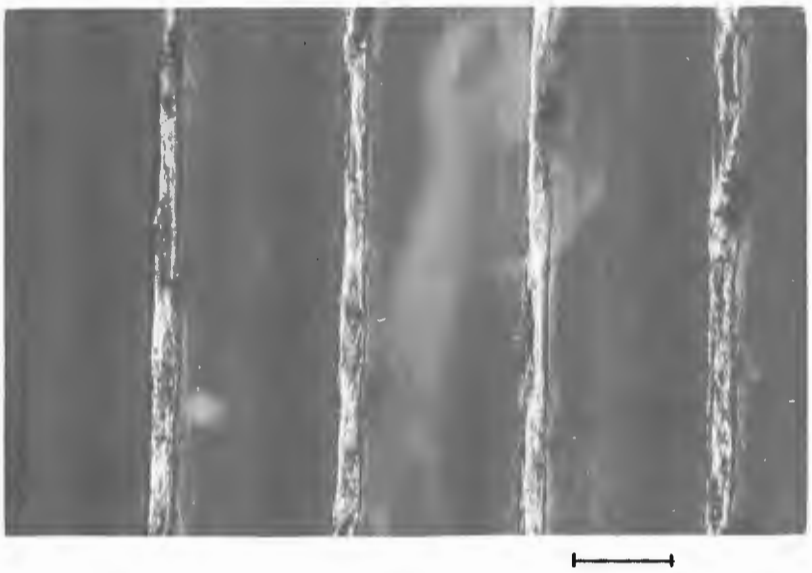

No. 1

Top view

Magnification 131x 1/10 mm

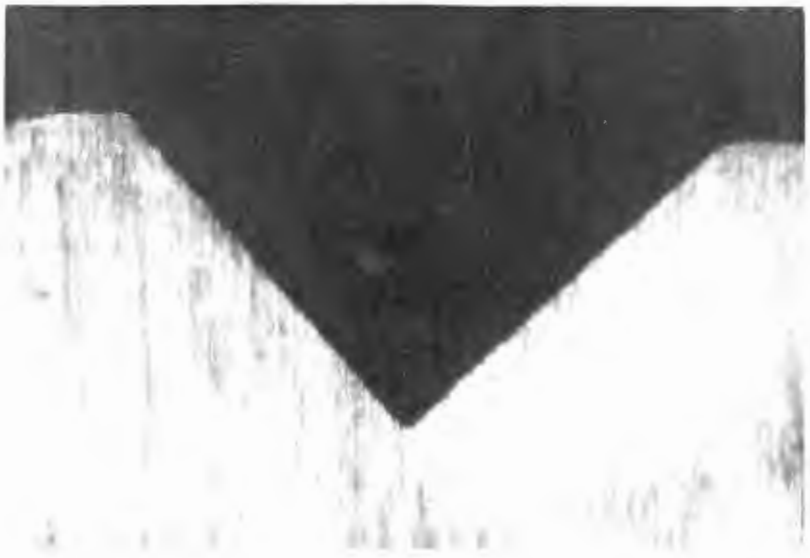

No. 23

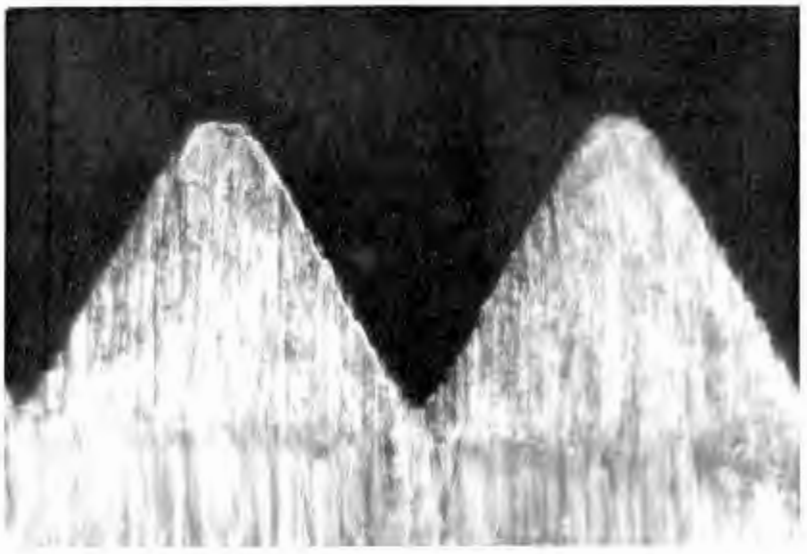

No. 22

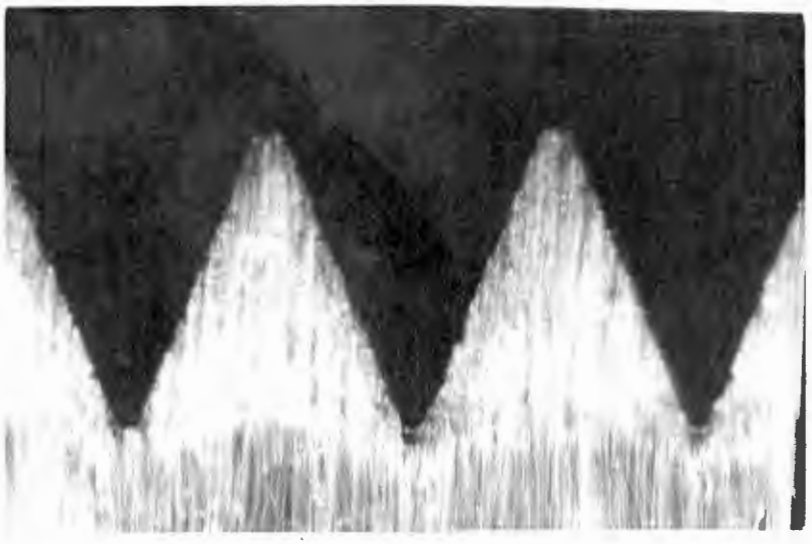

No. 21

Magnification 19x

1mm

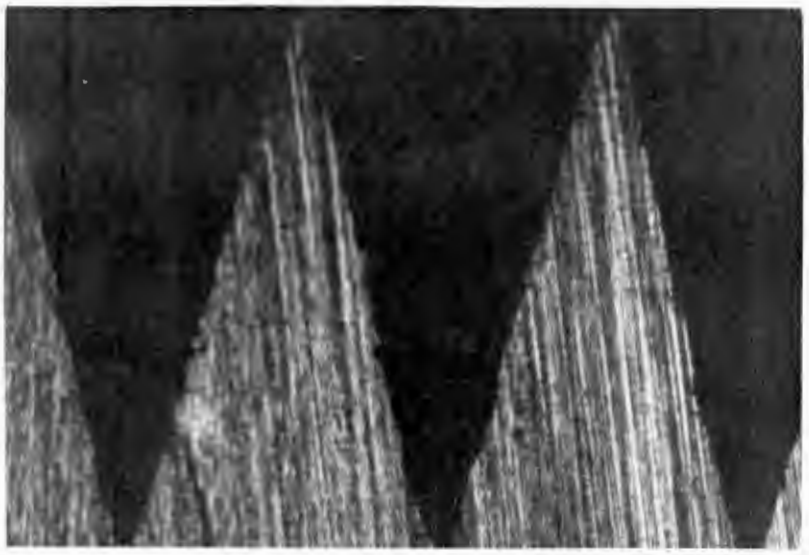

No. 20

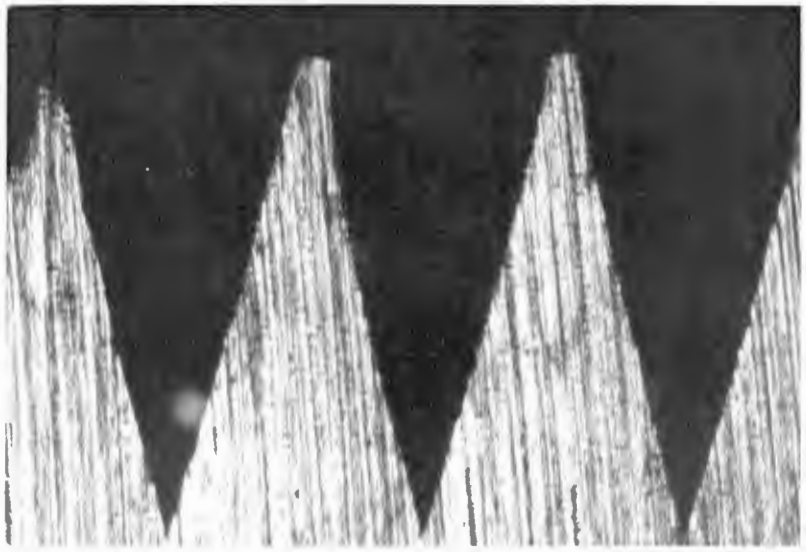

No. 19

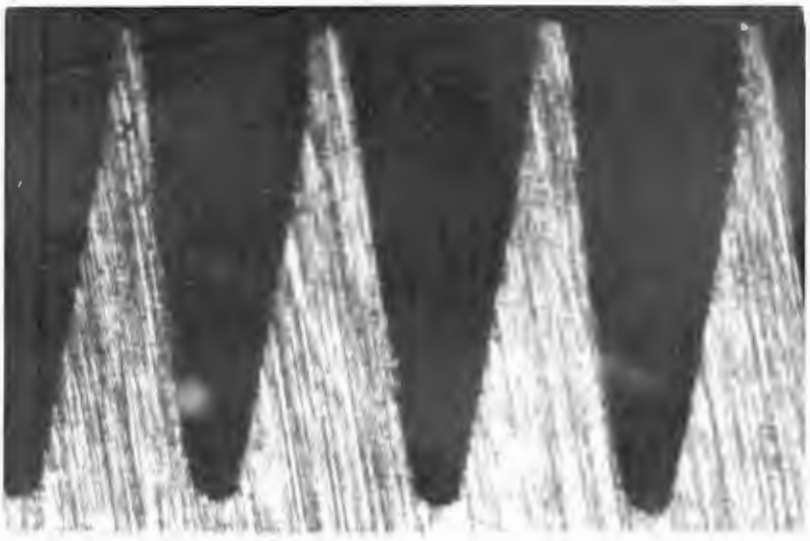

No. 18

Magnification 32,5x ⟵1 mm⟶

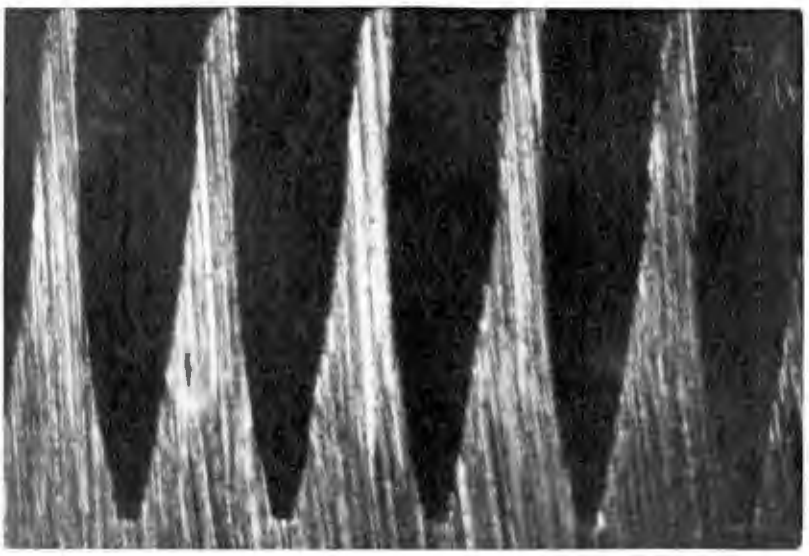

No. 17

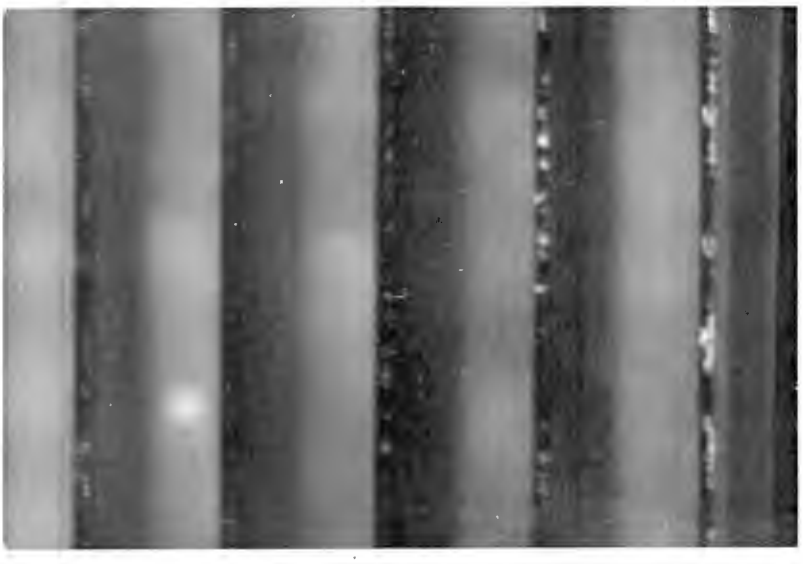

No. 17

Top view

Magnification 32,5x ⊢——1 mm——⊣

APPENDIX G

Sample Calculations

(Specimen No. 28)

I. Relevant Equations

As shown in Section 3.4, the experimental investigation is based on Eqs. (44), (45), (47), and (48):

$$\eta = \frac{\dot{m}\,(\bar{c}_{p2}\,T_2 - \bar{c}_{p1}\,T_1)}{EA}\;100\,\%$$

$$\eta_{rel} = \frac{\eta}{\eta_{32}}$$

$$q_1 = \dot{m}^*(\bar{c}^*_{p1}\,T^*_1 - \bar{c}^*_{p2}\,T^*_2)$$

$$\alpha_{eff} = \frac{\dot{m}\,(\bar{c}_{p2}\,T_2 - \bar{c}_{p1}\,T_1) + \dot{m}^*(\bar{c}^*_{p1}\,T^*_1 - \bar{c}^*_{p2}\,T^*_2)}{EA}$$

These equations were used in a calculator program (Texas Instruments SR 52) for evaluation of results.

II. Readings Obtained for Specimen No. 28

By using the experimental procedure as described in Section 3.4.2, the following readings were obtained for specimen No. 28 :

(The corresponding temperature recording chart is attached)

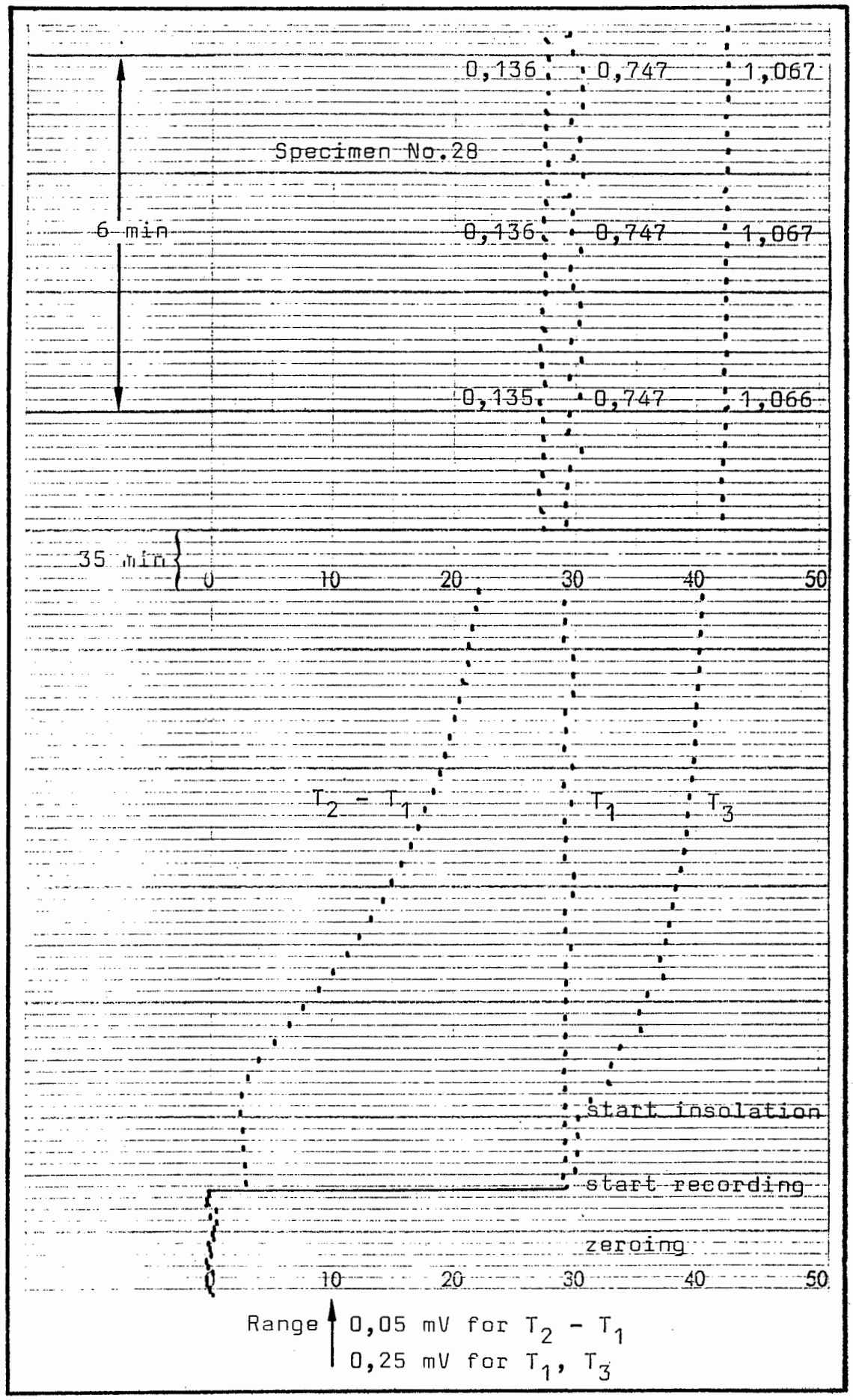

Temperature recording chart.

Readings:

Irradiance on specimen	E	= 15,86	mV
Flow rate of glycol	$\dot{m}$	= 204,4	g/6 min
Ambient air temperature	T_0	= 18,5	^{o}C
Glycol temperature at calorimeter inlet	T_1	= 0,136	mV
Temperature difference of glycol between calorimeter outlet and inlet	$T_2 - T_1$	= 0,747	mV
Surface temperature of specimen	T_3	= 1,067	mV

III. Conversion and Interpolation Equations

The readings were entered in the calculator program for conversion and computation. The following conversion procedures and interpolation equations were used in the program:

a) Given calibration for solarimeter,

$$1 \text{ mV EMF} = 0{,}0118^{-1} \text{ W/m}^2 .$$

b) The copper-constantan thermocouples were calibrated in situ by means of a 3rd degree Lagrange interpolation equation applied to 4 key temperatures (0 ^{o}C, 33,00 ^{o}C, 66,00 ^{o}C, 99,68 ^{o}C). The smooth temperature-EMF relationship,

$$T\,[^{o}C] = f(U\,[\text{mV EMF}]),$$

generated by this method is

$$T = 25{,}78\ U - 0{,}6392\ U^2 + 0{,}015568\ U^3 .$$

c) The temperature dependent specific heat of glycol (99 % ethylene glycol) was determined by applying a linear interpolation equation to 2 key values taken from [46]. The temperature-specific-heat relationship,

$$c_p\ [Wh/kg^oC] = f(T\ [^oC]),$$

generated by this method is

$$c_p = 0{,}0013\ T + 0{,}647 .$$

d) The total heat losses, q_1, of the system at the temperature difference $(T_3 - T_0)^*$ were found by using a least square method. As shown in App. K, a least square curve fit was applied to the relevant experimental results for q_1, which are plotted in App. I. For realistic approximation, a quartic regression equation of the type

$$q = a\ \Delta T + b\ \Delta T^4$$

was chosen. With reference to specimen No. 28 and App. K the relevant regression equation is

$$q_1 = 0{,}153\ (T_3 - T_0) + 0{,}787 \times 10^{-7}\ (T_3 - T_0)^4 .$$

e) The efficiency η_{32} of the flat reference specimen No. 32 at the temperature difference $(T_3 - T_0)^*$ was also found by using a least square curve fit. A linear regression equation was applied to the relevant experimental results obtained for η_{32}. With reference to App. K

the relevant regression equation is

$$\eta_{32} = 44{,}20 - 1{,}873\,(T_3 - T_0)\,.$$

This equation provides also a means for determining the absorptance of brass, the material from which all specimens were machined. Under the hypothetic assumption that no heat losses occur, i.e., $T_3 - T_0 = 0$, $\eta_{32}/100$ equals α_{32} (see Eqs. (44) and (48)). Hence it follows, in agreement with App. J, that

$$\alpha_{brass} = \alpha_{32} = \eta_{32}/100 = 0{,}44\,.$$

IV. Experimental Results for Specimen No. 28

Subject to Sections II and III, the final results for specimen No. 28 are as follows:

E	=	1344	W/m^2
A	=	0,006221	m^2
$\dot{m}$	=	2,044	kg/h
T_0	=	18,50	^oC
T_1	=	18,91	^oC
T_2	=	22,28	^oC
T_3	=	26,80	^oC
$\bar{c}_{p1}$	=	0,659	Wh/kg^oC
$\bar{c}_{p2}$	=	0,661	Wh/kg^oC
$T_3 - T_0$	=	8,3	^oC
q_1	=	1,27	W
η_{32}	=	28,65	%
α	=	0,44	

The computation (program) yields:

$$\eta = \frac{2{,}044\ (0{,}661 \times 22{,}28 - 0{,}659 \times 18{,}91)}{1344 \times 0{,}006221} \times 100\,\%$$

$$= 55{,}38\,\%$$

$$\eta_{rel} = \frac{55{,}38}{28{,}65}$$

$$= 1{,}93$$

$$\alpha_{eff} = \frac{2{,}044\ (0{,}661 \times 22{,}28 - 0{,}659 \times 18{,}91) + 1{,}27}{1344 \times 0{,}006221}$$

$$= 0{,}71$$

These experimental results, $\alpha_{eff} = 0{,}71$ and $\eta_{rel} = 1{,}93$, are labeled with Z_1 in Fig. 29 and Z_2 in Fig. 30 respectively.

V. Theoretical Results for Specimen No. 28

The corresponding theoretical (nominal) values for α_{eff}, plotted in Fig. 29 for the purpose of comparison, are labeled with

- Z_3 using actual groove data and assuming diffuse surface properties,
- Z_4 using nominal groove data and assuming diffuse surface properties,
- Z_5 using nominal groove data and assuming specular surface properties.

The different values for α_{eff} are computed by evaluation of Eq. (40) in conjunction with Eqs. (28) and (37) (cf. Section 2.4). Using the relevant actual/nominal groove parameters

$$\theta = 30^{o}$$

$$\frac{w}{l} = 2\frac{d}{l}\tan\frac{\theta}{2} = 17,12 \;/\; 6,7$$

for specimen No. 28 (App. E), it follows:

$$\alpha_{a,d} = 0,44\left(\frac{1}{2 - (1 - 0,44)(1 + \cos 30^{o})} + \frac{1}{2 - (1 - 0,44)(1 - \sin 15^{o})}\right)$$

$$= 0,74$$

$$\alpha_{a,s} = 1 - (1 - 0,44)^{6}$$

$$= 0,97$$

With respect to Z_3:

$$\alpha_{eff,d} = \frac{0,74 \times 17,12 + 0,44}{1 + 17,12}$$

$$= 0,72$$

With respect to Z_4:

$$\alpha_{eff,d} = \frac{0,74 \times 6,7 + 0,44}{1 + 6,7}$$

$$= 0,70$$

With respect to Z_5:

$$\alpha_{eff,s} = \frac{0,97 \times 6,7 + 0,44}{1 + 6,7}$$

$$= 0,90$$

It may be seen that--in this case--the experimentally obtained effective absorptance, α_{eff}, equals the theoretically obtained effective absorptance (cf. Z_1 and Z_3 in Fig. 29). The accuracy of the above results is discussed in App. H (Error Analysis).

APPENDIX H

Error Analysis

I. Introduction

From the point of view of reliability estimates, experiments--in general--fall into two main categories: single-sample experiments and multiple-sample experiments. Uncertainties of the latter are evaluated by repetition and estimated by means of statistical methods, thus providing a high reliability and accuracy.

Multiple-sample experiments were carried out with the flat reference specimen No. 32 as shown in App. J. It was found that the resulting absorptance of this specimen, $\alpha = 0{,}44$, can be regarded with 95 % confidence as being accurate within $\pm$ 2,8 %.

All other experiments fall into the first category. Although they are not single-sample experiments (they were carried out at least twice), further repetitions were neither sensible nor possible because of the length of time involved. It must be remembered that each experiment (620 in total) required a settling time between 30 and 120 minutes. What is more, the absolute values of absorptance and efficiency are of less significance than

their overall trend. This has been discussed in Chapter 5.

However, the analysis will show that the errors in measurements were so small as not to affect the trends being inferred from the experimental results.

II. Analysis

Inspection of Eq. (44) and (48) reveals that the main experimental results for η and α_{eff} are governed by the expression

$$e = \frac{\dot{m}\, c_p\, \Delta T}{E\, A} .$$

The overall, most probable, error in evaluation of the above expression can be defined according to the Error Propagation Law:

$$(\delta e)^2 = \left(\frac{\delta e}{\delta \dot{m}}\, \delta \dot{m}\right)^2 + \left(\frac{\delta e}{\delta c_p}\, \delta c_p\right)^2 + \left(\frac{\delta e}{\delta \Delta T}\, \delta \Delta T\right)^2 + \left(\frac{\delta e}{\delta E}\, \delta E\right)^2 + \left(\frac{\delta e}{\delta A}\, \delta A\right)^2$$

Performing the partial derivations and dividing by e yields

$$\frac{\delta e}{e} = \left[\left(\frac{\delta \dot{m}}{\dot{m}}\right)^2 + \left(\frac{\delta c_p}{c_p}\right)^2 + \left(\frac{\delta \Delta T}{\Delta T}\right)^2 + \left(\frac{\delta E}{E}\right)^2\right]^{1/2}.$$

For evaluation of this fractional error, $\delta e/e$, the four error contributions, $\delta \dot{m}$, δc_p, $\delta \Delta T$, and δE, have to be

determined as follows:

a) The flow rate of the glycol was measured by means of a stopwatch and a balance, resulting in

$$\dot{m} = G\,[g]/t\,[sec]\,.$$

Assuming an error of $\pm$ 0,2 g in weighting and an error of $\pm$ 0,2 sec in measuring the time interval (6 min), the maximum error in the average flow rate, $\bar{\dot{m}}$ = 200 g / 6 min, can be calculated as follows:

$$\delta\bar{\dot{m}} = \pm \left(\frac{\delta\bar{\dot{m}}}{\delta G}\,\delta G + \frac{\delta\bar{\dot{m}}}{\delta t}\,\delta t \right)$$

$$= \pm \left(\frac{\delta G}{t} + \frac{G}{t^2}\,\delta t \right)$$

$$= \pm \left(\frac{0,2}{360} + \frac{200}{360^2} \times 0,2 \right) g/sec$$

$$= \pm\ 0,009\ kg/h$$

b) The specific heat of ethylene glycol, as taken from [46], can be regarded as being accurate within $\pm$ 0,005 cal/g^{o}C. Hence it appears that c_p is accurate within $\pm$ 0,006 Wh/kg^{o}C.

c) The temperature readings taken after in situ calibration of the thermocouples (see App. G-3) proved to be accurate within $\pm$ 0,05 ^{o}C, as compared to standard thermometer readings. Hence ΔT is accurate within $\pm$ 0,05 ^{o}C.

d) The uncertainty of the measured irradiance E is a function of the following factors:

1. The stability (<3 %) of the irradiation incident on the specimen surface area
2. The manufacturer's stated accuracy of the solarimeter being <± 1 % of output
3. The manufacturer's stated accuracy of the digital millivoltmeter being ± (0,03 % of reading ± 0,02 % of range)

It is obvious that the errors caused by the instruments are negligible, as compared to the fluctuation in irradiance. Therefore, the irradiance can be regarded as being accurate within ± 3 %.

With this information (a-d) on hand, the overall, most probable error, $\delta e/e$, can be evaluated. This is carried out for the experimental results obtained for specimen No. 28 (see App. G-5) as follows:

$$\frac{\delta e}{e} = \left[\left(\frac{0,009}{2,044}\right)^2 + \left(\frac{0,006}{0,659}\right)^2 + \left(\frac{0,05}{8,3}\right)^2 + (0,03)^2\right]^{1/2} \times 100\,\%$$

$$= (1,9 \times 10^{-5} + 8,3 \times 10^{-5} + 3,6 \times 10^{-5} + 9 \times 10^{-4})^{1/2} \times 100\,\%$$

$$= 3\,\%$$

Inspection of the above computation reveals that the overall error is mainly affected by the error in E, i.e., by the stability of the irradiation.

Applying the above overall error of 3 % to the results obtained for specimen No. 28 shows that the trend of the experimental points plotted in Figs. 29 and 30 can hardly be affected:

$$\eta_{rel} = 1{,}93 \pm 0{,}06$$

$$\alpha_{eff} = 0{,}71 \pm 0{,}02$$

The calculated overall error of 3 % compares favourably with the error in α of specimen No. 32 , which was found to be 2,8 % (see App. J).

APPENDIX I

Total Heat Losses of Specimens

Comment:

The experimental determination (described in Section 3.4.3) of the total heat losses of a selection of specimens was required for the evaluation of Eq. (48), i.e., of α_{eff}. It is worth mentioning that, as far as the working temperatures are concerned, the groove depth as well as the groove angle had no significant influence on the total heat loss of a specimen. A significant increase in heat loss with decreasing groove angle occured only at high temperatures (see App. I-4).

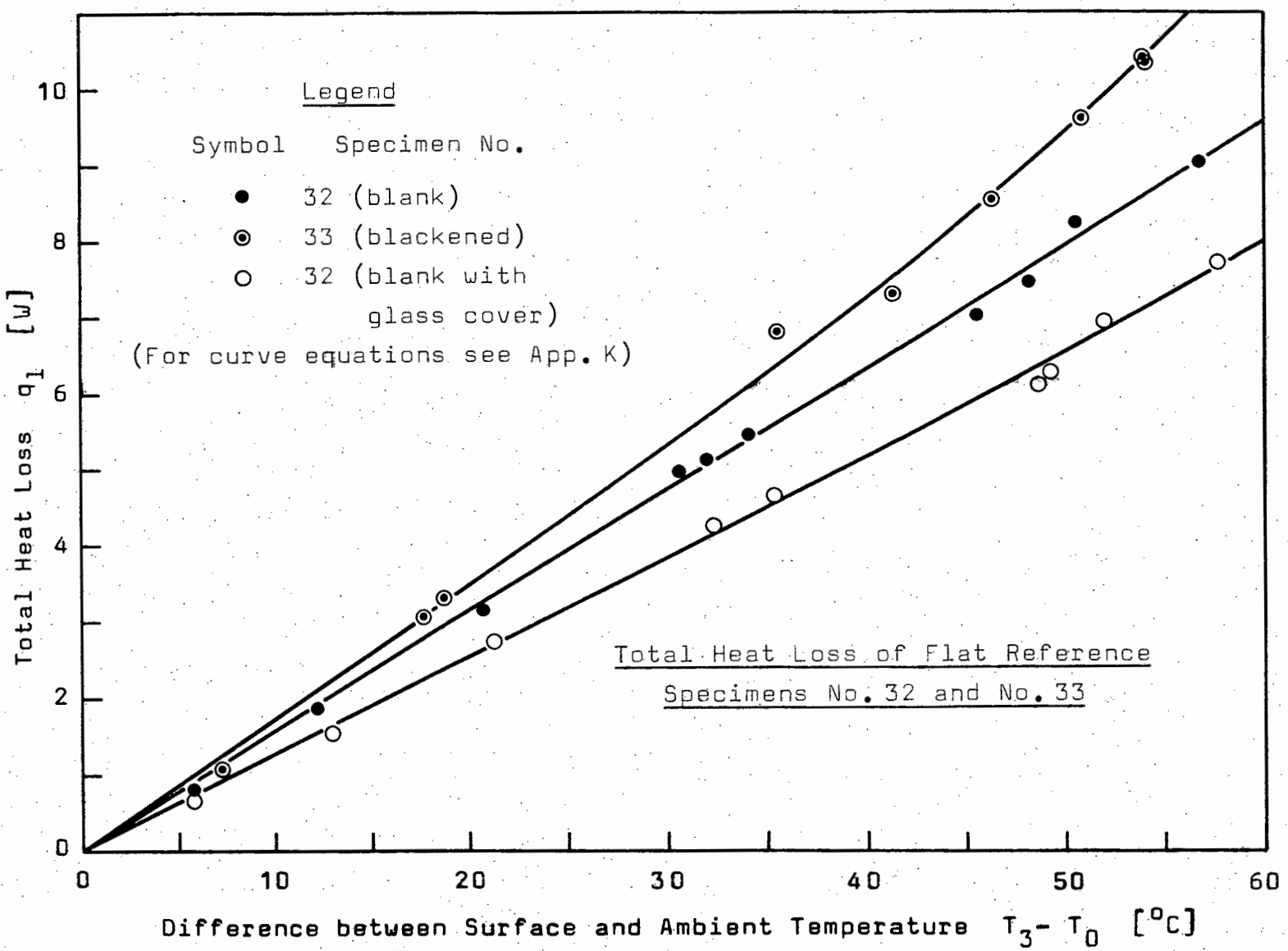
Legend
Symbol Specimen No.
32 (blank)
33 (blackened)
32 (blank with glass cover)
(For curve equations see App. K)
Total Heat Loss of Flat Reference Specimens No. 32 and No. 33
Total Heat Loss q_1 [W]
Difference between Surface and Ambient Temperature $T_3 - T_0$ [°C]
0
2
4
6
8
10
0
10
20
30
40
50
60

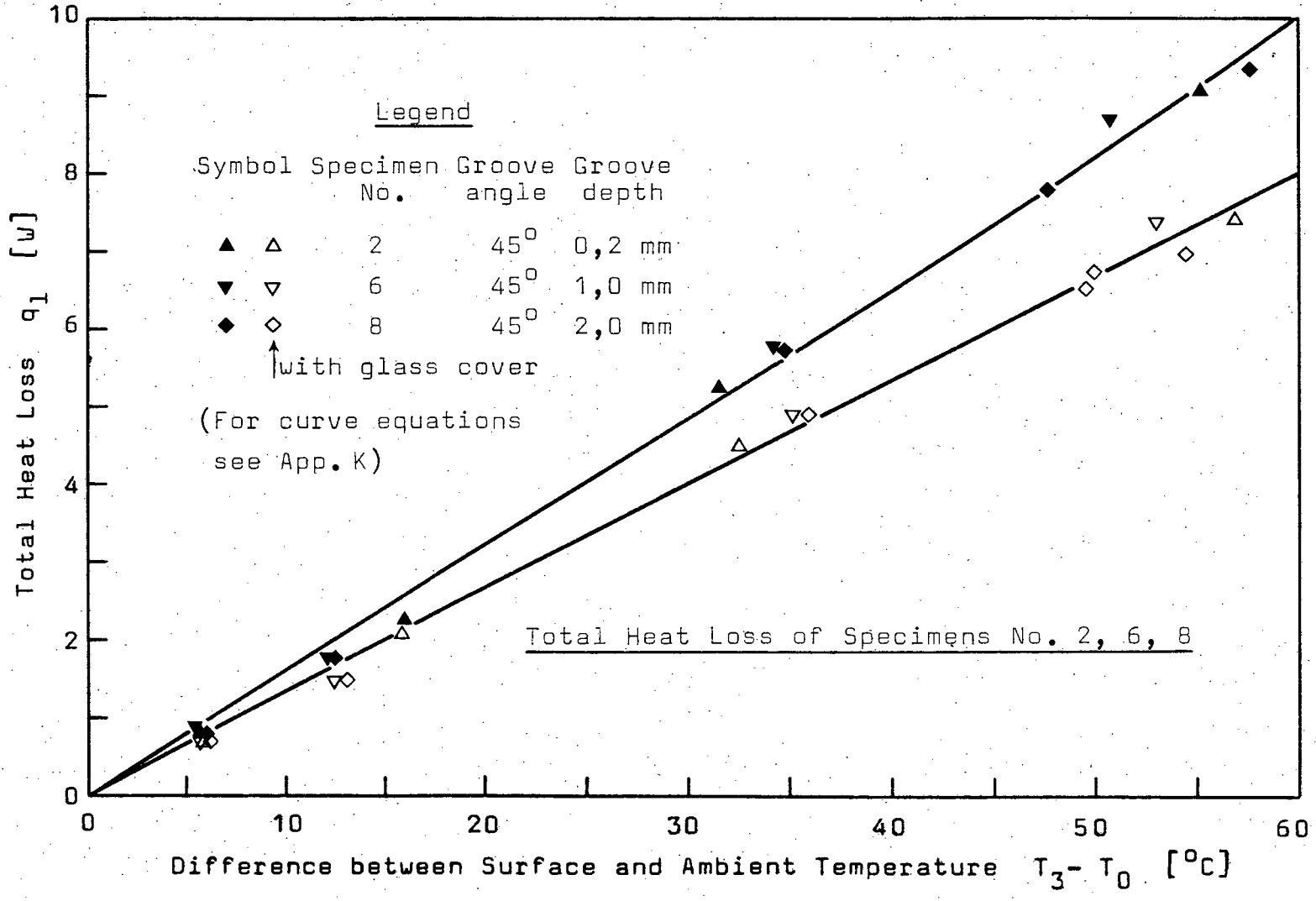
Legend
Symbol Specimen No. Groove angle Groove depth
2 45° 0,2 mm
6 45° 1,0 mm
8 45° 2,0 mm
with glass cover
(For curve equations see App. K)
Total Heat Loss of Specimens No. 2, 6, 8
Total Heat Loss q_1 [w]
Difference between Surface and Ambient Temperature $T_3 - T_0$ [°C]
0
2
4
6
8
10
0
10
20
30
40
50
60

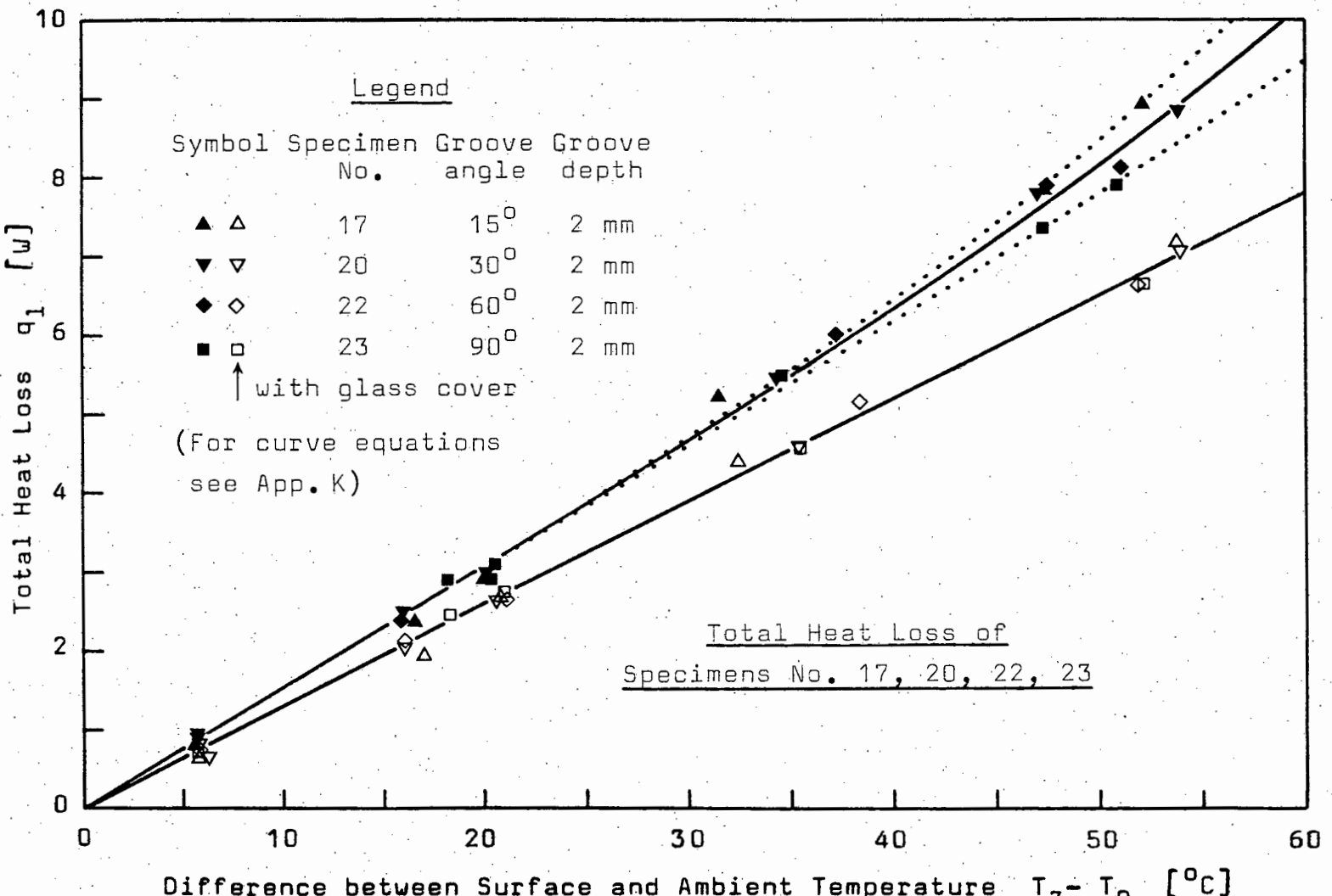
Legend
Symbol Specimen No. Groove angle Groove depth
17 15° 2 mm
20 30° 2 mm
22 60° 2 mm
23 90° 2 mm
with glass cover
(For curve equations see App. K)
Total Heat Loss of Specimens No. 17, 20, 22, 23
Total Heat Loss q_1 [W]
Difference between Surface and Ambient Temperature $T_3 - T_0$ [°C]
0
2
4
6
8
10
0
10
20
30
40
50
60

APPENDIX J

Absorptance of Flat Reference Specimen No. 32

Comment:

The experimental determination of the absorptance α of the flat reference specimen No. 32 was required for the evaluation of Eq. (40). The following results, plotted versus $T_3 - T_0$, show that α is independent of temperature; a necessary condition for further experiments. The confidence limits, being $\pm$ 2,8 % of the true mean of α, correspond very well with the overall measuring error of $\pm$ 3 % (cf. Error Analysis, App. H).

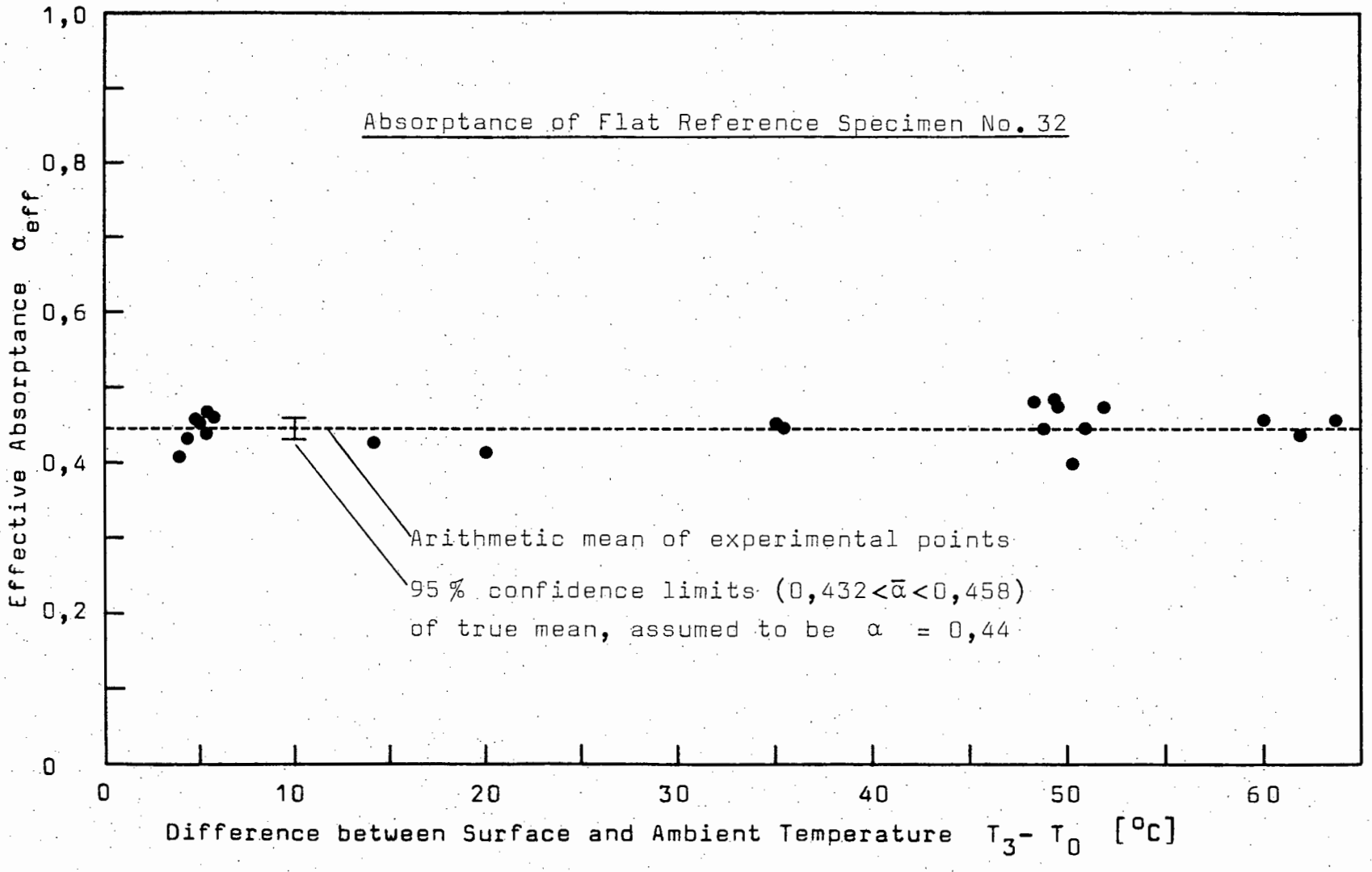
Absorptance of Flat Reference Specimen No. 32
Effective Absorptance α_{eff}
1,0
0,8
0,6
0,4
0,2
0
0
10
20
30
40
50
60
Difference between Surface and Ambient Temperature $T_3 - T_0$ [°C]
Arithmetic mean of experimental points
95 % confidence limits (0,432 < $\bar{\alpha}$ < 0,458)
of true mean, assumed to be α = 0,44

APPENDIX K

Least Square Curve Fit Equations

Specimen No.		Symbol	Regression Equation ($\Delta T \equiv T_3 - T_0$)
2,6,8	App. I-3	▲ ▼ ◆	$q_1 = 0,161\,\Delta T + 0,31 \times 10^{-7}\,\Delta T^4$
2,6,8	"	△ ▽ ◇	$q_1 = 0,134\,\Delta T$
17	App. I-4	▲	$q_1 = 0,153\,\Delta T + 1,317 \times 10^{-7}\,\Delta T^4$
23	"	■	$q_1 = 0,153\,\Delta T + 0,246 \times 10^{-7}\,\Delta T^4$
17,20,22,23	"	▲ ▼ ◆ ■	$q_1 = 0,153\,\Delta T + 0,787 \times 10^{-7}\,\Delta T^4$
17,20,22,23	"	△ ▽ ◇ □	$q_1 = 0,130\,\Delta T + 0,013 \times 10^{-7}\,\Delta T^4$
32	App. I-2	●	$q_1 = 0,158\,\Delta T + 0,062 \times 10^{-7}\,\Delta T^4$
32	"	○	$q_1 = 0,127\,\Delta T + 0,296 \times 10^{-7}\,\Delta T^4$
33	"	◉	$q_1 = 0,173\,\Delta T + 1,233 \times 10^{-7}\,\Delta T^4$
32	Fig. 31	○	$\eta = 44,2 - 1,873\,\Delta T$
33	"	●	$\eta = 102,5 - 1,935\,\Delta T - 0,005\,\Delta T^2$
34	"	◇	$\eta = 42,2 - 1,887\,\Delta T$
35	"	△	$\eta = 73,7 - 1,725\,\Delta T - 0,003\,\Delta T^2$
36	"	▲	$\eta = 107,4 - 2,176\,\Delta T - 0,001\,\Delta T^2$
37	"	◆	$\eta = 94,7 - 1,843\,\Delta T - 0,001\,\Delta T^2$

APPENDIX L

Solar Energy Collection in Space

1. A flat black surface (e.g. specimen No. 33) is used for solar energy collection in space. The surface absorptance for solar radiation (λ = 0-2 μm) is, ideally, assumed to be α_{0-2} = 0,95 , whereas the infrared emittance (λ = 2-∞ μm) is assumed to be $\varepsilon_{2-\infty}$ = 0,94 . The surface is to be maintained at a temperature of T_s = 116 ^{o}C = 389 K by extracting useful energy. Then the net energy which can be extracted is given as follows:

$$q_{net} = q_{absorbed} - q_{emitted}$$

$$= E(\alpha_{0-2} f'_{0-2} + \alpha_{2-\infty} f'_{2-\infty}) - \sigma T_s^4 (\varepsilon_{0-2} f''_{0-2} + \varepsilon_{2-\infty} f''_{2-\infty})$$

where

E	= 1353 W/m^2	(Solar irradiance)
σ	= 5,6693 x 10^{-8} W/m^{2}K^4	(Stefan-Boltzmann constant)
f'_{0-2}	= 0,94504	(Fraction of blackbody function for cutoff-wavelength-temperature-product $\lambda_c T_{sun}$ = 2 x 6000 μmK)
f''_{0-2}	= 0,106 x 10^{-4}	($\lambda_c T_{surface}$ = 2 x 389 μmK)

With these values, and since ideal cutoff at 2 μm is assumed, i.e., $\alpha_{0-2} = \varepsilon_{0-2}$ and $\alpha_{2-\infty} = \varepsilon_{2-\infty}$, the above

equation can be solved:

$$q_{net} = 1353(0,95 \times 0,94504 + 0,94(1 - 0,94504)) - 5,6693 \times 10^{-8} \times 389^4 (0,95 \times 0,106 \times 10^{-4} + 0,94(1 - 0,106 \times 10^{-4})) \; W/m^2$$

$$= 1285 - 1220 \; W/m^2$$

$$= 65 \; W/m^2$$

2. Instead of a flat black surface, a flat chromium plated surface (e.g. specimen No. 34) is to be used. The solar absorptance of the chromium plating proved to be $\alpha = 0,42$, whereas an infrared emittance of $\epsilon = 0,1$ can be assumed. With these data the above calculations yield:

$$q_{net} = 1353(0,42 \times 0,94504 + 0,1(1 - 0,94504)) - 5,6693 \times 10^{-8} \times 389^4 (0,42 \times 0,106 \times 10^{-4} + 0,1(1 - 0,106 \times 10^{-4})) \; W/m^2$$

$$= 544 - 130 \; W/m^2$$

$$= 414 \; W/m^2$$

3. By V-grooving, the absorptance of the chromium plated surface increases to $\alpha_{eff} = 0,94$ (see results for specimen No. 37). Assuming that Eqs. (40) and (30) can be applied to the emittance $\epsilon = 0,1$, it follows that $\epsilon_{eff} = 0,29$. With these data the above calculations yield:

$$q_{net} = 1353(0,94 \times 0,94504 + 0,29(1 - 0,94504)) -$$

$$5{,}6693 \times 10^{-8} \times 389^4 (0{,}94 \times 0{,}106 \times 10^{-4} + 0{,}29(1 - 0{,}106 \times 10^{-4}))\ W/m^2$$

$$= 1223 - 376\ W/m^2$$

$$= 847\ W/m^2$$

Although these examples are very special cases, they nevertheless demonstrate the advantageous effect of V-grooves applied to specular surfaces.

NOMENCLATURE

(Symbols cited in the literature survey as well as common mathematical symbols are not listed to avoid confusion.)

	Unit
projected surface area of specimen	m^2
grooved surface area of specimen	m^2
constant	-
constant	-
specific heat capacity of glycol	Wh/kg^oC
diameter of specimens	mm
depth of V-groove	mm
irradiance per unit area (flux density)	W/m^2
local irradiance per unit surface area	W/m^2
error as defined in App. H	-
configuration factor	-
blackbody function	-
weight of glycol	kg
thickness of specimens	mm
number of reflections	-
kernel of integral equation	-
quantity as defined by Eq. (36)	-
width of V-groove side	mm
width of V-groove side as shown in Fig. 6	mm
width of land between V-grooves as shown in Figs. 9 and 13	mm
flow rate of glycol	kg/h
total number of V-grooves on a specimen	-
pitch of V-grooves as shown in Fig. 13	mm
heat transfer rate	W
temperature	^oC
time interval	sec
thermocouple EMF	mV
width of V-groove opening	mm
dimensionless coordinate (x/L)	-
coordinate	mm
dimensionless coordinate (y/L)	-
coordinate	mm
coordinate	mm

Symbol		Unit
α	absorptance	-
β	substituted function as defined by Eqs. (14) and (16)	-
γ	substitution as defined by Eq. (15)	-
δ	angle of reflection	deg
ϵ	emittance	-
η	absorption efficiency	%
θ	groove angle	deg
λ	wavelength	μm
ξ	dimensionless variable	-
ρ	reflectance	-
σ	Stefan-Boltzmann constant	W/m^2K^4
τ	transmittance	-
Φ	radiant flux	W
φ	image angle as shown in Fig. 6	deg

Subscripts / Superscripts

a	apparent
c	cutoff
d	diffuse
eff	effective
i	number of reflections
l	losses
rel	relative
s	specular, or surface
α	absorbed
0	ambient
1	inlet of calorimeter
2	outlet of calorimeter
3	surface of specimen
*	quantity related to $(T_3 - T_0)^*$
'	auxiliary quantity